Study of PZT Multilayer Piezoelectric Transformers

SUBMITTED BY

Zhang Yu

FOR THE DEGREE OF

MASTER OF PHILOSOPHY IN PHYSICS

AT

DEPARTMENT OF APPLIED PHYSICS
'HE HONG KONG POLYTECHNIC UNIVERSITY

2001

Acknowledgements

Firstly, I would like to thank my chief supervisor Prof. C.L. Choy and co-supervisor Prof. Helen L.W. Chan for their close supervision and invaluable suggestions throughout the period of this research work.

It's also a pleasure to thank Dr. Qifa Zhou of the Department of Physics of the Zhongshan University in Guangzhou, China for his skilful assistance in the fabrication of sol-gel PZT thin film. I would also like to acknowledge the expert help from Dr. Junhui Hu and Dr. Guorong Li.

Moreover, thanks are also due to many people, namely Mr. Deming Lei of the Department of Physics of the Zhongshan University and technicians in our department for their technical support and assistance.

I gratefully acknowledge the financial support from The Hong Kong Polytechnic University. Finally, I would like to thank my family for their understanding and support to complete the thesis.

Abstract

Two types of lead zirconate titanate (PZT) multilayer structures have been investigated in this work. The first one, which consisted of thick PZT films fabricated by roll-casting and platinum (Pt) interleaving electrodes, was sintered at high temperature (1280°C). Thickness mode and length mode multilayer transformers have been fabricated from this type of multilayer structure and tested. The second type of multilayer PZT structure was fabricated by a sol-gel technique. A conductive oxide, lanthanum nickel oxide (LNO), was used as the electrode and the PZT/LNO multilayers were co-fired at below 650°C to make the process compatible with the integrated circuit (IC) technology. Original contributions reported in this thesis included:

(1) Besides fabricating and evaluating PZT multilayer transformers based on the usual thickness mode, a new length mode multilayer transformer has been fabricated and its performance characterized.

(2) A PZT/LNO multilayer structure was studied. A buffer layer consisting of a mixture of PZT and LNO was introduced at the interface to enhance the adhesion between the PZT and LNO.

(3) To fabricate LNO films thick enough to be used as electrode, a modified sol-gel process has been used. LNO powder was introduced into the LNO sol-gel solution to induce a seeding effect in the film formation process and the annealing temperature has been reduced.

Table of Contents

Chapter Four

Chapter Five

Figure Captions

Chapter 1

Introduction and Review

In recent years, piezoelectric transformer has a rapid development and a number of ways for improving the device characteristic have been invented.[1-9] The multilayer piezoelectric transformer fabricated by the co-fire and hot-press lamination method has attracted considerable attention. This kind of transformer has a number of advantages, including: strengthening of the vibration, increasing the voltage ratio, smaller size, good mechanical properties, high Q_m factor, etc. Several international research groups in Japan and western Europe have devoted great efforts in this field, and good results have been obtained. For example, NEC of Japan has worked on this project for more than 10 years, and they have obtained more than 26 patents in piezoelectric transformers. One of the most important patent is on the fabrication of multilayer transformer, which can achieve high voltage ratio and more than 92% power transmission efficiency.[10]

In this thesis, study on how to fabricate lead zirconate titanate (PZT) multilayer transformer and the details of the process are reported. Several different types of multilayer piezoelectric transformer (MPT) were invented, such as thickness mode MPT, third half wave-length vibration mode MPT, etc. Besides that, study of fabricating multilayer PZT thin film with conductive oxide electrode, namely, lanthanum nickel oxide (LNO), is also presented. And the optimization of the fabrication process of LNO thin film by introducing the nano-sized LNO powder as seeds for inducing the grain growth of the ceramic was also tested.

1.1 Piezoelectric Transformer

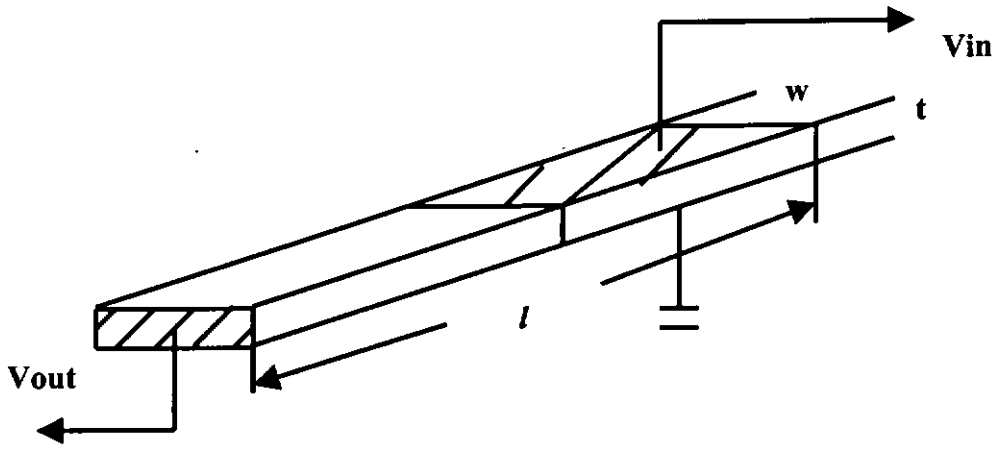

Fig. 1.1. The Rosen type piezoelectric transformer (PT).

A typical conventional piezoelectric transformer (PT), known as the **Rosen type transformer,** and shown in Fig.1.1[11], is operated by applying an ac voltage to its input (or driving) section. A thickness vibration excites a vibration along the length direction through an electromechanical coupling coefficient k_{31}. The k_{31} generator portion with a length vibration gives a voltage output corresponding to a 33 mode with an electromechanical coupling coefficient k_{33}. As a result, higher (if the impedance of the output portion is higher than the input portion) or lower (if the impedance of the output portion is lower than the input portion) voltage output can be obtained.

The vibration frequency is mainly decided by the size of the device, the materials characteristics, and the fabrication process. Also the painting and connection of external electrode will affect the performance of the final device. For example: A typical Rosen type transformer, fabricated by Ferroton, China, with a thickness of 2 mm, width of 8 mm, and length of 42 mm, and a mechanical qualification factor Q_m of 100, will have a fundamental length mode vibration frequency at about 140 kHz given by equation (1.1):

$$f_s = \frac{v^E}{2l} = \frac{1}{2l}\sqrt{\frac{1}{s_{33}^E}} \qquad (1.1)$$

where f_s is the one wave-length mode resonant frequency, l is the length of the transformer, v^E is the speed of sound in the ceramic, $s_{33}^E = 2.4E\text{-}11(m^2/N) = 1/Y$ and Y is the Young's modulus.

A piezoelectric transformer is different from an electromagnetic transformer in that it has several sharp resonance peaks. As we have mentioned before, these resonant frequencies depend on the material characteristics and thickness of the electrodes. They also depend on the fabrication parameters such as the sintering time and temperature. The resonant frequency can also be influenced by the external driving circuit. With increasing mechanical quality factor Q_m, the power transmission efficiency of a PT can become higher.

The design of a PT is based on an understanding of its piezoelectric mechanical resonance characteristics [2-4]. The most important point is to lift the energy exchange efficiency. However, the efficiency relates to a lot of factors such as: properties of the piezoelectric material, device size and shape, preparation of electrode, electrical loading and the driver circuit working conditions, etc. Every factor should be optimized to yield the best performance.

1.1.1 Simplified model of a piezoelectric transformer

To consider some of the formulae pertaining to the performance of a piezoelectric transformer, we must look at the factors that could limit its performance [12]. Some of the factors are listed below:

1. Internal mechanical losses due to finite mechanical quality factor Q_m.
2. Internal dielectric losses due to finite electrical quality factor Q_e.
3. Dielectric breakdown.
4. Frequency drift due to internal heating.

The first factor is more important, since the device operates at high dynamic stress levels. Factor (3) is of less importance. While at high output electric field levels factor (2)

becomes important. Factor (4) is, from a practical standpoint, also important as a change of the resonance frequency due to heating will cause fluctuation in the output voltage.

The following list of parameters holds at the length mode resonance.[9,11,12]

$C_{oi}=\epsilon_{33}^{T}(1-k_{31}^{2})\ l w/t$ (Clamped capacitance of the input section)

$C_{oo}=\epsilon_{33}^{T}\ (1-k_{33}^{2})\ wt/l$ (Clamped capacitance of the output section)

$\phi=wd_{31}/(s^{E}_{11} \times E)$

$\psi=k_{33}^{2}wt/(g_{33}\ l)$

$R=(\ \pi/Q_m\ )\rho v wt$

$X=2\pi r\rho v wt;$

Where $\epsilon_0\epsilon_{33}^{T}$ is the dielectric constant, ρ is density in kg/m^3; v is velocity = 2N; N is the frequency constant; $r = f_r/f_a$, where f_r and f_a are the resonance and anti-resonance frequencies, respectively. ϕ and ψ are the calculated exchange ratio in the input and output sections of the equivalent circuit, respectively. R is the resistance calculated from the equivalent circuit. A simplified equivalent circuit for the transformer is shown in Fig.1.2[12,13].

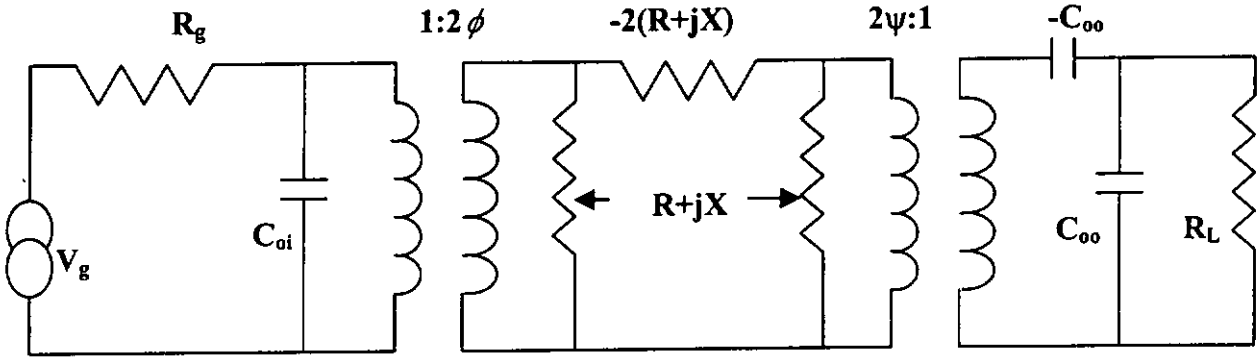

Fig. 1.2. Equivalent circuit of a Rosen type PT.[3]

1.2 Fabrication of Lead Zirconate Titanate (PZT) Ceramics by the Mixed Oxide Method

Conventional mixed oxide method for the fabrication of PZT ceramic is shown in Fig. 1.3.

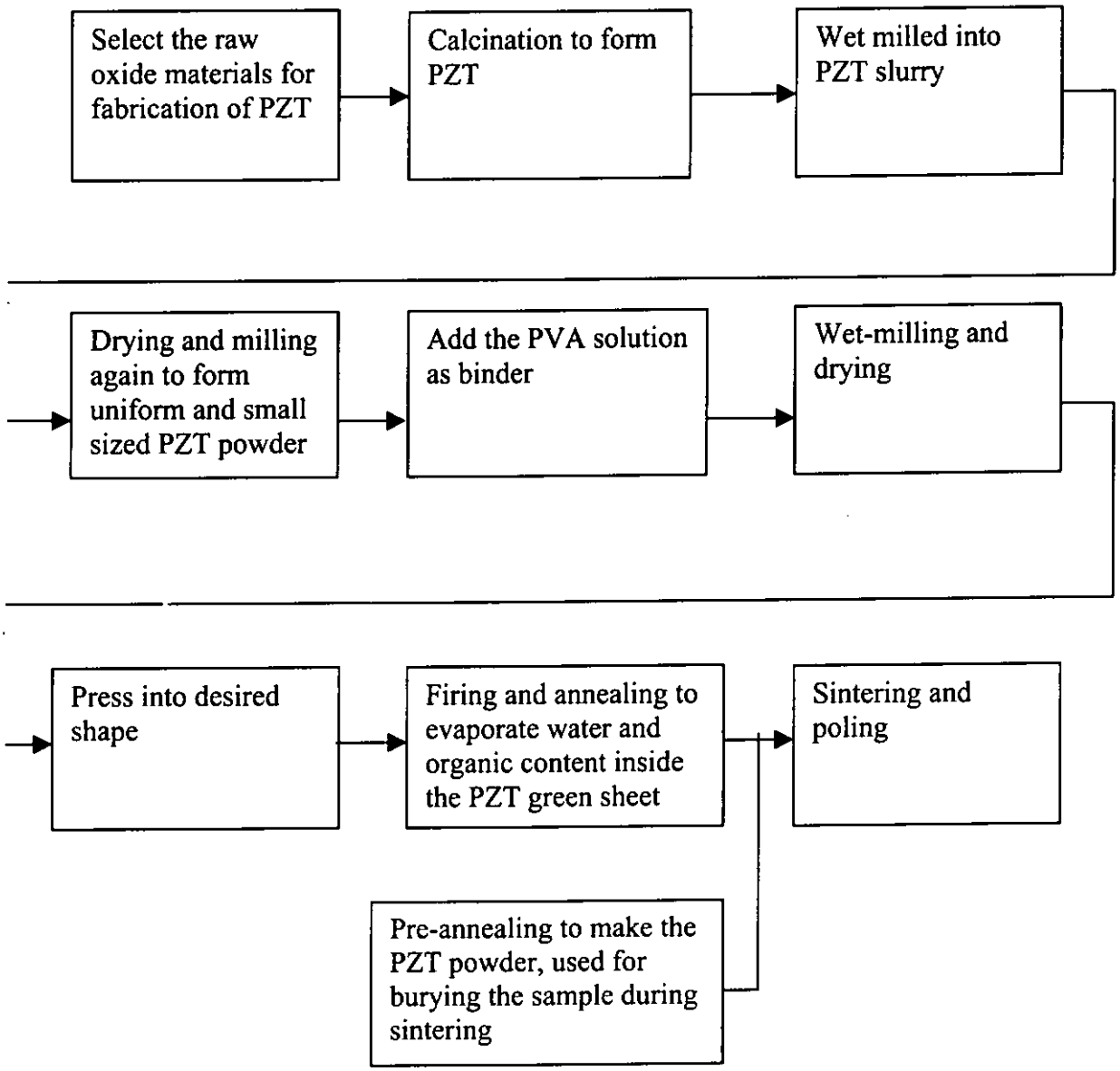

Fig. 1.3. Common fabrication procedure of piezoelectric ceramic.

As shown in the flowchart Fig 1.3, ten main steps are used to fabricate PZT ceramics. In more detail:

1. The first four steps are used to fabricate PZT with certain characteristics. There are two major type of PZT commonly used. The first one is a soft PZT, which is doped with low valence ions such as potassium (K^+). This kind of PZT can be used for fabricating piezoelectric sensors or actuators for it has lower Q_m value and large strain can be induced. However, hysteresis effect is quite large in the soft PZT, and it is also relatively easy to depole. Another type of PZT is a hard PZT which is doped with high valence ions such as manganese (Mn^{5+}). This kind of PZT can be used to fabricate high Q_m PZT ceramic which can bear high power transmission value but with lower induced strain. In the present project, the hard PZT ceramic (PKI 801 from Piezo-Kinetics. USA) is used. This ceramic has high Q_m factor and is used to fabricate the multilayer PZT transformer described in Chapters 2-4.

2. Polyvinyl alcohol PVA solution is produced by dissolving PVA in water with a weight percentage of 25%, then a small amount of glycerin is added to adjust its viscosity. The PVA is selected with a lower molecular weight of about 3000~4000 amu, which gives good adhesive strength to bind the PZT powder together but does not stick to the surface of the steel moulds.

3. Wet-milling and drying are used to reduce the PZT powder into smaller size. The diameter of the PZT powder is about 2~5 μm after milling.

4. The powder is shaped in a stainless steel mould. The pressure used is about 1500 kg/cm^2 for a bulk PZT. But a lower pressure of 650~850 kg/cm^2 is used for laminating and hot-pressing of the thick PZT films for multilayer transformer fabrication as described in section 2.4.1.

5. To get rid of the water and organic components, the PZT is heated at 200°C for about 2 hours. Then the temperature is slowly increased to about 500°C

and dwell for another two hours to burn out the PVA binder inside the sample. The sample is cooled to room temperature at a rate of no more than 5°C/min.

6. In order to reduce the lead loss during high temperature sintering, the PZT sample is covered with PZT powder. The PZT powder has been previously heated to 750°C to reduce its surface activity and prevent it from sticking onto the sample during sintering.

7. Sintering and poling are the final steps for fabricating a PZT ceramic with desirable piezoelectric properties. The best sintering temperature for PKI 801 PZT is about 1300°C, and the poling voltage is 6 kV/mm. The detailed technical procedure is discussed in Chapter 2.

1.3 Piezoelectric Parameters of PZT

PZT with a Zr/Ti of 52/48, product no. PKI 801 from Piezo-kinetic in USA was used in fabricating the thickness mode and length mode MPT reported in Chapters 2-4. The piezoelectric parameters of PKI 801 are given in Table 1.1.

Table. 1.1. The piezoelectric parameters of PKI 801[6]

k_{31}	0.31	k_{33}	0.7
k_{15}	0.54	k_t	0.4
d_{31}	-100 (pm/V)	d_{33}	230 (pm/V)
s^E_{11}	1.1*E*-11 (m^2/N)	s^E_{13}	4. 9*E*-12 (m^2/N)
s^E_{33}	1. 54*E*-11 (m^2/N)	s^D_{11}	1*E*-11 (m^2/N)
s^D_{13}	1.7*E*-12 (m^2/N)	s^D_{33}	0.7*E*-11 (m^2/N)

Q_m	800	$\tan\delta_e$	0.03
v^E_{33}	3300m/s	v^D_{33}	4200m/s
e_{33}	11.83 (C/m^2)	e_{31}	-3.59 (C/m^2)
Frequency constant N_1	1732 (Hz-m)	Frequency constant N_{3t}	2098 (Hz-m)
Frequency constant N_p	2328 (Hz-m)	Frequency constant N_5	1131 (Hz-m)
Density	7600 (kg/m^3)	$\varepsilon^T_{33}/\varepsilon_0$	1100
Piezoelectric voltage constant g_{33}	27.6 ($X\ 10^{-3}\ m^2\ C^{-1}$)	Piezoelectric voltage constant g_{31}	-11.6 ($X\ 10^{-3}\ m^2\ C^{-1}$)
Piezoelectric voltage constant g_{15}	26 ($X\ 10^{-3}\ m^2\ C^{-1}$)	Constant electric field elastic stiffness c^E_{13}	9.4*E*10 (N/m^2)
Constant electric field elastic stiffness c^E_{33}	1.3*E*11 (N/m^2)	Constant electric field elastic stiffness c^E_{44}	3.6*E*10 (N/m^2)

1.4 Measurement of Piezoelectric Transformer

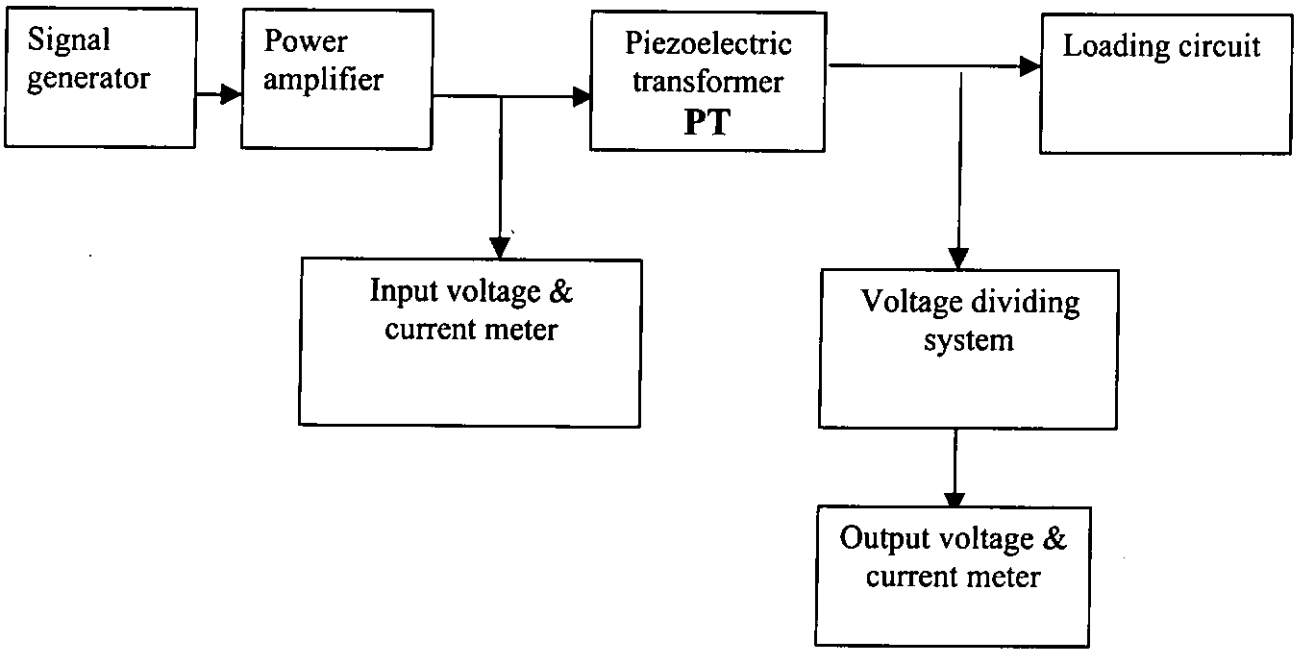

Fig. 1.4. Schematic set up for measuring the voltage exchange ratio of PT

First a stable voltage is applied, then different loading impedance are used, and the input frequency is adjusted. The input frequency is the resonance frequency of the transformer and is determined by the selected level of resonance. Normally, the fundamental resonance frequency is chosen as the working frequency because most likely the highest power transmission efficiency is obtained.

After transformed, the output voltage and current are measured through a voltage dividing system. As the output voltage might be very high, so by using a voltage dividing system, we can measure a lower voltage and then calculate the actual output voltage of the transformer through the measured value. One important factor should be noted: The output frequency can be different from the input frequency because the loading

impedance of the input and output working circuit are different. By comparing the different electrical properties of the input and output parts, we can find out some of the relationships between the voltage exchange ratio, the resonance frequency and the optimum loading impedance.

1.5 Multilayer Transformer

The multilayer technology was first introduced in the middle of this century in which several divided sheets were laminated together. To fabricate multilayer ceramic devices, two processes were commonly used. One was a cut-and-bond method and the other were tape-casting or roll-casting method. In the roll-casting method, ceramic green sheets were produced by roll-casting, then they were printed with electrodes, laminated and co-fired with internal electrodes. By using multilayers, low driving voltage and high displacement can be achieved.

The individual PZT sheet was poled in a direction opposite to its neighboring layers and each layer is connected electrically in parallel, but mechanically in series. In this way, a low input voltage can be used to obtain a high field because each layer is quite thin (~250 μm). A typical multilayer structure is shown schematically in Fig. 1.5.

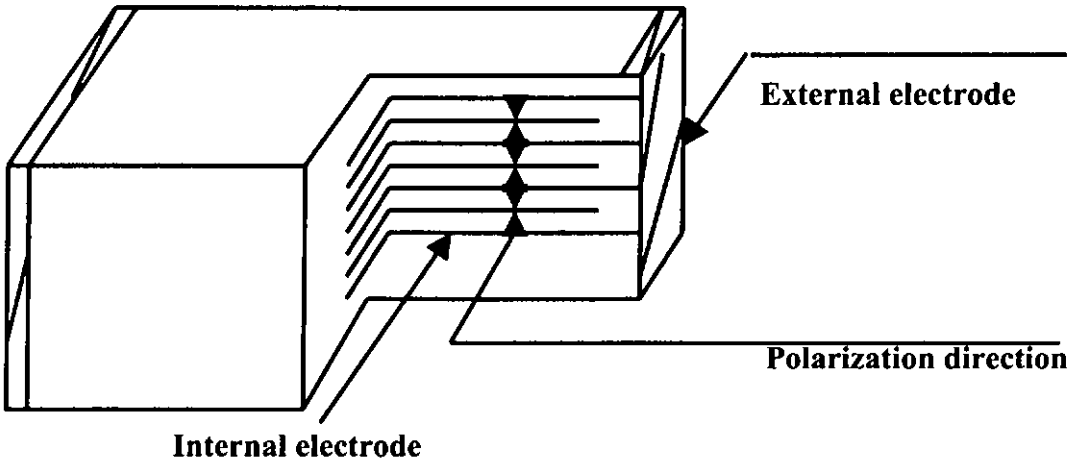

Fig. 1.5. Schematic diagram of a multilayer strucutre.

1.6 Working Principles of a Multilayer Piezoelectric Transformer

In order to compare the performance of a multilayer transformer with a single sheet piezoelectric transformer, the Rosen type transformer is chosen as an example and its working principle is discussed.

Fig. 1.6 shows two third-level Rosen type piezoelectric ceramic transformer, which have been designed both in a single sheet and a multilayer structure. (Note: Third-level Rosen type PT has two driving parts and the vibration wave transmits through the device with two nodes when it operates at the fundamental resonance frequency, as shown in Fig.1.6.)

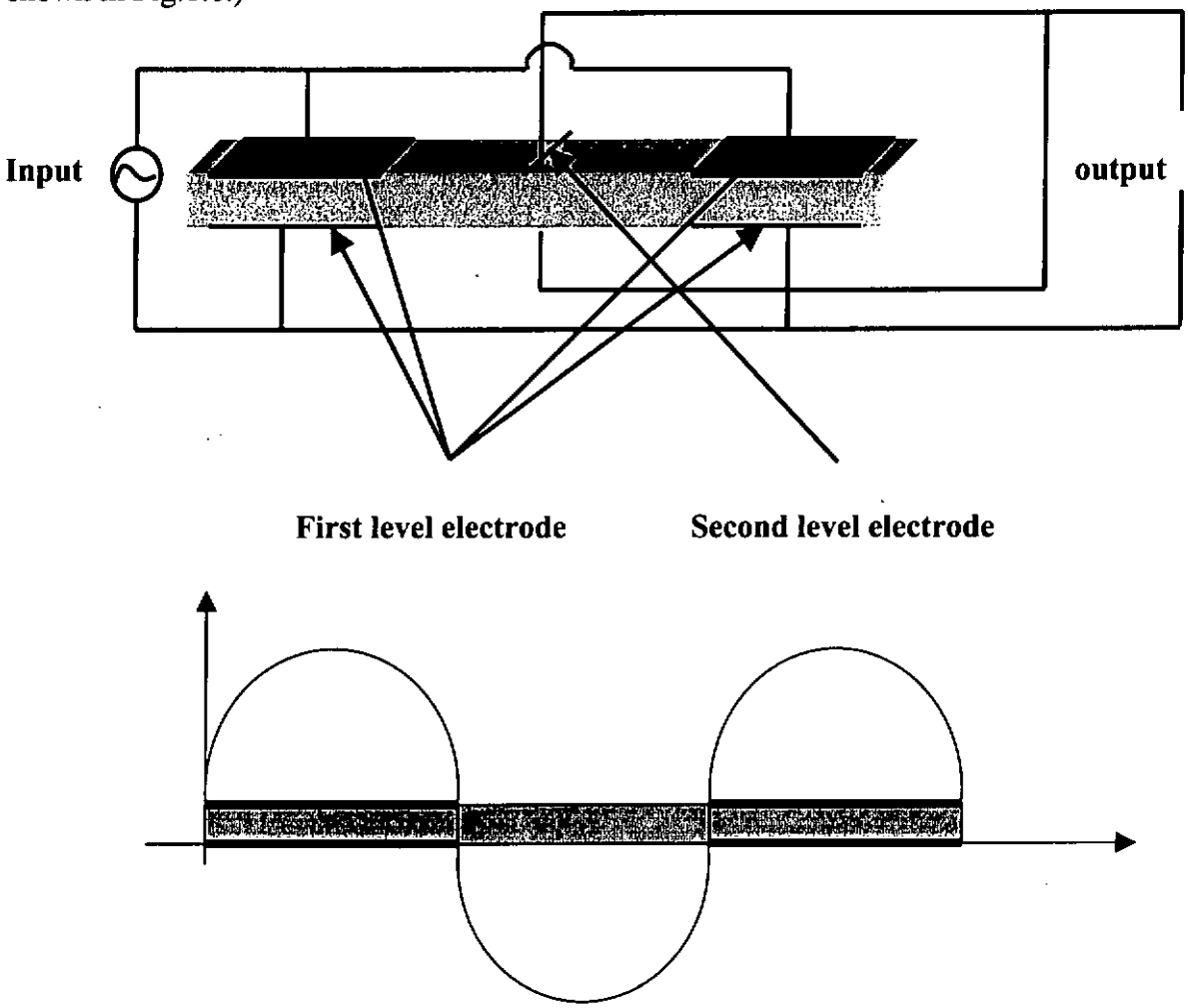

Fig. 1.6. Third-level Rosen type single sheet piezoelectric transformer and its fundamental vibration mode.

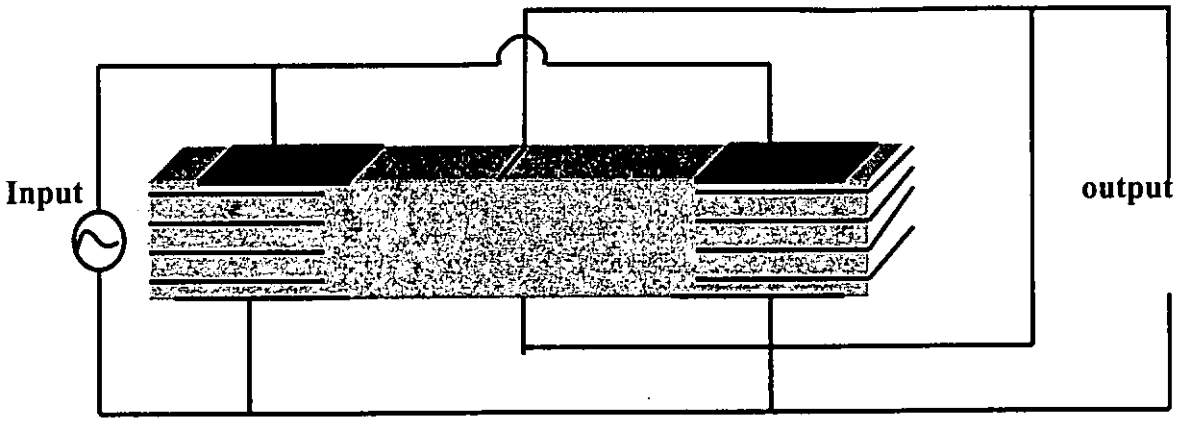

Fig. 1.7. Third-level Rosen type multilayer piezoelectric transformer.

Similar to a single sheet piezoelectric ceramic transformer, in a multilayer transformer, the output and input voltage ratio has a definite relationship. Due to this reason, the transformer must be produced with long length or thin thickness in order to achieve a high length to thickness ratio. On the other hand, the output power density of the transformer has a direct relationship with the cross sectional area of this device. So if the ratio increases, in order to maintain a constant power density, we must extend the width. But this will cause a vibration in the width direction. This spurious vibration interferes the normal operation of the transformer, hence the increase in width couldn't be too large [14,15,16].

Compared with a single sheet device, Fig.1.7 shows a multilayer co-fired structure which uses the PZT materials with interleaving metallic electrodes. It has the following characteristics:

1). The mechanical quality factor Q_m can maintain a high value even with many layers and it can have a high power transmission efficiency. The co-fired method, which is different from the adhesion method, can give a more stable characteristic and a lower decrease in the Q_m value. There is a direct relationship between the output and input voltage ratio with the number of layers n, so if we decrease the sheet thickness and increase n, the output and input voltage ratio can be lifted and a smaller input voltage can be used. (See Chapter 3)

2). In contrast to the single sheet device, multilayer can work with high impedance (>100 kΩ) and gives a high output and input voltage ratio (>40) together with a high power transformation ratio (>90%).

1.7 Advantages and Potential Applications of Multilayer Piezoelectric Transformer

Multilayer piezoelectric transformer (MPT) is a new kind of power converter. It has the advantages of high output and input voltage exchange ratio, low driving voltage, small volume, automatic cut-off without burning in case of overload due to short circuiting, high power density, and low electromagnetic interference. Step-up MPT can be used in devices with high output voltage and low output current, such as the back-light in LCD display. Step-down MPT has important applications in portable charger and internal adapter in note-book computer. The main MPT research carried out so far included the searching for high-performance ceramic materials and their application in MPT, fabrication technology, structure, working principles and application development of MPT.

1.8 Multilayer Transformer Fabrication Process

Multilayer piezoelectric ceramic device used in a small-sized electrical and mechanical energy transmission system has several merits including close lamination density, high interfacial fracture strength, good mechanical quality and reliability, and are used as high performance electronic components. [16,19,20]

Tape-casting or roll-casting, interleaving electrode printing, lamination and co-firing are necessary steps for the fabrication of multilayer ceramic devices and variations in these processes can have significant effects on the final product. [19,20] Two of the most important steps are lamination and co-firing. The lamination process involves

several variables (pressure, temperature, and time) which are also related to the properties of the green sheet and to the sintering behavior. In the co-fire process, the shrinkage matching and the interfacial bonding between the metal and the ceramic is another important aspect in fabricating multilayer ceramic devices. Detailed fabrication process will be described in Chapter 2.

1.9 Scope of the Present Study

In the present study, we first use platinum (Pt) alloy as the internal electrode material and $PbTi_{0.52}Zr_{0.48}O_3$ (PZT) as the starting material. A systematic investigation of the lamination process and co-fire technology has been carried out to reveal the relationship between the process parameters and the properties of the multilayer. A thickness mode (k_{33}) multilayer piezoelectric transformer (MPT) fabricated by using the Pt alloy as interleaving electrode and a new type of length mode (k_{31}) MPT, which has two separated multilayer structural driving sections laying beside the generator portion, was also built. To minimize the inter-diffusion between the electrode and PZT, a two-step sintering process was used to lower the sintering temperature. Using this two-step sintering method and by choosing a suitable PZT from Ferrotron in China, less costly palladium/silver (Pd/Ag) electrodes can be used as the electrodes. Finally, a study of using oxide interleaving electrode that provides better thermal matching to PZT thin film in fabricating multilayer structures was carried out. The modified sol-gel PZT films were co-fired with the lanthanum nickel oxide (LNO) thin films and a buffer-layer structure was used to improve the interfacial adhesive strength. The seeding effect was also used to reduce the annealing temperature of LNO in order to provide a better match to the PZT thin film fabrication.

1.10 Significance of the Present Work

The following are original work reported in this thesis:

(1). A new length mode (k_{31}) multilayer piezoelectric transformer (MPT) was designed and fabricated. (Chinese patent pending.)

(2). The co-fire technology for fabricating PZT and LNO multilayer structure with buffer-layer. The PZT film was made by a modified sol-gel method and the LNO film was made by a metal-organic deposition (MOD) method. The micro-structure of the specimen was studied and good conductivity in the LNO ceramic layer was achieved. (Results published in Thin Solid Films.)

(3). Using the seeding effect to reduce the annealing temperature of LNO film in order to provide better match to the PZT layers. (Results published in 2000 MRS Proceedings.)

Chapter Two

Fabrication of Multilayer Transformer with Metallic Interleaving Electrodes

2.1 Introduction

The fabrication process of multilayer device with metallic interleaving electrodes has been developed for almost 20 years, but the use of co-fire and conventional green-sheet technique to produce a practical piezoelectric multilayer transformer is still developing. Although a co-fired multilayer transformer can generate higher voltage than a single plate transformer and can be operated at high efficiency, its commercialization has still been limited by difficulties in meeting performance and reliability requirements at an acceptable manufacturing cost. Apparently, multilayer ceramic fabrication technology that allows capacitors to be manufactured at a low cost has not been translated into the low-cost fabrication of multilayer transformers. Considerable additional developments of piezoelectric and electrode materials, as well as multilayer fabrication methods, are still required for the commercialization of MPT. These include:

a) To select piezoelectric ceramic materials with a reasonable high Q_m factor and can withstand high driving voltages.

b) More reliable internal electrodes should be fabricated. They should have good conductivity and minimum loss.

c) The hot-press lamination process should be well-controlled with optimum pressure and temperature to allow for proper interfacial development between the ceramic green sheet and the electrode layer.

d) The heating rate and co-fire procedure should be adjusted to avoid excessive shrinkage mismatch and interfacial diffusion between the ceramic and the internal electrode.

2.2 Tape-casting and Roll-casting Method for Producing PZT Green Sheets

First, PZT(52/48) powder was milled for 3 hours to give an average particle size of 2~5μm, then some polyvinyl alcohol (PVA) solution was added as the binder and plasticizer and they were mixed for 1 hour to form a slurry. This PVA solution composed of polyvinyl alcohol (20%), butyl phthalyl butyl glycolate (BPBG) (5%), ethyl alcohol (<10%), and water (>65%). (This ratio was based on weight percentage.) A green sheet of about 100 ~ 400μm in thickness can be fabricated by the roll-casting process, as shown in Fig. 2. 1.

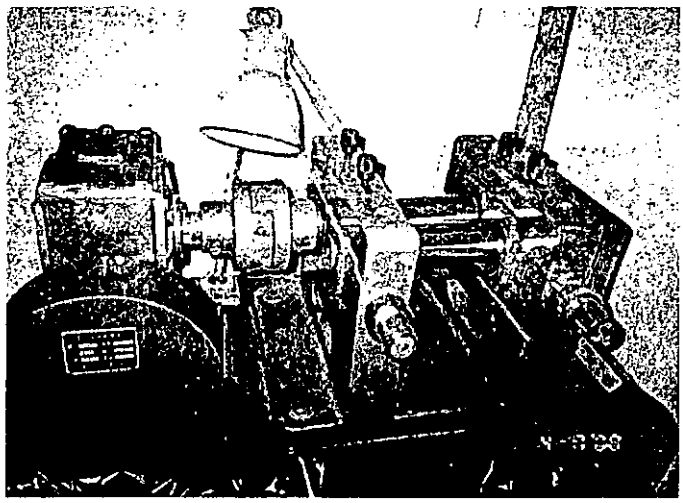

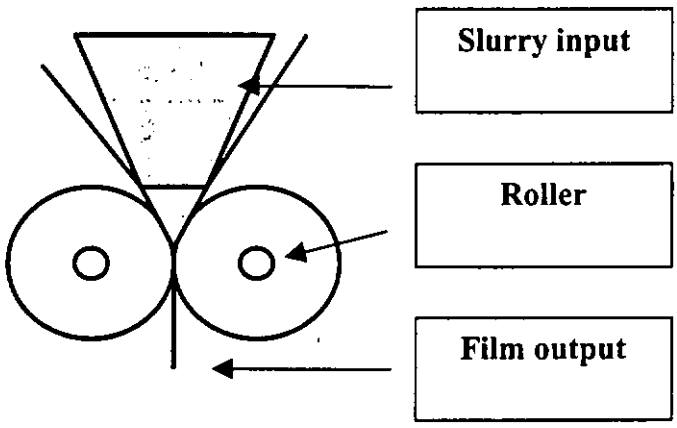

Fig.2.1. Photo and schematic diagram of the roll-casting method.

In the tape-casting process, two steps are quite important: The first one is the added percentage of the PVA solution, which is about 35% by weight. The second one is how to make a uniform slurry and how to remove the air bubbles inside the slurry. There are two main methods: The first method is by using a vacuum stirring machine which can pump out the air bubbles inside the slurry within a few minutes, but it requires an elaborate vacuum system. The second method that we actually used is to heat the slurry to about 80°C, then cooled it at a very slow rate while stirring the slurry slowly. By this method, the bubble inside the slurry can separate out little by little, and this method can be applied to deal with different amount of slurry. By using the tape-casting technique, ceramic sheet with a thickness of about 40 μm can be fabricated. In our work, a model of DP-160 doctor-blade tape casting machine from BAYAMA POKEN LTD. in Japan was used, a picture and a schematic diagram of the machine used in the tape-casting method is shown in Fig. 2.2.

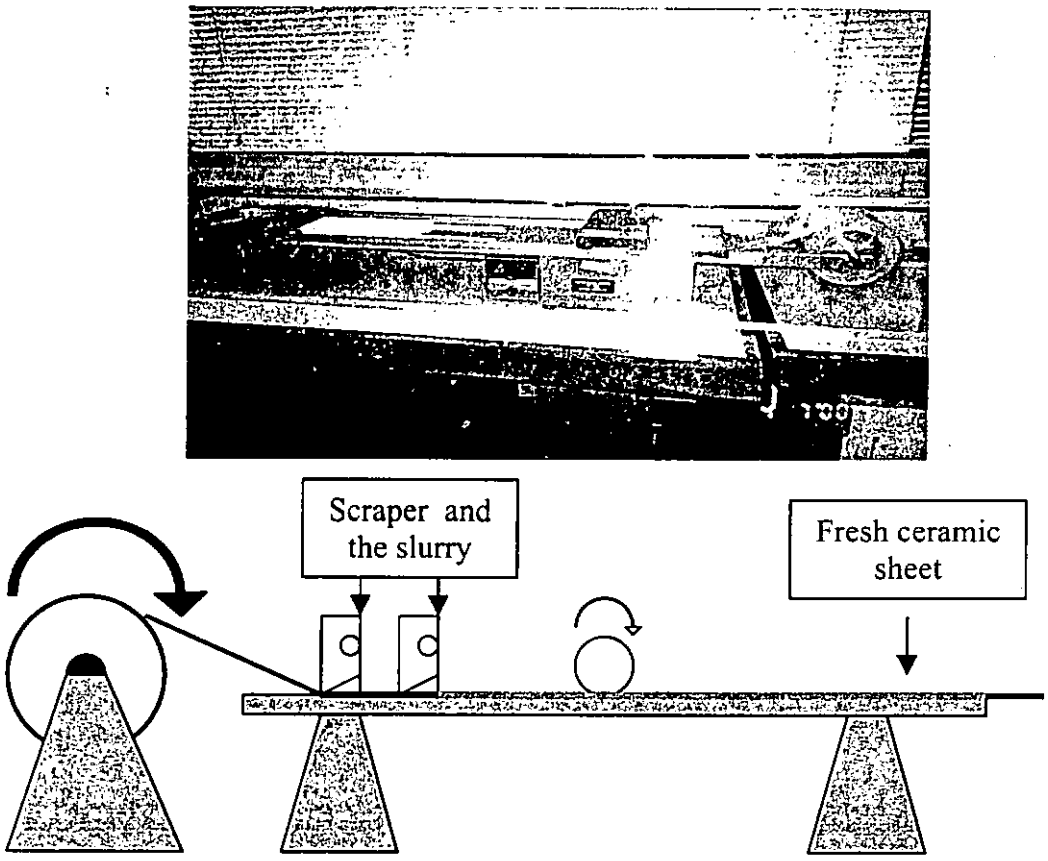

Fig.2.2. Photo and a schematic diagram of the tape-casting method

2.3 Designing and Painting the Interleaving Electrodes

In order to make connection to the external electrodes, the internal interleaving electrodes were painted as shown in Fig. 2.3.

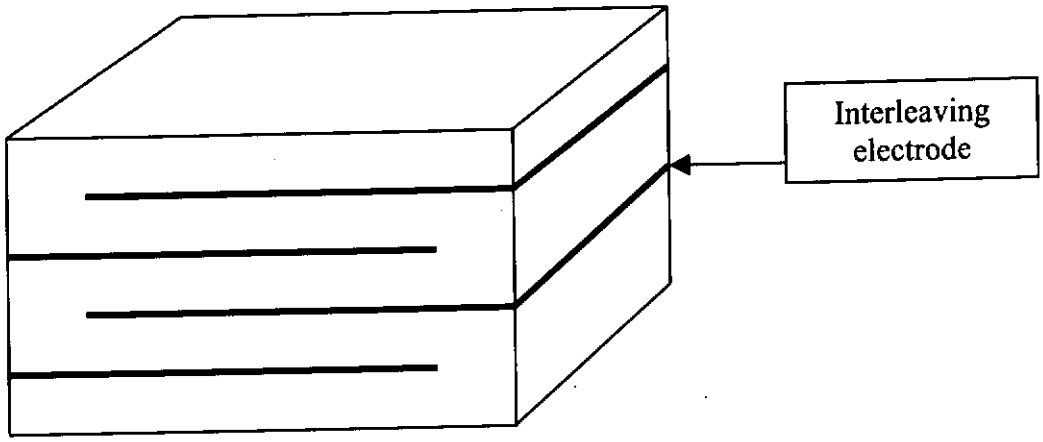

Fig. 2.3. Multilayer structure with partially overlapped interleaving electrodes.

The uniformity and good conductivity of the interleaving electrodes are very important for the device to ensure a minimum electrical loss. A platinum (Pt) alloy slurry was used in fabricating interleaving electrodes. A flat tip brush was used for painting, and then a small knife was used to scrap the electrode surface to make it smooth. This step should be repeated two or three times in order to attain a suitable electrode thickness which is about 5 μm. Between each steps, the painted electrode should be dried by baking at 150°C for 3 hours[23-27].

2.4 Hot-press Lamination Process for Forming the Multilayer Structure

2.4.1 Introduction

The lamination process involves several variables (pressure, temperature, and time) which relates to the properties of the green sheet and to the sintering behavior.

The green sheet is cut to 38 mm × 38 mm square plates. After electrodes are painted, seven layers will then be placed in a mould and pressed using a uniaxial stress. The pressure during lamination is varied from 650~800 kg/cm^2, and the temperature from 80~150°C, with the time fixed at 3 hours[25,26,27]. Fig. 2.4 shows a schematic diagram of the lamination process.

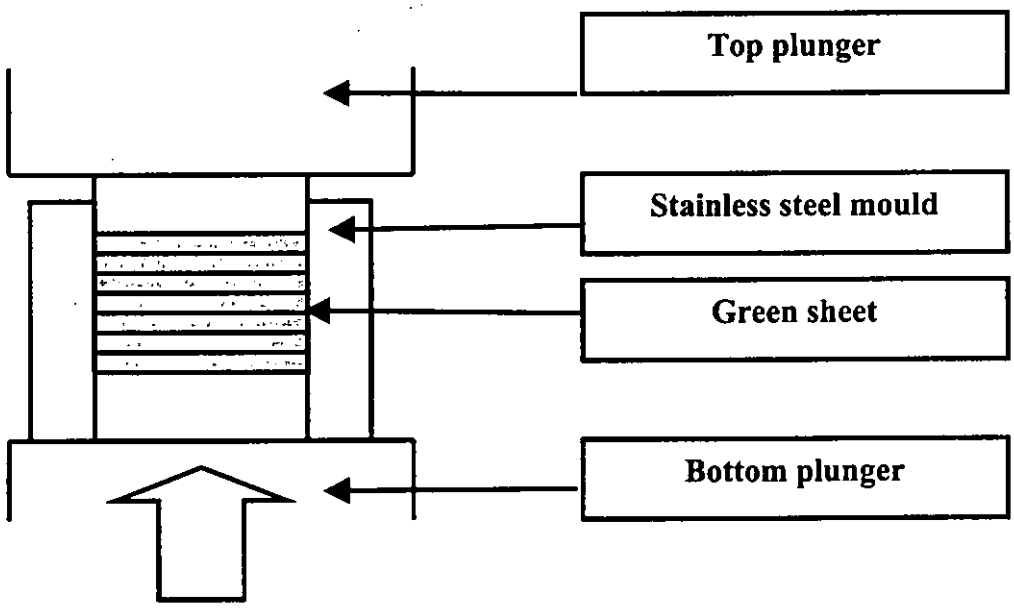

Fig. 2.4. Schematic lamination process

2.4.2 Viscous Flow at the Interface of Ceramic with Metallic Electrodes

Table 2.1. Changes in thickness and volume shrinkage of the specimen after being laminated and co-fired at 1280°C

Lamination Temperature/pressure °C/(kg/cm^2)	Changes in thickness (%)	Volume shrinkage (%) (after be sintered at 1280°C)
80/500	8.6	Since the hot-press and laminating condition is not suitable for making these PZT green sheets into one multilayer block, so the sample showed de-lamination after co-fire and its shrinkage cannot be measured.
80/650	11.7	
80/700	12.3	
80/800	14.5	
120/500	11.2	
120/650	13.2	
120/700	16.8	
120/800	19.6	38
150/500	17	36
150/650	17.5	38
150/700	20.3	40
150/800	24.6	43
170/1000	Lost of lamination structure and merged into one block	

The green sheet contained some polymeric binders that softened with increased temperature, thereby increasing the viscous flow of the ceramic green sheet, especially at the ceramic/electrode interface. This effect of viscous flow will strengthen the interface diffusion between the ceramic green sheets and the printed internal electrodes, as shown in Fig. 2.5.

There are many small cracks and holes on the surface of the ceramic green sheet. After applying heat and pressure onto the multilayer specimen, some of the metallic internal electrode slurry will easily diffuse into the cracks and holes, so that the contacting area between the interleaving electrodes and the ceramic layers is much increased due to this kind of micro-interfacial structure. At the same time, the soft ceramic green sheet will also reduce the cracks and holes, and will improve its uniform and quality of the whole multilayer structure. Hence applying adequate pressure will help to enhance the adhesion between the ceramic green sheets and the metallic slurry. This is a key step for controlling the interfacial fracture strength between the ceramics and the metallic internal electrode layers, and has a direct influence on the properties of the multilayer device[12-16,27-29].

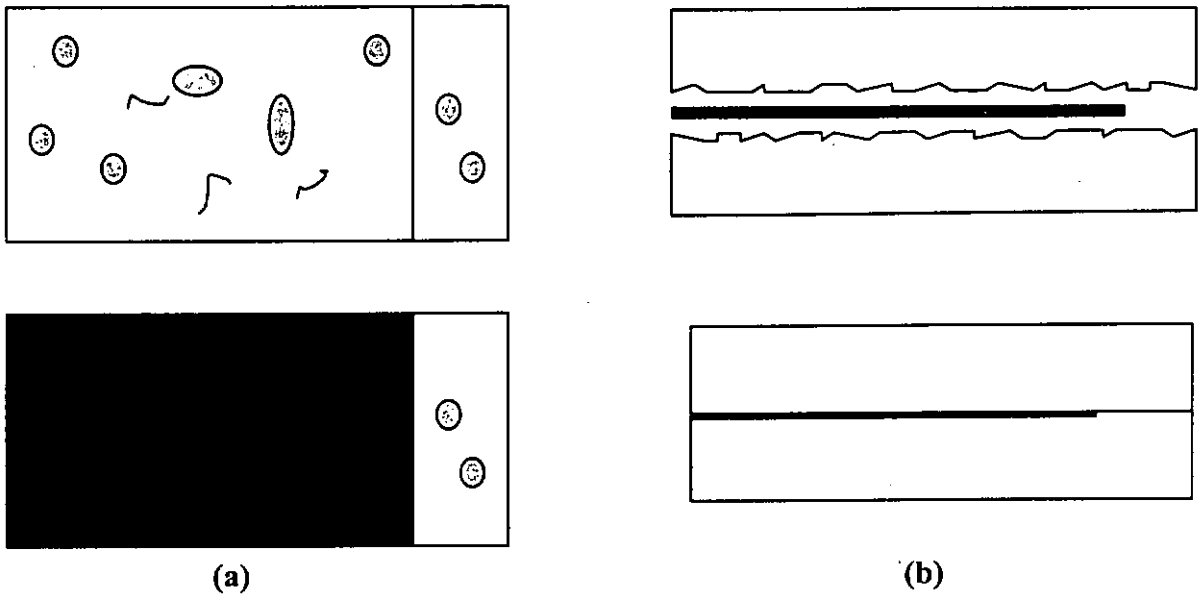

Fig. 2.5. Schematic interfacial structure of the ceramic green sheets with internal electrode slurry, before and after hot-pressing. (a) Top view, (b) Cross section

2.4.3 Experimental Procedure

A flow chart showing the main steps in fabricating a multilayer piezoelectric transformer (MPT) is shown in Fig.2.6.

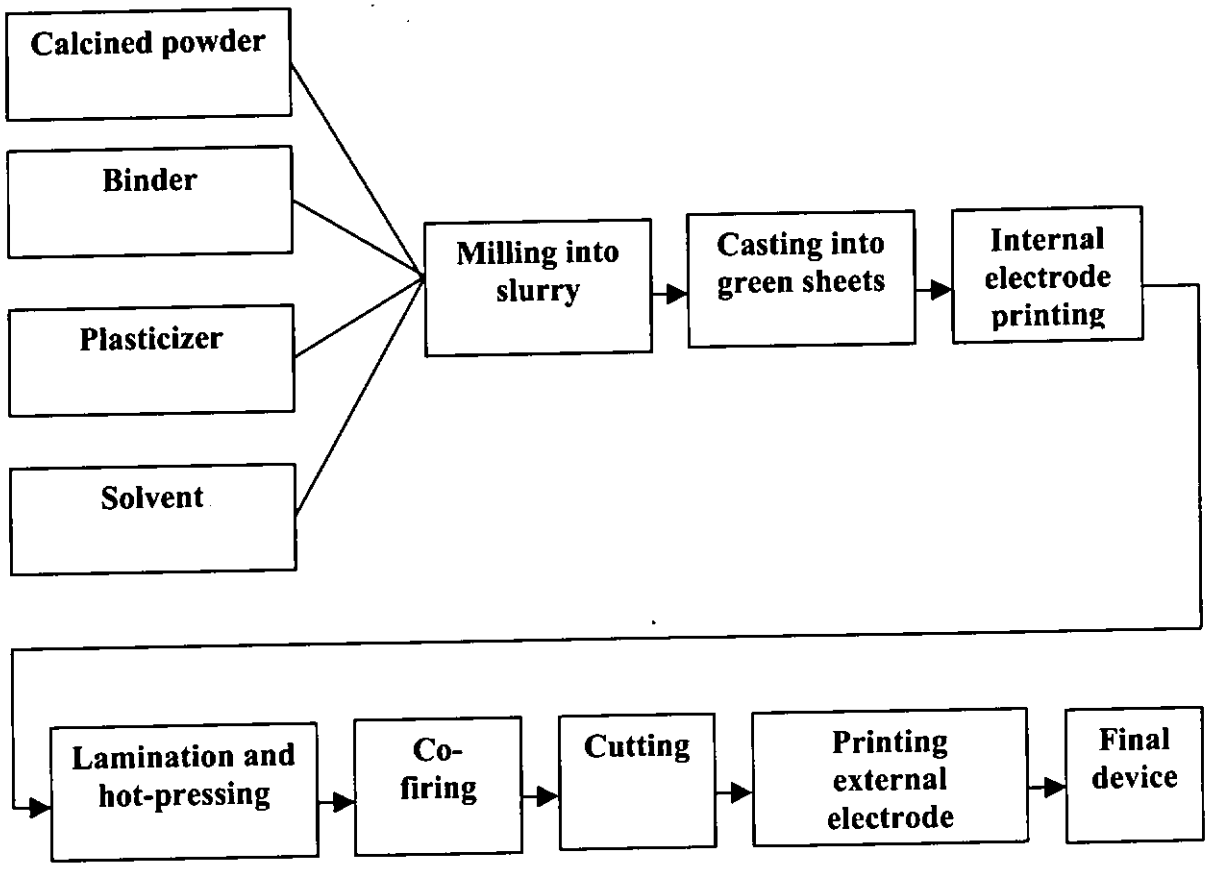

Fig. 2.6. Fabrication process of MPT

2.4.4 Results and Analysis

Pt alloy internal electrodes can withstand very high sintering temperature, because it does not evaporate or chemically react with other materials during the high temperature sintering process. Fig. 2.7 shows the SEM images of the fractured surface of the multilayer. Samples are dealt at different conditions. Fig. 2.7 (a) simple is pressed at 500 kg/cm^2 and heated at 80°C; Fig. 2.7 (b) simple is pressed at 1000 kg/cm^2 and heated at 170°C; Fig. 2.7 (c) simple is pressed at 700 kg/cm^2 and heated at 150°C, which is the optimum condition. Each layer of the green ceramic sheet is ~250 μm thick, and the internal electrode layer is about 2 μm thick. As explained earlier, during hot-pressing, the metallic internal electrode slurry diffused into the small cracks and holes on the surface of the PZT green sheets, providing adhesion at the interface of the distinctive material layers after being sintered, as shown in Fig. 2.8. [21,22]

This is the first step for improving the interface adhesive strength between the two distinctive layers. From these images we can see, if the lamination process is adjusted to an optimum condition, the resulting multilayer structure will have a well-defined layered structure. Otherwise it will either crack or curve or merge into a single block and lose the interface between the internal electrodes and the ceramic sheets.

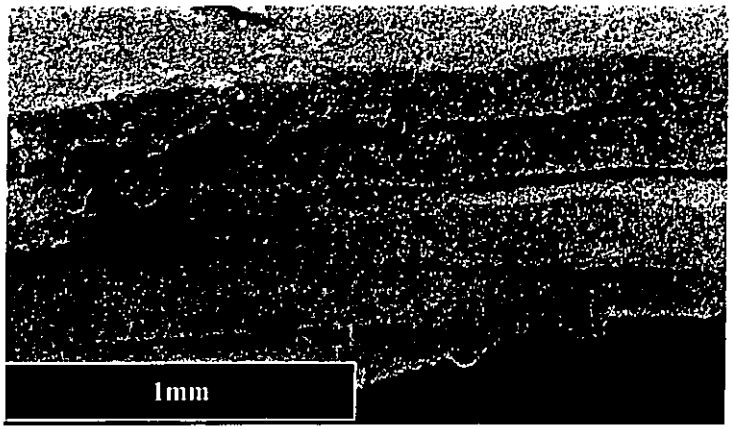

(a) Hot-pressed at 500 kg/cm^2 and 80°C; There are gaps between the layers.

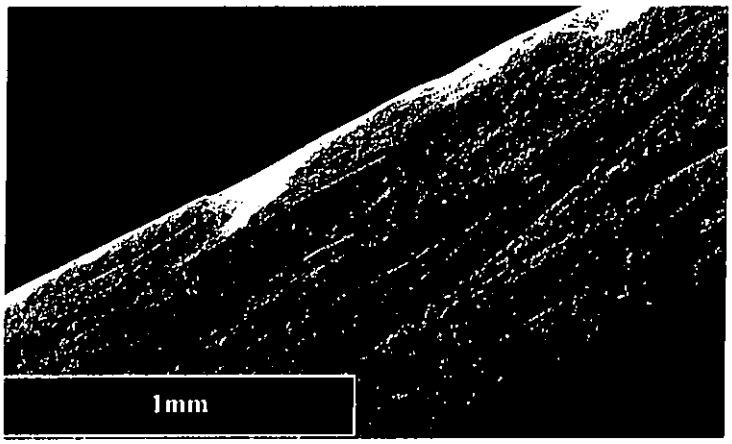

(b) Hot-pressed at 1000 kg/cm^2 and 170°C; The layer structure disappears.

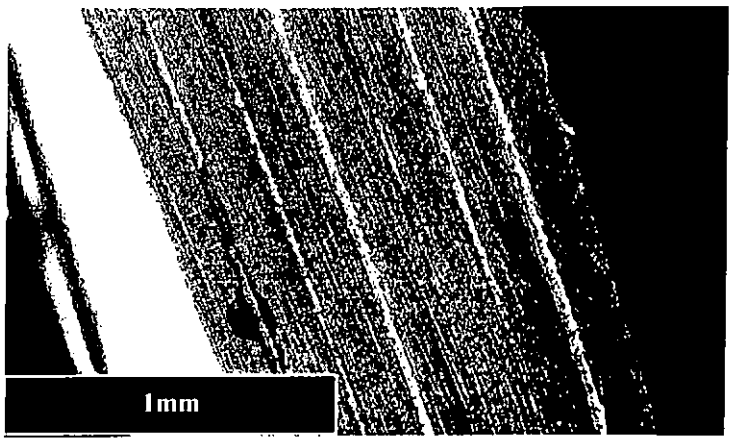

(c) Hot-pressed at 700 kg/cm^2 and 150°C which is the optimum condition for fabricating multilayer structure

Fig. 2.7. SEM images of the multilayer specimen formed under different hot-press conditions and after being sintered at 1280°C for 1.5 hours.

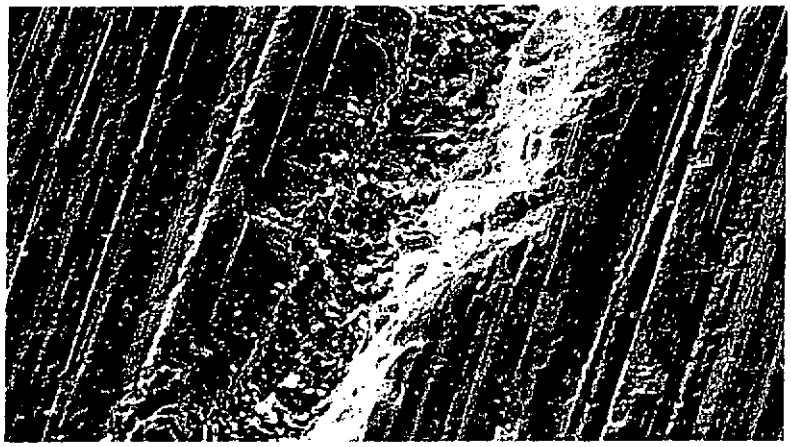

Fig. 2.8. SEM micrograph of the interfacial structure between PZT sheets and the Pt interleaving electrode in the MPT.

2.5 Sintering Process

2.5.1 Introduction

During sintering, there are several parameters which need to be optimized:

1). The heating and cooling rates which have very important effects on the shrinkage of the multilayer device.

2). The sintering temperature and the dwelling time which are used to control the interfacial reactions between the ceramic sheets and the metallic interleaving electrodes, and also to limit the loss of lead due to evaporation.

3). The relative time spent at different stages of the sintering, which mainly includes the binder burnout, a sintering step with slow heating rate to 1280°C which lasted at this temperature for more than 1.5 hours, then followed by a cooling step. (see Chapter 3&4)

4). During the whole heating process, the sample should be kept in a lead rich environment.

5). Since the multilayer device is very easy to curve when sintered, so a pressure should be applied to balance the curving force.

2.5.2 The Relationship of Shrinkage Matching and Heating Rate

Fig. 2.9 shows the SEM micrographs of the top view of the ceramic and internal electrode after the sintering process with (a) being the PZT ceramic grain and (b) the ceramic grains with Pt internal electrode. Compare these two figures, Fig. 2.9 (b) shows some light circling streak lines on the surface of each of the ceramic grain.

(a) The PZT ceramic grain

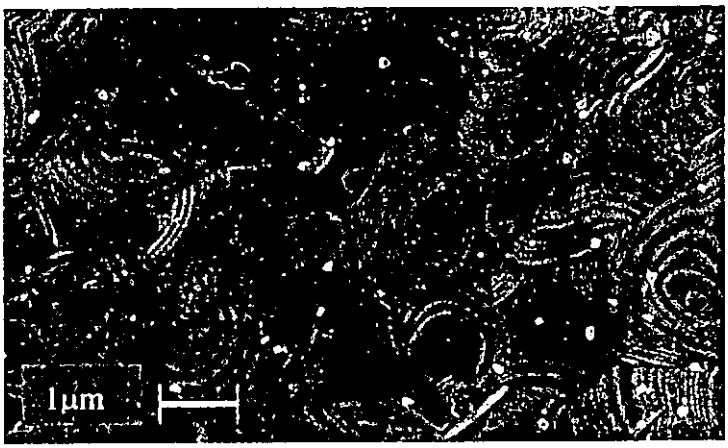

(b) The ceramic grain with Pt internal electrode painted on its surface

Fig. 2.9. SEM micrographs of the top view of the ceramic and internal electrode after the sintering process.

The specimen is sintered at 1280°C, which is a considerably high sintering temperature for the PZT ceramic. During the heating process, solid bonds are formed between particles of both the ceramic and metallic internal electrode. [1-4, 21-27] The objective is to achieve sintering in both materials simultaneously without distortion or the formation of defects. [22] Co-firing requires that the two materials follow the same shrinkage pathway, even though they may exhibit differences in basic properties. By adjusting the heating speed to a slower rate (about 1.5°C/min), and extending the sintering duration to 1.5 hours ~ 2 hours, the metallic internal electrode is partially melted and has a viscous flow at the highest temperature. (The heating rate can influence the co-firing results during annealing and sintering.) This enables the metallic internal electrode to spread uniformly on the surface of the ceramic sheets and ease the shrinkage match problem between these two different materials. After the high temperature sintering step, the PZT green sheets became ceramics, the Pt alloy is used as internal electrode crystallized along the ceramics grain boundary, and freeze into a stable form as the temperature dropped. Sometimes if the metallic internal electrode is thick enough and the sintering condition is suitable, this crystallization behavior can form some light circling streak lines on the surface of the Pt alloy [23-29]. That is what happens in our fabrication process, as shown in Fig.2.9 (b). By decreasing the heating rate and extending the sintering duration and under a certain sintering temperature, enough time is allowed for the interfacial reaction between the metallic electrode and ceramic sheet to occur. A multilayer block with good mechanical and piezoelectric properties will be obtained.

2.5.3 Diffusion of Interleaving Electrode

During the high temperature sintering process, the Pt alloy partially melted and diffused into the small cracks or pin-holes in the ceramic surface, which adversely affect the piezoelectric property of the ceramic multilayer.

Since the diffusion of electrode is determined mainly by the temperature and the duration of heating, so decreasing the sintering temperature and reducing the heating duration are good ways to minimize the problem. In our experiment, 1280°C was used as the sintering temperature and the heating duration was 1.5 hours.

2.6 Poling of the Multilayer Transformer

2.6.1 Painting of the External Electrode

Good external electrodes should be uniform and flat, since this has a significant effect on the vibration modes. The pattern of the external electrode is also quite important, and proper design can help to reduce the difficulties in the wire connection and the disturbing effect caused by the soldering. Fired-on silver is usually used as external electrodes.

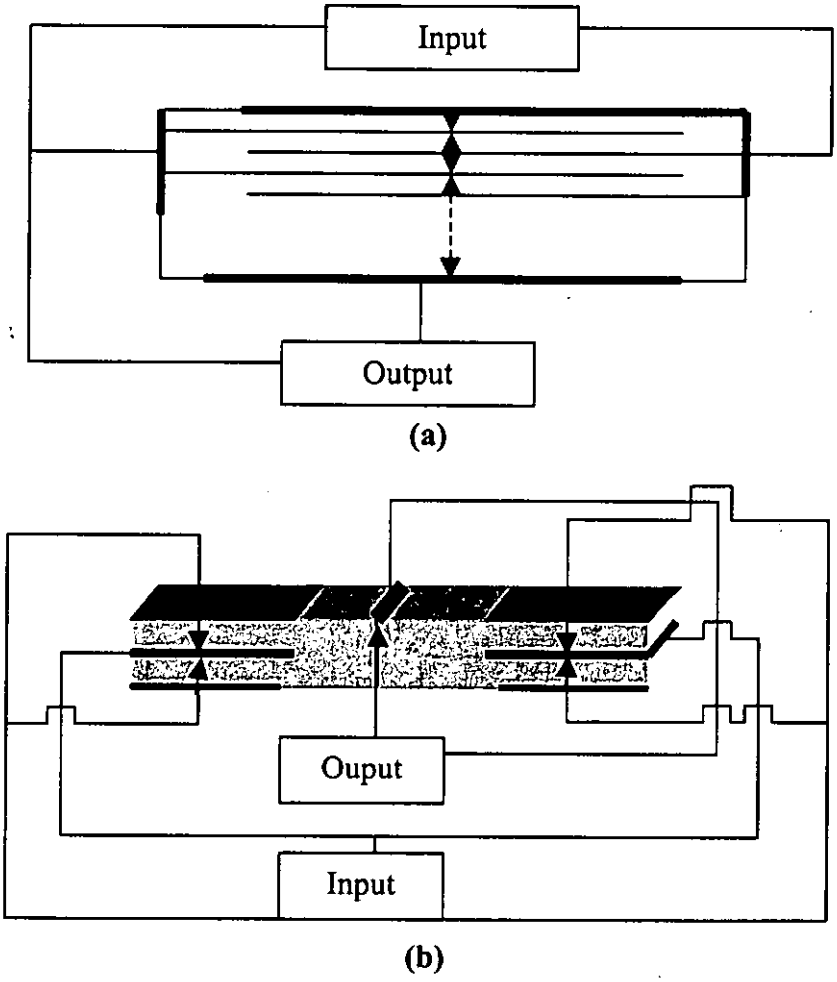

Fig. 2.10. External electrode patterns of (a) a thickness mode multilayer transformer; (b) a length mode (k_{31}) multilayer piezoelectric transformer

After the external electrodes were painted with the desired shape, they were dried in an oven at a temperature of 150°C, then the sample was annealed at 650°C for 2 hours to fire the silver electrodes onto the ceramic surface. After soldering the wire onto the device, the solder joints were covered with air-dried silver paint to improve the electrical contact.

2.6.2 Effect of Poling Conditions on the Properties of the Final Device

Poling condition is another important factor that affects the mechanical and electrical properties of the transformer. In our work, the poling temperature was 120°C to 130°C, and the poling voltage was 6~6.5 kV/mm. The exact experimental condition depended on the properties of PZT and the electrode pattern used in the transformer. A step-wise method was used to increase the applied poling voltage. The increase in voltage was taken in steps as shown in Fig. 2.12. In between each step, we short circuited the poling voltage once in order to relax the internal stress caused by the ferroelectric grain orientation. Each step lasted for 20 minutes. This process helped to increase the poling voltage and to improve the properties of the transformer[23-25].

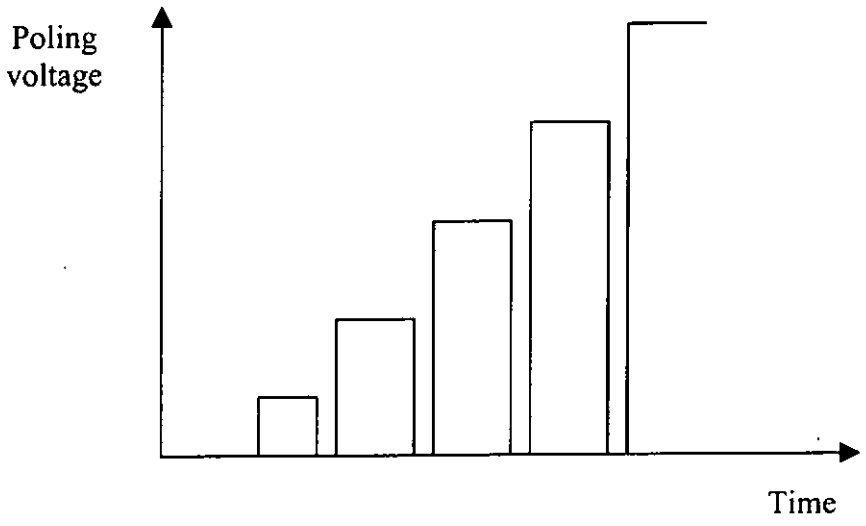

Fig. 2.11. Schematic of the step-wise poling process

After poling, the mechanical factor (Q_m) and piezoelectric constant d_{33} of samples with different sintering and laminating conditions were compared.

The relationship between mechanical quality factor (Q_m) and the heating rate and the sintering duration is also shown in Figs. 2.13 (a) & (b). The sintering temperature was kept at 1280°C. It is seen that if the heating rate is low and the high temperature sintering duration is longer, Q_m increases. When the sintering duration at the highest temperature is more than 1.5 hours, the ceramic growth process has almost finished and Q_m does not increase further. If the sintering duration extends for too long, due to the evaporation of the lead ions inside the PZT ceramic, the Q_m factor decreases. Hence, the changing of the Q_m is mostly affected by the interfacial reaction during the co-firing process.

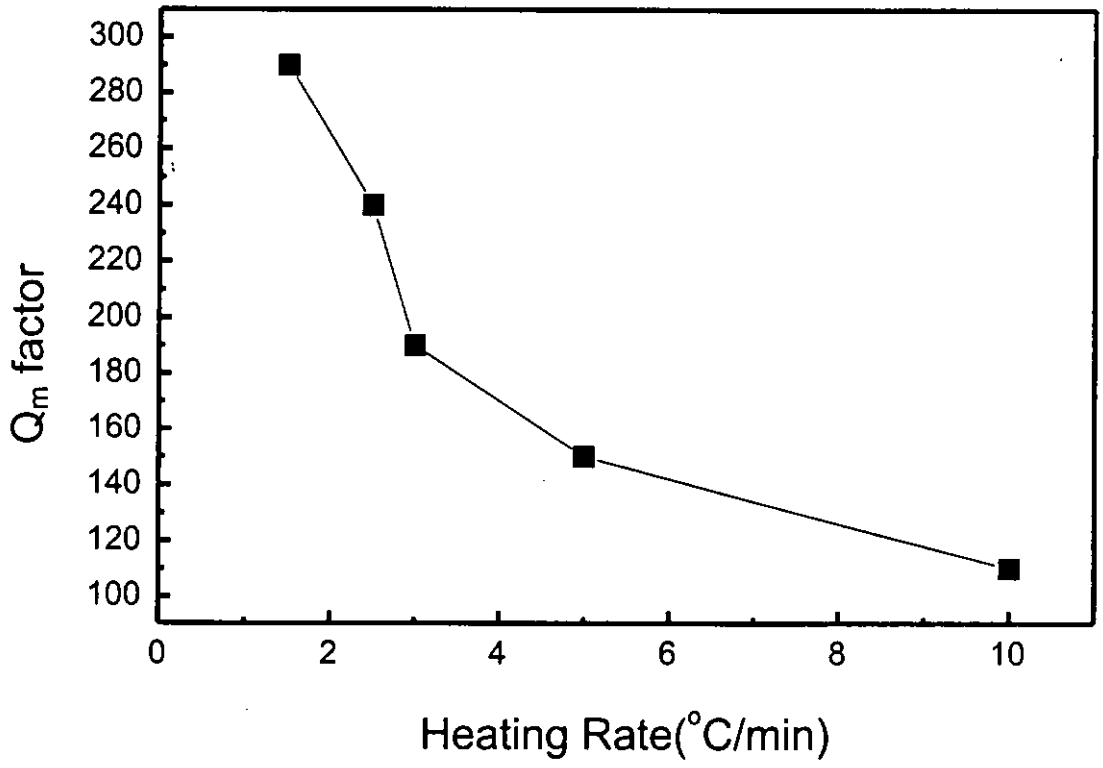

(a)

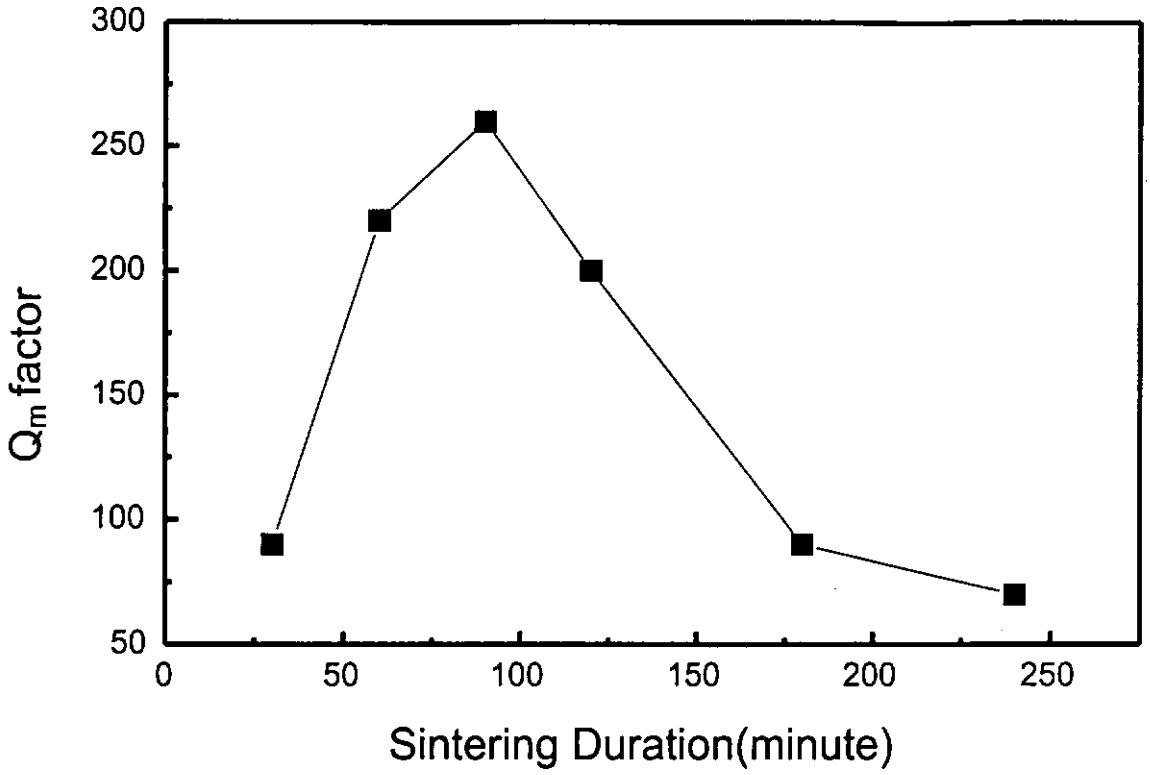

(b)

Fig. 2.12. The relationship between (a) mechanical quality factor (Q_m) and the heating rate while the duration is 1 h; (b) the Q_m and the sintering duration while the heating rate is 1°C/min

Chapter Three

Fabrication and Measurement of Thickness Mode PZT/Pt Multilayer Piezoelectric Transformer

3.1 Introduction

With the onset of miniaturization, many applications in the electronics industry now require small components with a high efficiency of operation. Electromagnetic transformers, having thousands of wire turns around a ferrite core, have become an obstacle to the progress of miniaturization, as they are among the most bulky devices on a circuit board. Piezoelectric transformers have recently received considerable attention as a possible alternative.

In this chapter, a thickness mode multilayer transformer has been introduced. Both its structure and fabricate process have been discussed. Some of its physical properties have been measured, especially voltage gain and power transmission characteristics.

A piezoelectric transformer essentially consists of two mechanically coupled and electrically insulated piezoelectric resonators. When an electrical signal near the frequency of mechanical resonance is applied to the input section of the transformer, strong mechanical vibration occurs due to the converse piezoelectric effect. This vibration is transferred to the output section, inducing a voltage on its electrodes due to the direct piezoelectric effect, with a consequent voltage gain [1-9, 21-23].

It is now possible to manufacture piezoelectric films of sufficient thickness and quality to make thin film piezoelectric transformers through the use of a roll-casting method. A thickness mode transformer with vibrating motion in the thickness direction has been fabricated with an operating frequency of ~1 MHz and an output voltage gain of 6.

Current work has been focused in optimizing the material parameters of the film and the procedure of fabricating the piezoelectric multilayer device, as well as developing a method of measuring the piezoelectric parameters.

3.2 Design of the Thickness Mode Transformer and its Working Principle

In the present piezoelectric transformer, the thickness extensional mode is used and the voltage ratio depends on the ratio of the thickness of the input plate compare to the thickness of the output plate, and also relies on the piezoelectric properties of the piezoelectric ceramic. The transformer generally comprises two blocks of piezoelectric ceramic plates of equal cross section rigidly bonded together. Using multilayer piezoelectric stacks as the primary increases the power handling capability of the transformer. The schematic structure is shown in Fig. 3.1.

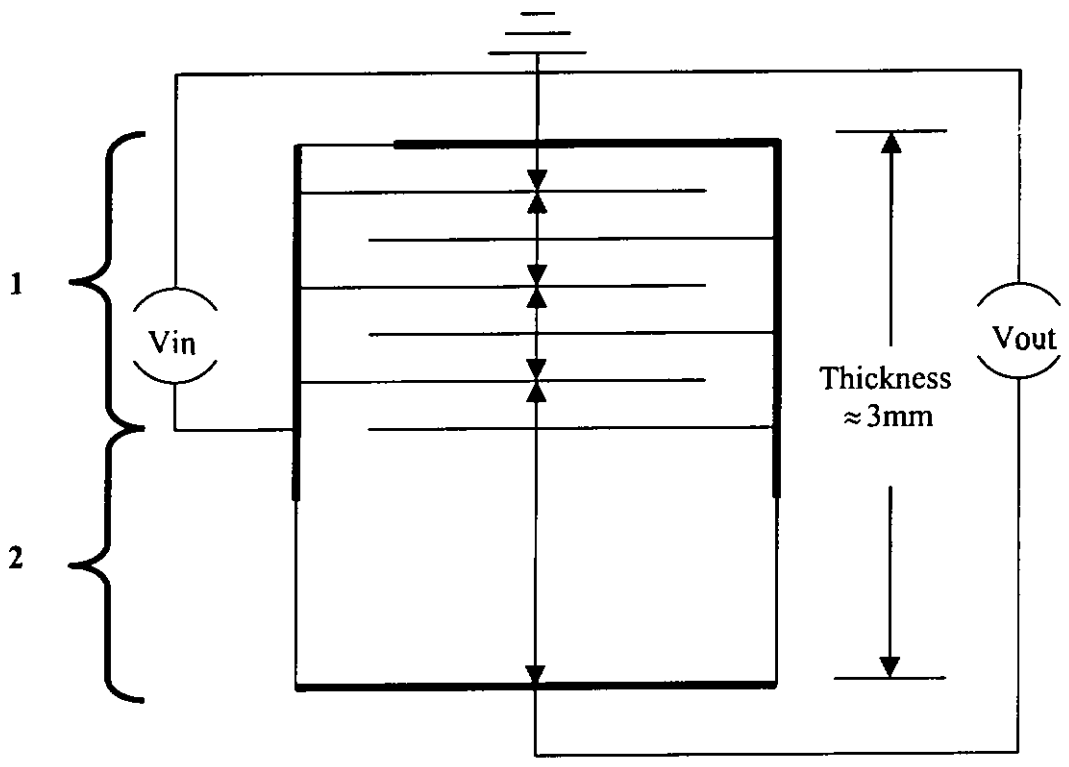

Fig. 3.1. Thickness mode multilayer transformer (The arrow in each layer indicates the direction of polarization.)

The multilayer driver section 1 was polarized in a thickness direction. The Pt inner electrodes were partially overlapped and each layer was poled with a polarization as shown in Fig. 3.1. An output section 2 was also poled in the thickness direction. Each of the ceramic sheets in drive section 1 is about 250 μm thick, and the output section 2 is about 1.5 mm thick. A piezoelectric transformer of this structure can improve the input current and power transmission characteristics. A photo of the prototype thickness mode MPT with the size of: 12 mm(Length) x 10 mm(Width) x 3 mm(Thickness) is shown in Fig.3.2.

Fig. 3.2. Photograph of the prototype thickness mode MPT

3.3 Fabrication Procedure

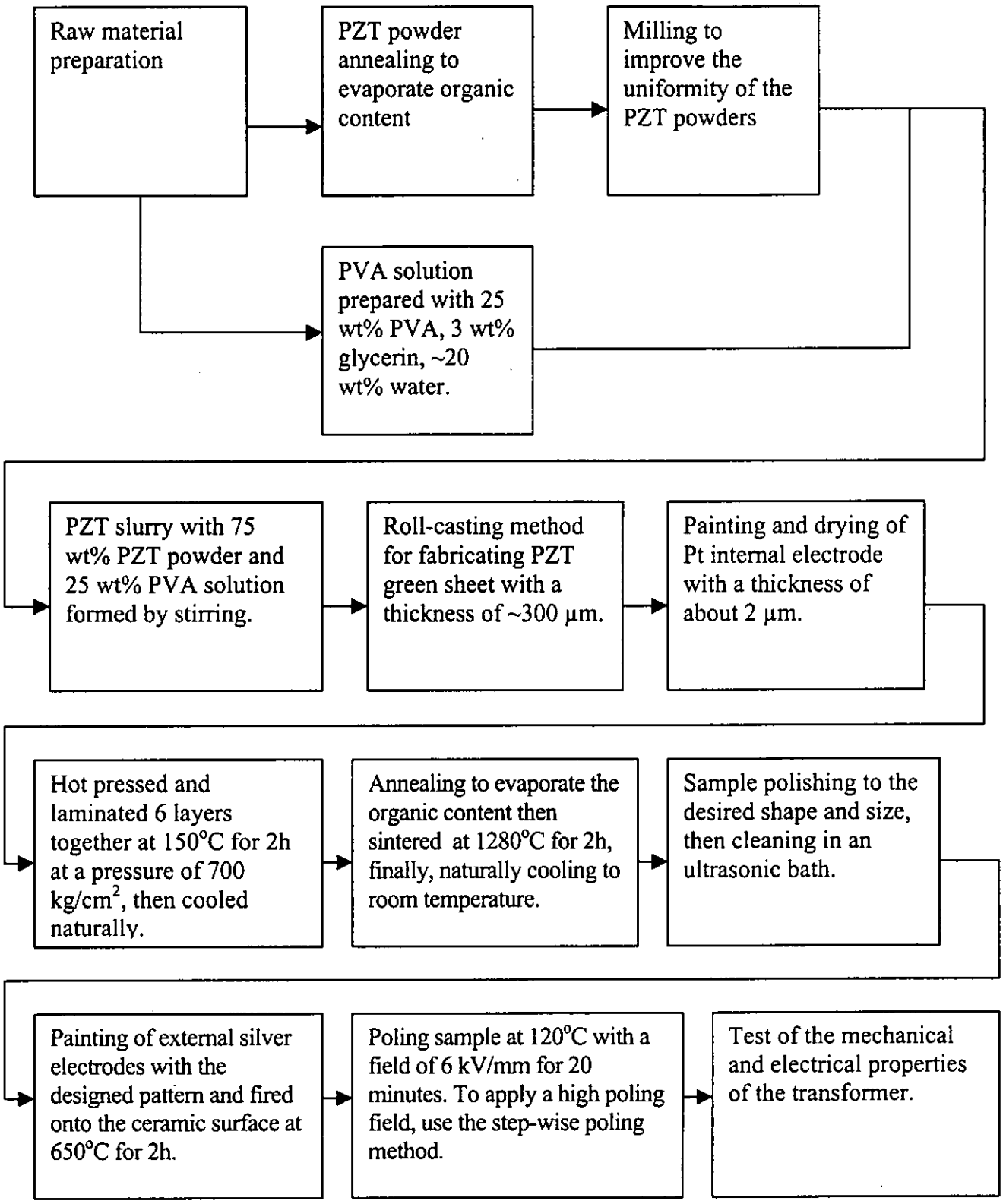

Fig. 3.3. Flowchart of the MPT fabrication procedure.

3.3.1 Fabrication of the Interleaving Electrode

One of the most important processes in the transformer fabrication is to apply the internal electrode. Since the internal electrode, which is made of Pt metallic alloy, will be co-fired with PZT ceramic at a very high temperature of 1280°C and part of the electrode will diffuse into the ceramic and lose its conductivity. So the thickness of the dried internal electrode should be at least 2~3 μm thick. The interleaving electrode has to be uniform and flat because of the shrinkage mismatch problem. PZT ceramic and Pt alloy have different shrinkage ratios under high temperature sintering. Even with a low heating rate and by adding pressure onto the sample, it is still very easy to break at the ceramic/Pt electrode interface[12], hence the quality of the paint-on electrode is quite important to the final sintering result.

In order to improve the quality of the painted internal electrodes, a flat painting brush was used to paint the Pt slurry onto the PZT green sheet three times. After being dried, a soft cotton wool was used to polish the surface in order to obtain a smooth and flat surface finish. (See Chapter 2 for more detail.)

3.3.2 Sintering

In a conventional sintering process, PKI-801 (from Piezo-kinetic, USA) has a normal sintering temperature of 1340°C for the bulk ceramic. In a multilayer structure of PKI802/Pt electrodes, the sintering temperature can be 60°C lower than the bulk ceramic, which is 1280°C.

An important factor of the sintering process is the heating rate. Because of the different shrinkage ratio between PZT ceramic sheet and the Pt metallic internal electrode, stress will be generated at the interfaces. So if the heating rate is too high, stress will not have sufficient time to relax and breakage will occur through the interface.

In our experiment, the sintering procedure as shown in Fig. 3.4 was used. Pressure was applied to the MPT during sintering by placing some Al_2O_3 fire bricks on top of the MPT. This can help to prevent the MPT from curving up.

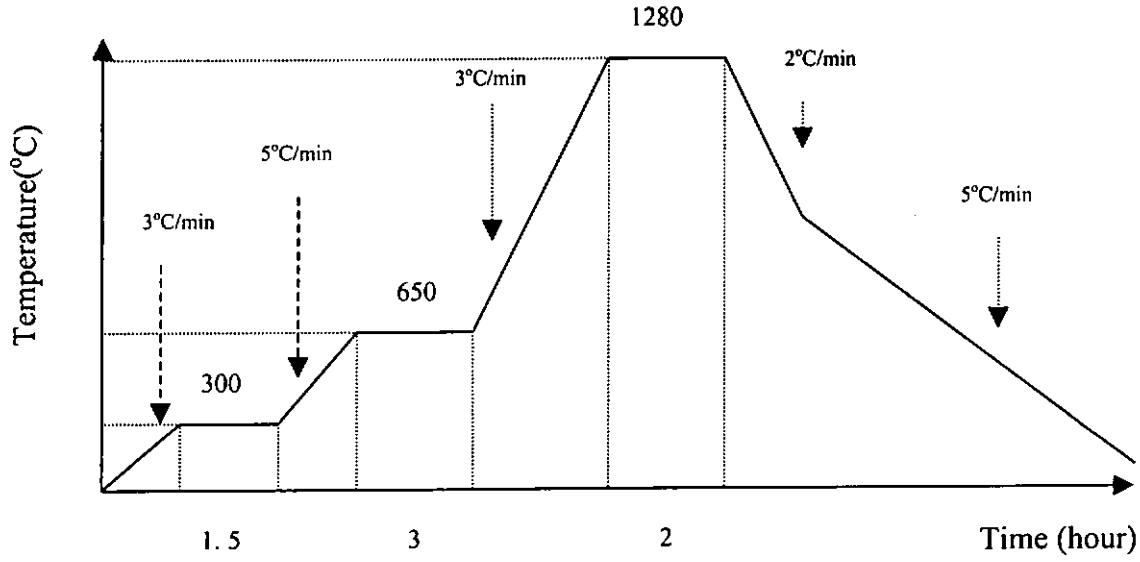

Fig. 3.4. Schematic procedure of the sintering process of PKI-801 MPT.

3.3.3 Fabrication of the External Electrodes

Before painting the electrode on the outer surface of the device, the sample was cleaned in an ultrasonic bath. After drying, silver slurry was applied onto the device by tracing the original designed pattern as shown in Fig. 3.1. This silver slurry needs to be dried at 150°C for 8 hours, followed by annealing at 650°C for 2 hour. This procedure was used to give good adhesive strength between the external electrodes and the ceramic layer.

The ultrasonic bath should be operated for no more than 10 minutes, because prolonged vibration will cause damage to the device. Also during the silver external electrode annealing process, the temperature should be kept below 700°C, as silver will diffuse into the ceramic. Also if the temperature is higher than 700°C, lead ions of the PZT ceramic will begin to evaporate which results in a lead depletion and decrease the piezoelectric properties of the transformer[23-29].

3.3.4 Poling of the Multilayer Transformer

Poling is the last process in fabricating a multilayer piezoelectric transformer. Taking into account the structure of the transformer, the poling process was carried out in two steps. First, the input multilayers were poled with a lower voltage. As each layer is ~250 μm thick, a poling field of 6 kV/mm was applied. The poling temperature was 120°C, and the field was kept for 20 minutes. The output part was poled with the same field, but due to its increased thickness, the actual poling voltage was higher. A step-wise poling method (Chapter 2, Fig. 2.12) was used to apply a considerable high poling voltage on the sample in order to confirm the poling result of the transformer.

3.4 Measurement and Analysis

3.4.1 Lumped Equivalent Circuit of MPT

The MPT fabricated in the present study has equal thickness ($l = l'$) in the input and output sections. Also it is assumed that the wave velocities in the driver section and generator section are equal. A complete lumped constant equivalent circuit of the thickness mode piezoelectric transformer as shown in Fig 3.5 can be used to model the MPT. [3-9]

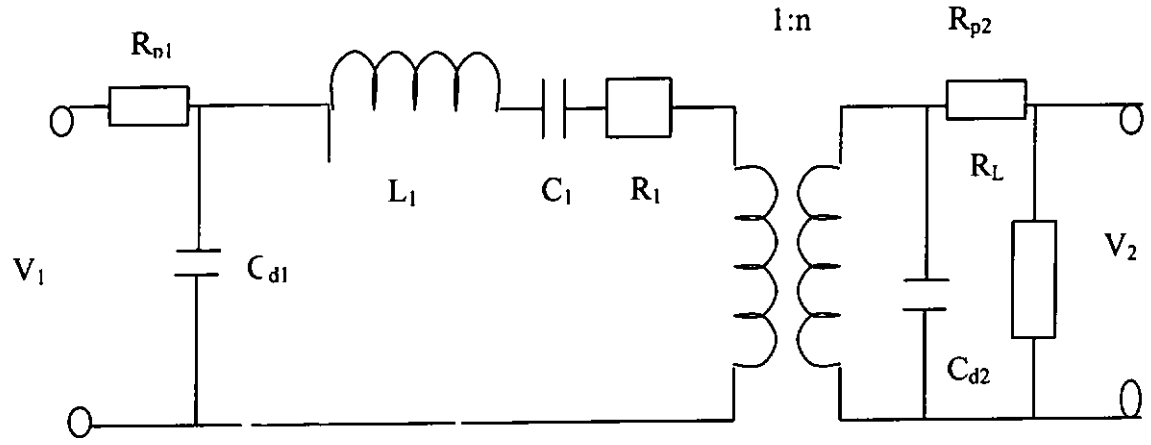

Fig. 3.5. Lumped equivalent circuit of the MPT.

In the above equivalent circuit, the dielectric losses are neglected because they are usually small. If the dielectric losses are required, they can be expressed as resistances and inserted into the electrical part of the equivalent circuit. R_L should be impedance in general, here it is expressed as a resistance to avoid complexity.

3.4.2 Physical Properties of the Thickness Mode MPT:

To calculate the resonant frequency, we first have to know the electromechanical properties of the thickness mode MPT using PKI 801 as raw material. The material's parameters of PKI 801 are shown in Table 1.1.

The driver section of our sample was laminated with 6 sheets, that means the layer number n=6. After fabrication, the measured parameters of the multilayer structure are shown in Table 3.1.

Table 3.1 Physical properties of the thickness mode MPT.

k_{31}	0.3	k_{33}	0.531
d_{31}	70 (pm/V)	d_{33}	110 (pm/V)
S^E_{33}	1.5*E*-11 (m^2/N)	Density	7350 (kg/m^3)
Q_m	190	Resonance Frequency	1.3 MHz
v^E_{33}	3300 m/s	Total thickness of the input and output sections	~3 mm
Length	12 mm	Width	10 mm

The results give an estimate of the acoustic velocity v of about 3300m/s, which is slightly slower than of the PZT ceramic (Table 1.1) due to the presence of the interleaving electrodes. The acoustic velocity is given by

$$v = f\lambda$$

where f is the resonance frequency and λ is the wavelength. When the specimen worked at the single wavelength vibration mode, λ should be 3 mm which is the same as the total thickness of the specimen, so the resonance frequency should be about 1.1 MHz. The calculated result agrees with the measurement which is about 1.26 MHz. The stress and displacement distribution of the thickness mode MPT is shown in Fig. 3. 6.

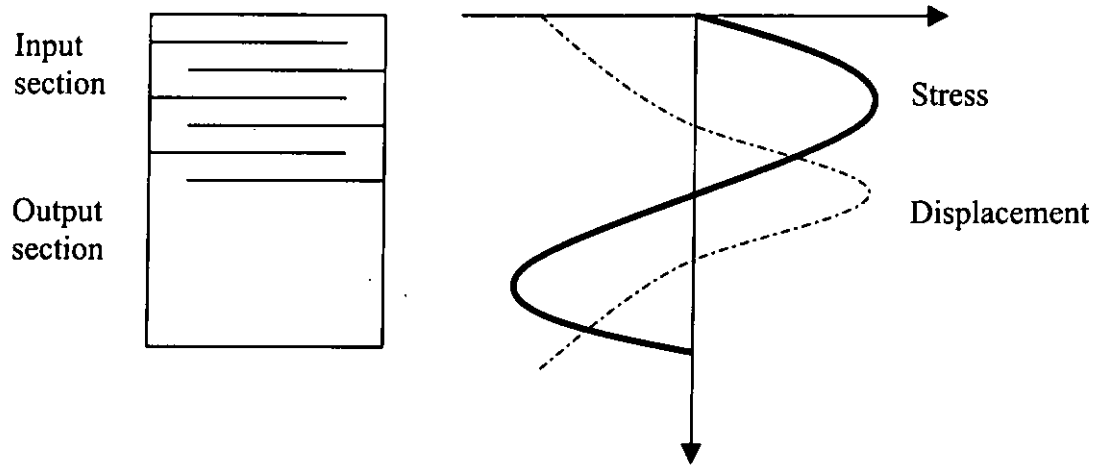

Fig. 3.6. Stress and displacement distributions in the thickness mode MPT.

MPT in the thickness vibration mode has a high resonance frequency, which is much higher than the longitudinal vibration mode, and its electromechanical coupling factor k_{33} is greater than k_{31}. Hence, MPT in the thickness vibration mode has larger output current and power than those in the longitudinal vibration mode. It is better to use ceramic with large piezoelectric anisotropy to suppress the spurious vibration.

By using the equivalent circuit shown in Fig. 3.5 for the thickness mode multilayer piezoelectric transformer, we can calculate the voltage ratio γ of the MPT by the equation of:

$$\gamma = K(\frac{Zout}{Zin})^{\frac{1}{2}} \approx K'(\frac{Cin}{Cout})^{\frac{1}{2}} \qquad (3.12)$$

where K and K' are constants, Z_{out} and Z_{in} are the electrical impedance of the generator section and the driver section, respectively, C_{out} and C_{in} are the capacitance of the generator section and each layer of the driver section, respectively. In the present MPT, γ is ~6.

In the MPT, the capacitance is

$$C = \frac{n \quad \varepsilon \quad \varepsilon_0 \quad S}{t} \tag{3.13}$$

where,

n = number of layers

$\varepsilon_0 \bullet \varepsilon$ = dielectric constant of the piezoelectric ceramic sheet

S = internal electrode area

t = thickness

Since the total thickness T is almost equal to nt, C may be written as

$$C = \frac{n^2 \quad \varepsilon \quad \varepsilon_0 \quad S}{T} \tag{3.14}$$

As the capacitance of the multilayer configuration is n^2 times larger than that of the single layer one, the impedance of the multilayer PT will be smaller than that of the single-layer PT.[9]

The output power of the MPT is related to the Q_m factor and the electro-mechanical coupling coefficient k_{33} of the device, and also it works as a function of the driving frequency of the transformer.

3.4.3 Measurements and Tests

In our measurement, we choose the impedance analysis method to model the MPT operation by the equivalent circuit shown in Fig. 3.5. In order to measure the input or output section of the MPT, we need to first short-circuit the output or the input portion, respectively, of the MPT, and find the equivalent circuit parameters near the resonance frequency of the proposed working mode. As we have calculated, the resonance frequency of our sample working at the thickness mode is about 1.3 MHz, we first find the resonance peak near this frequency and then calculate the parameters through the equivalent circuit option in the HP4194A impedance analyser.

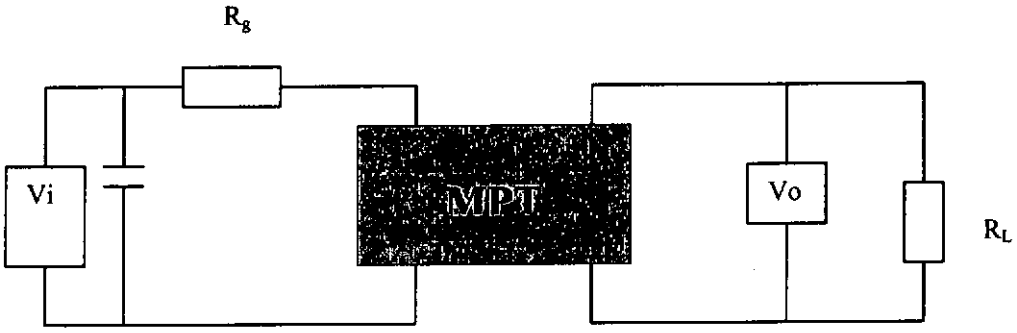

Fig. 3.7. Testing circuit of the impedance analyser

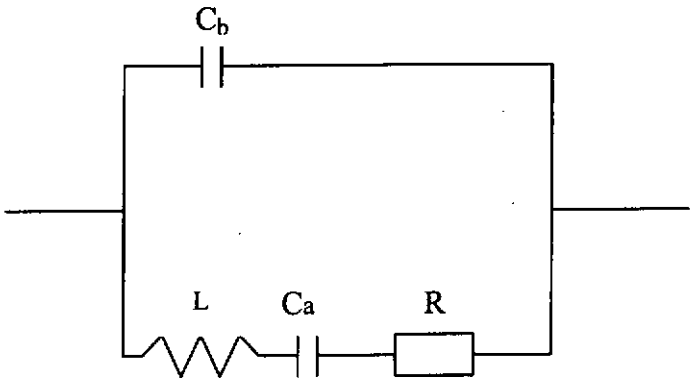

Fig. 3.8. Schematic diagram of the equivalent circuit of the input or output section.

To test the input section, we first short-circuit the output section and by stimulating the resonance near 1.26 MHz, the following parameters are found: (see Fig.3.5 & Fig.3.8)

Ca= 14.3 pF L= 7.78 mH R= 560 Ω

Cb= 266 pF

In this case: Q_m= 110,

where $Q_m = 2\pi f \frac{L}{R}$ (3.15)

Same process was applied to the output section and the test results are:

Ca= 13.9 pF L= 4.3 mH R= 272 Ω

C_b= 77 pF Q_m= 126

Then input the data to the equivalent circuit in Fig. 3.5. The theoretical performance of the thickness mode MPT is calculated by using the program shown in Appendix 2. The relation between the output voltage and frequency is shown in Fig. 3.9 and Fig 3.10 with a large load resistance of 5 MΩ(nearly open-circuit). In both cases, the input voltage is 1V. It can be seen that the MPT has the highest output voltage near the resonance frequency. As shown in Fig. 3.11, the output voltage decreases when the loading resistance becomes smaller as the MPT has a large input impedance which is more than 0.6 MΩ.

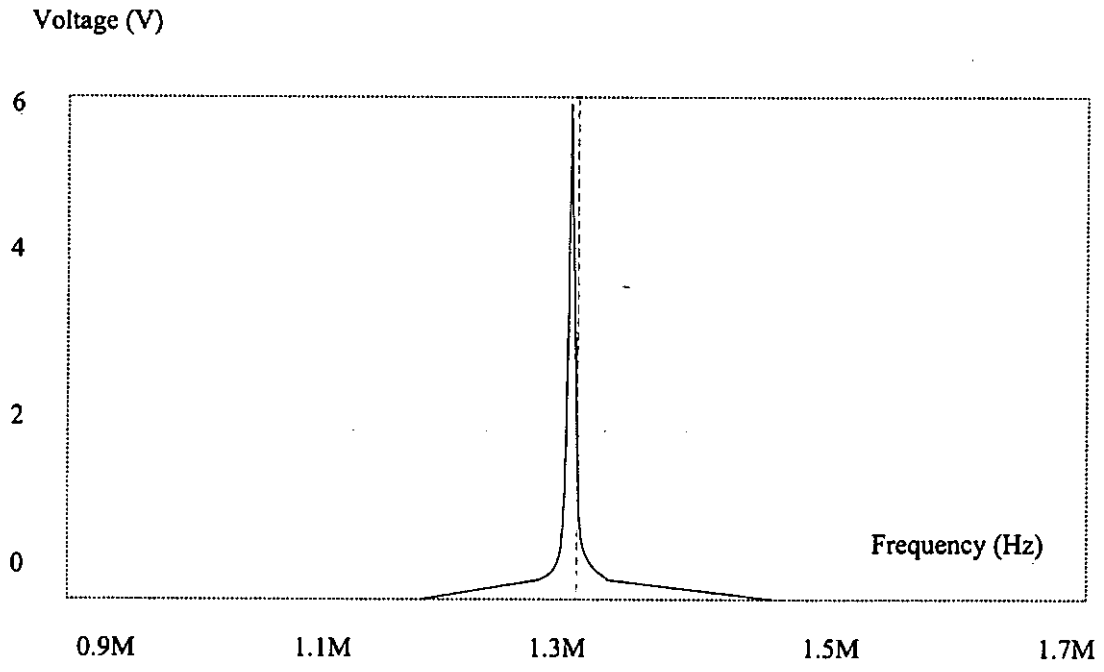

Fig. 3.9. Theoretical performance of MPT : Output voltage as a function of driving frequency at an input voltage of 1V. Frequency range from 0.9MHz to 1.7MHz

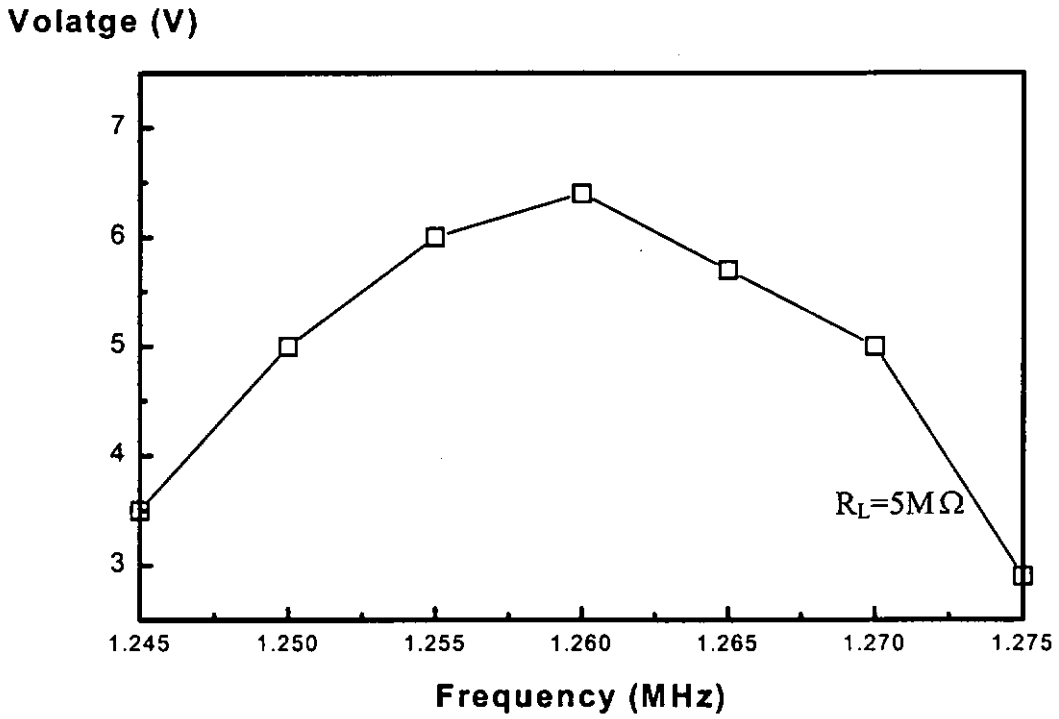

Fig. 3.10. Theoretical performance of MPT : Output voltage as a function of driving frequency at an input voltage of 1V. Frequency range from 1.245 MHz to 1.275 MHz, showing that the voltage gain is 6 at 1.26 MHz.

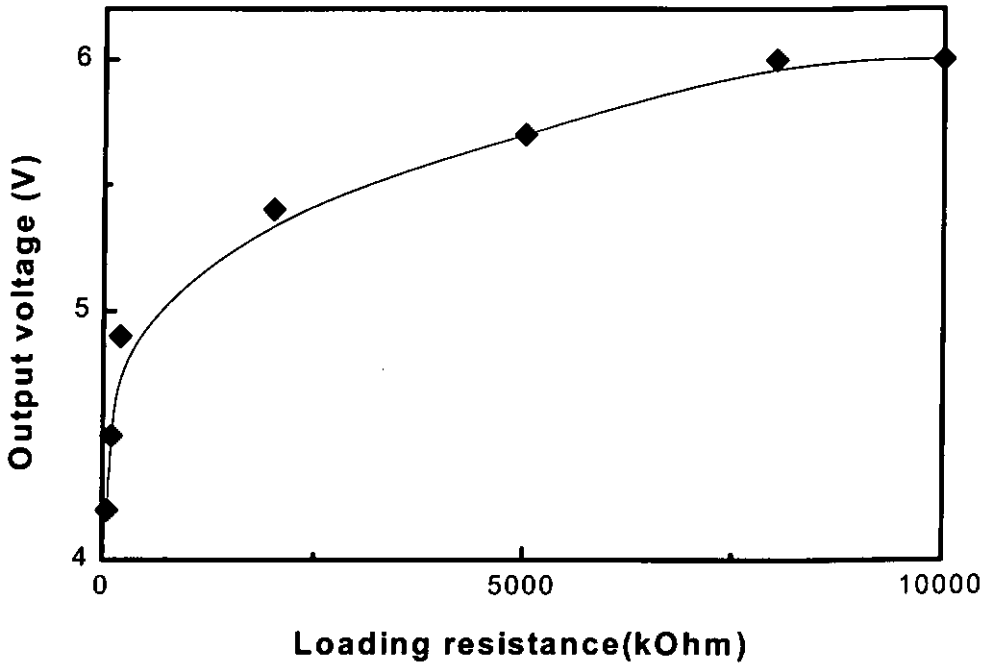

Fig. 3.11. Theoretical performance of MPT : Output voltage as a function of loading impedance at an input voltage of 1V.

Fig. 3.11 to Fig. 3.14 show the experimental results of the thickness mode MPT with a loading impedance R_L=5 MΩ. The voltage gains at 1.26 MHz are ~4.3 and ~4.5 when the input voltages are 50 V and 200 V, respectively. The curve line shows the same trend of the voltage exchange result, which has the highest voltage ratio at the resonance frequency of about 1.26 MHz. The difference of the practical voltage ratio, which are a little bit lower than the simulation result (Fig. 3.10) of 6, is mainly due to the thickness variation in the individual layer inside the MPT during the fabrication process which affects its operation and the voltage gain. Because the ratio of the input layer and output layer's thickness will decide the capacitance ratio of the input and output section, which effects to the device's final operation performance.

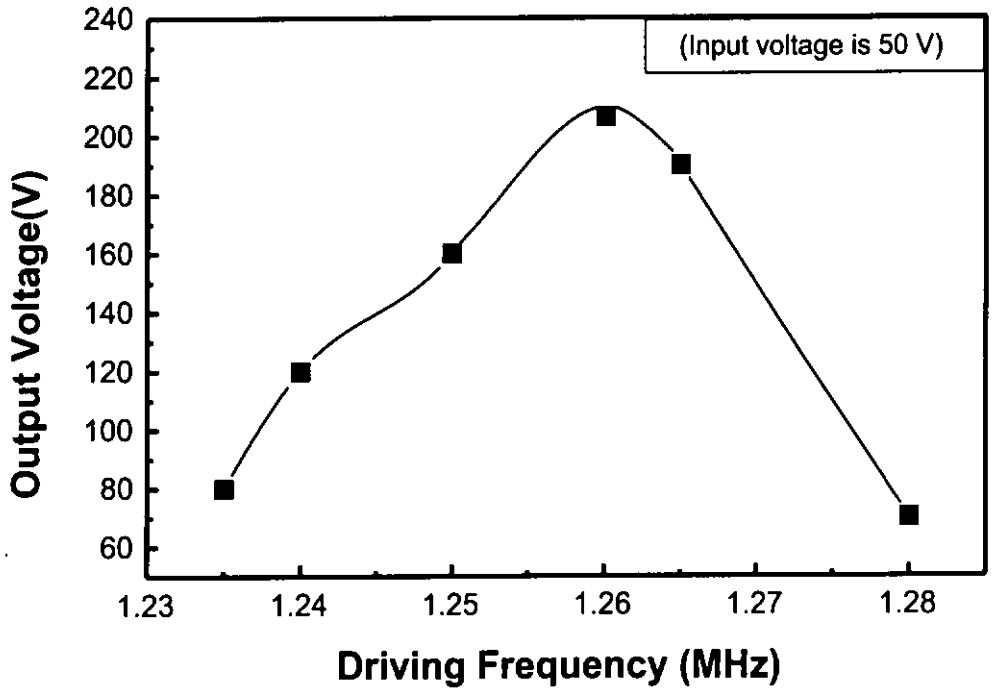

Fig. 3.12. Measured output voltage as a function of driving frequency at an input voltage of 50 V.

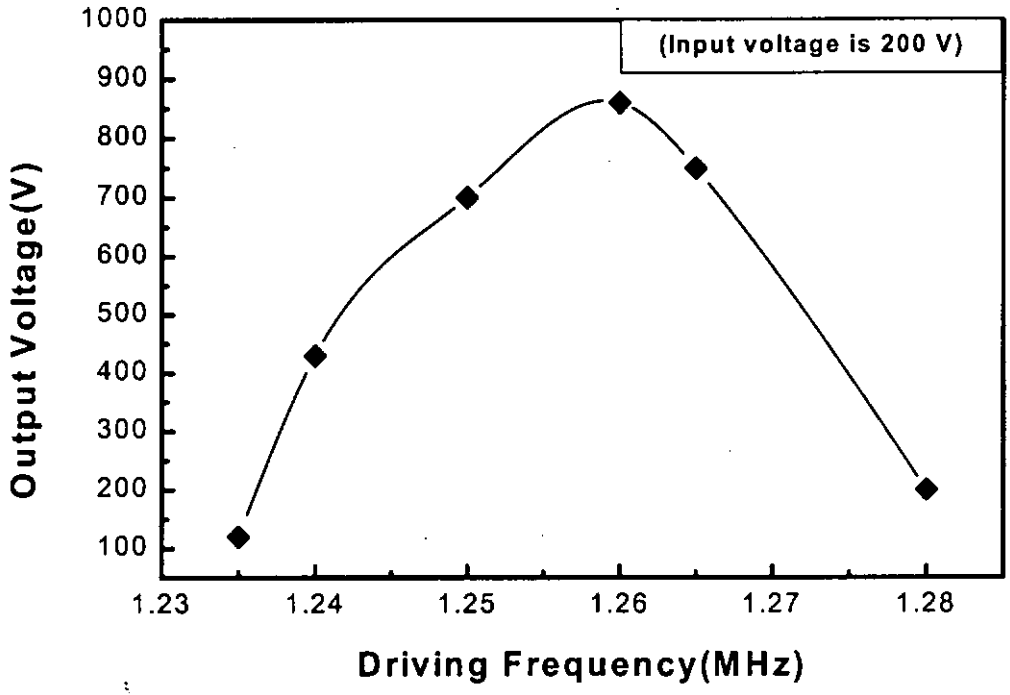

Fig. 3.13. Measured output voltage as a function of driving frequency at an input voltage of 200 V.

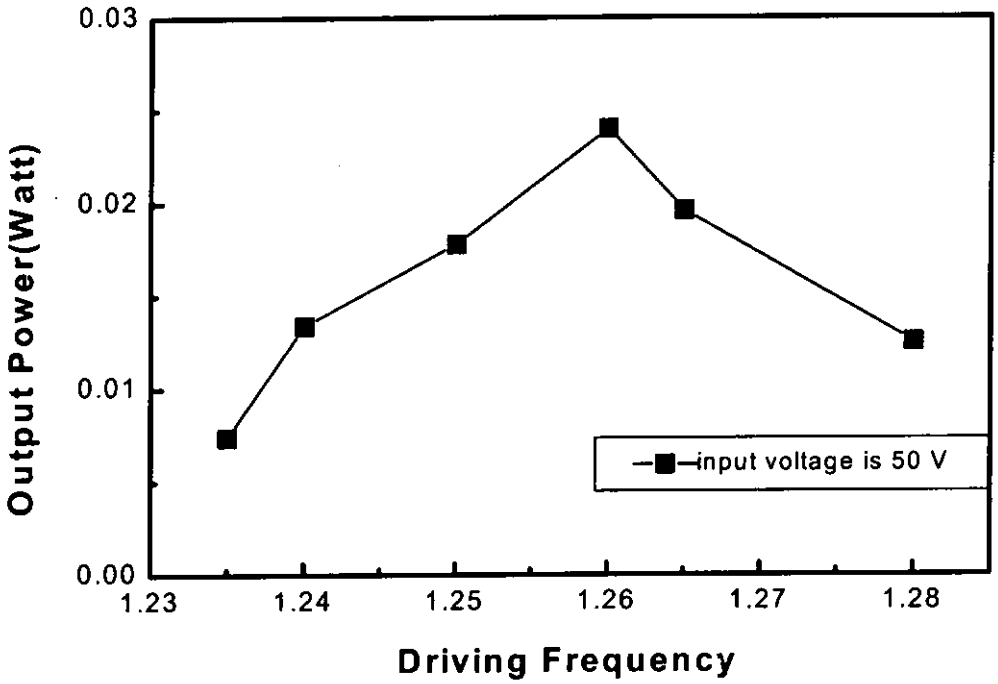

Fig. 3.14. Measured output power as a function of driving frequency at an input voltage of 50 V.

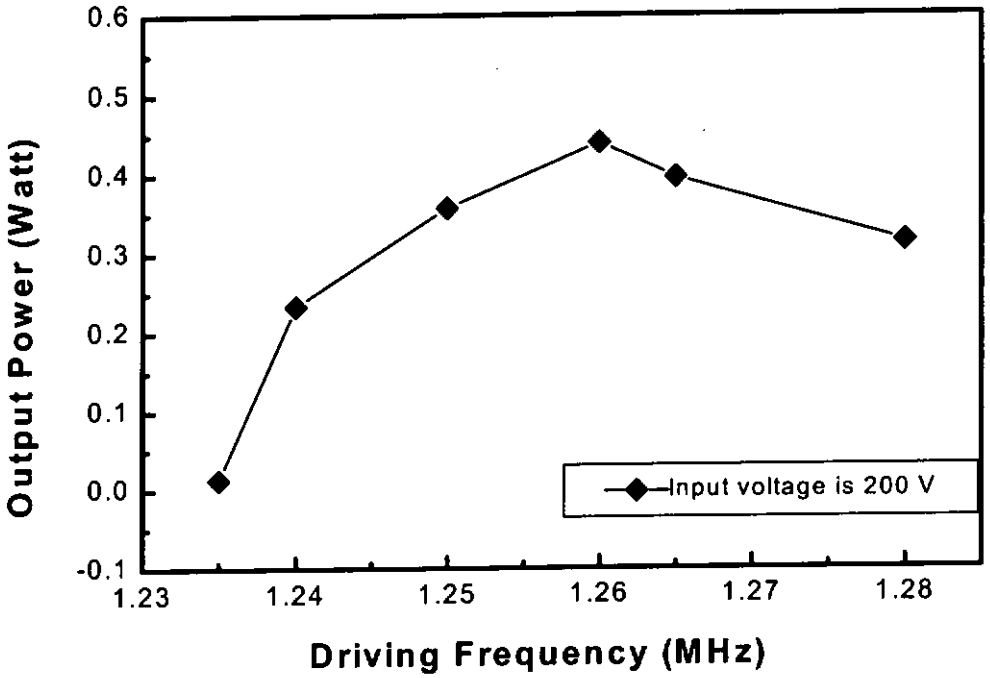

Fig. 3.15. Measured output power as a function of driving frequency at an input voltage of 200 V.

3.4.4 Energy Transmission Efficiency

Considering the characteristic of the piezoelectric transformer, the energy transmission efficiency also depends on the frequency, as shown in Fig. 3.16 and Fig. 3.17. From these two figures we can see the maximum efficiency is ~35% which is not very high. This result is mainly because the Q_m factor of the MPT is lowered by the introduction of the interleaving electrode, and the poling level of the MPT might not be high enough.

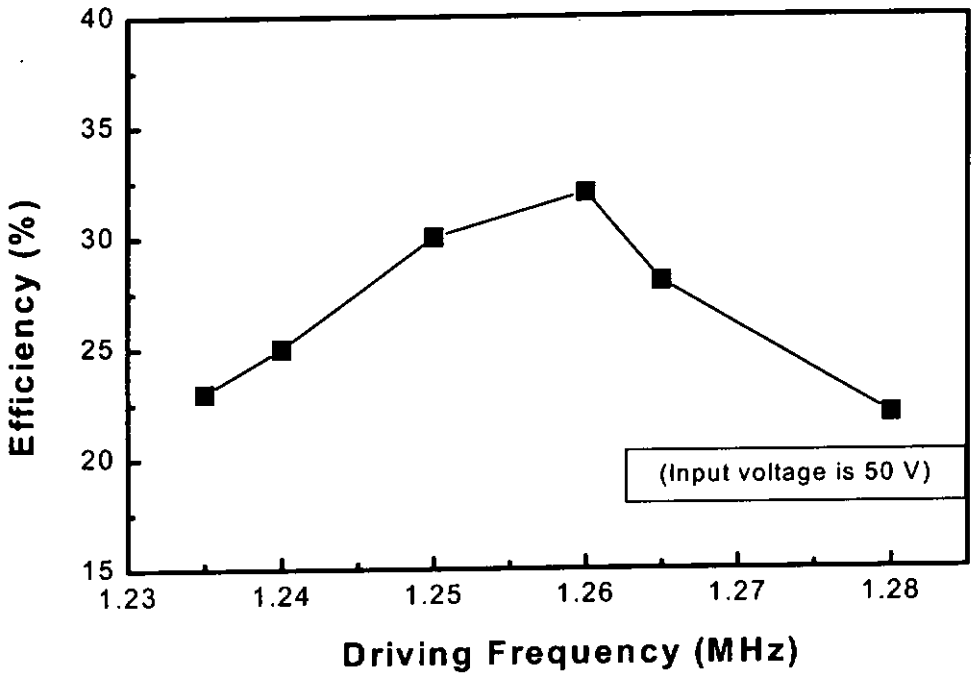

Fig. 3.16. Measured efficiency as a function of driving frequency at an input voltage of 50 V.

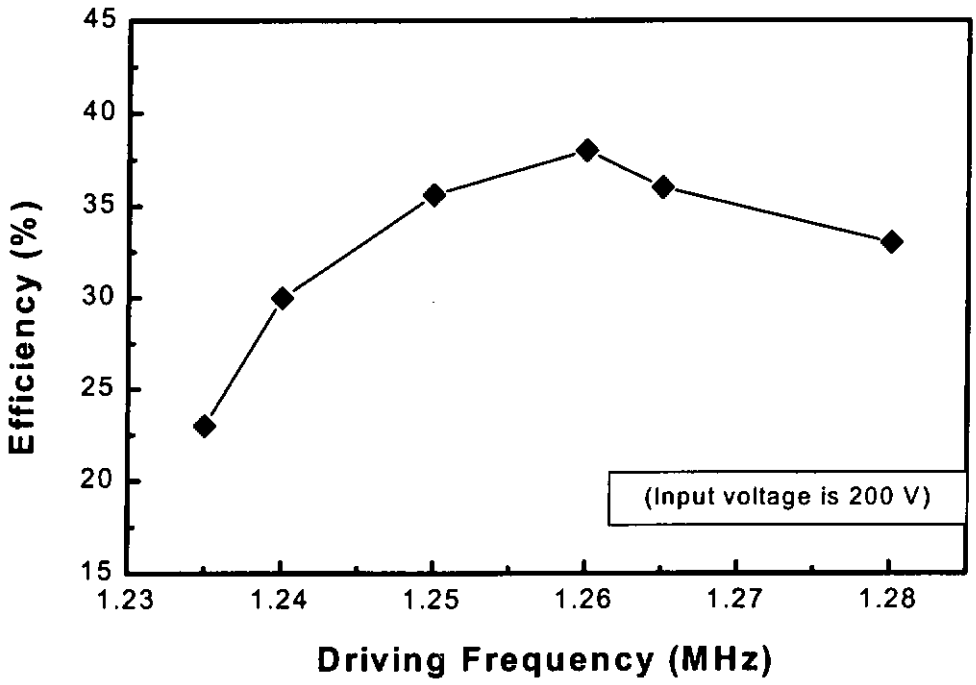

Fig. 3.17. Measured efficiency as a function of driving frequency at an input voltage of 200 V.

3.5. Conclusion

From the above analysis, whenever the driver section or the generator section adopts the multilayer structure, the whole multilayer piezoelectric transformer has a low input electrical impedance, which makes the driving circuit simpler. Hence, in a MPT the output power can be higher, or a smaller transformer can be used for equal power output [12-19].

The thickness mode MPT fabrication is not yet optimized. The efficiency of the multilayer transformer is less than that of the single-layer type PT. The reason may be due to the presence of the inner electrodes, the nonuniformity of the thickness in each layer, and the external electrode. Further optimization will be needed in future work. Moreover, with the increase in the number of the layers in the MPT, it is more difficult to fabricate the device and maintain a good electrical property. This is an important factor to be considered in the design of MPT.

Chapter Four

Length Mode Multilayer Piezoelectric Transformer

4.1 Introduction

Recently, multilayer transformer has got a rapid progress both in fabrication technology and in new structural designs. For example, after the thickness mode MPT was first invented in 1986, during the past fourteen years, many designs including those using the length mode, the bending mode and the k_{15} mode have been introduced, some of them have found practical applications. Characterization of the MPT, such as the voltage exchange ratio, power transmission efficiency, and high frequency working performance etc., have also been studied. In this work, a single layer transformer was turned into multilayer transformer design and a new fabrication process was introduced[22].

This new structural MPT uses the k_{31} effect to induce the length mode vibration and has several advantages. First, it can reach a high voltage-exchange ratio. Second, it can attain high power transmission. Third, it can be fabricated into a small size.

4.2 Device Structure and its Working Principle

The structure of the length mode (k_{31}) multilayer transformer is shown in Fig. 4.1. A special feature of this transformer is the electrode structure of the device. First, by using the multilayer structure at the input section, a lower input voltage can be used to induce the vibration. Then this vibration is transmitted through the length of the device. Since we choose to use the three half-wavelength ($3/2\lambda$) as its working mode, so the input and output section of the transformer should have the same length as shown in Fig. 4.1. In this case, the electrode pattern of the input and output sections should also have equal length.

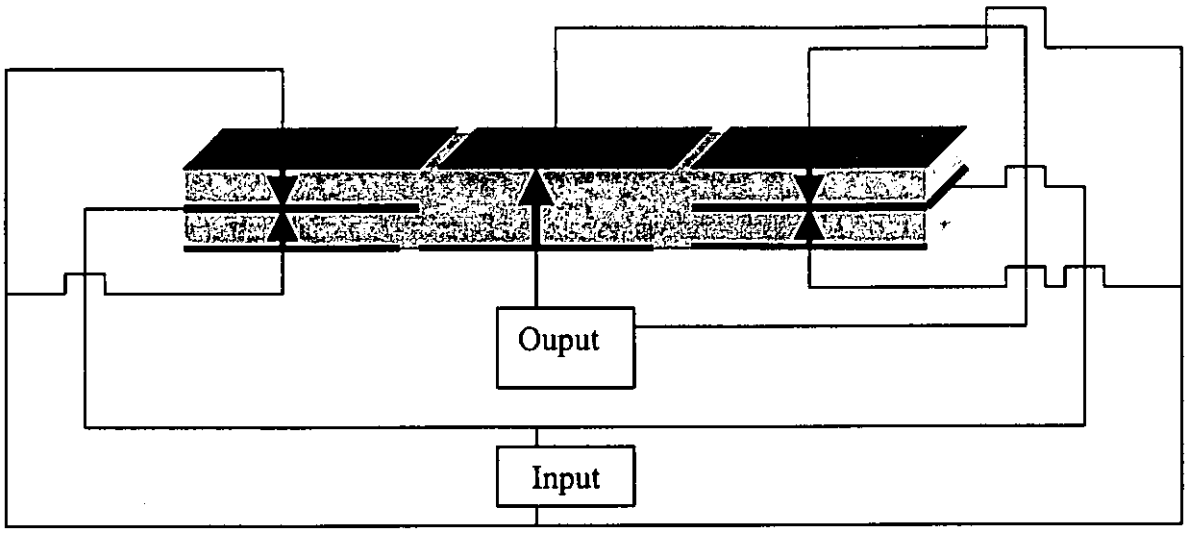

Fig.4.1. Length mode multilayer piezoelectric transformer.

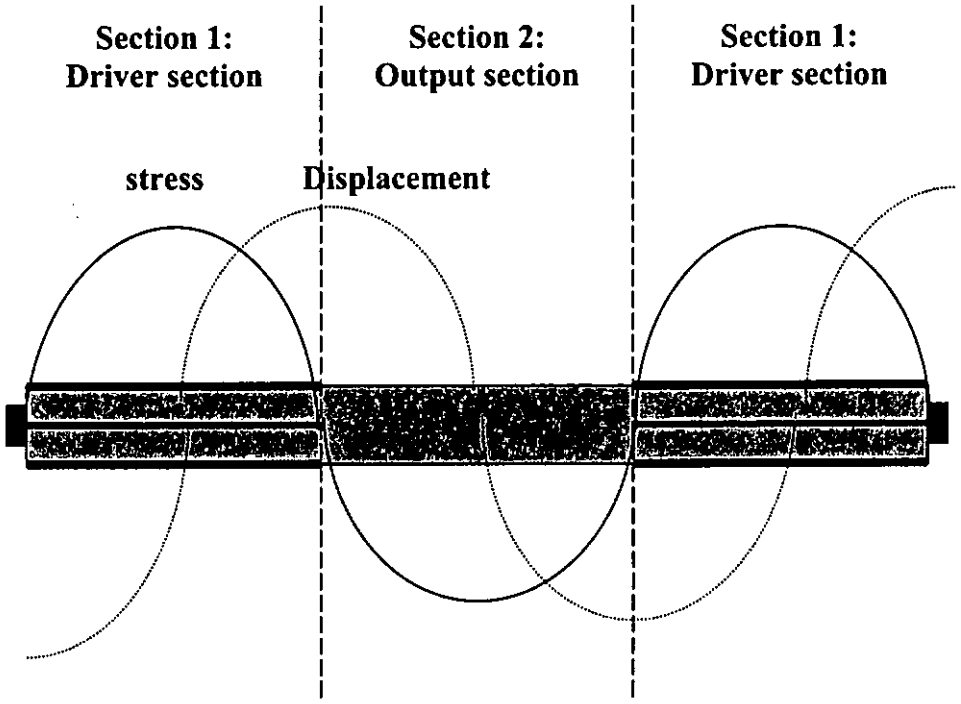

Fig. 4.2. Stress and displacement distributions in the length mode MPT.

The multilayer driver section 1 was polarized in a thickness direction. The Pt inner electrodes were partially overlapped and each layer was poled with polarization as shown in Fig. 4.1. An output section 2 was also poled in the thickness direction. The ceramic sheets of drive section 1 are about 600 μm thick, and the output section 2 is about 1.4 mm thick. A piezoelectric transformer of this structure can have improved voltage amplification characteristics. The driver section can induce a vibration through the longitudinal dimension of the ceramic, and a higher output voltage can be generated with the voltage amplification value of about 12 times the original input voltage value. This length mode (k_{31}) multilayer piezoelectric transformer works at three half-wavelength mode, that means its operating frequency is 3 times its fundamental resonance frequency. The displacement and stress distribution of this MPT is shown in Fig. 4.2. A photo of the length mode (k_{31}) MPT with the size of: 26 mm(Length) x 5 mm(Width) x 1.4 mm(Thickness) is shown in Fig.4.3.

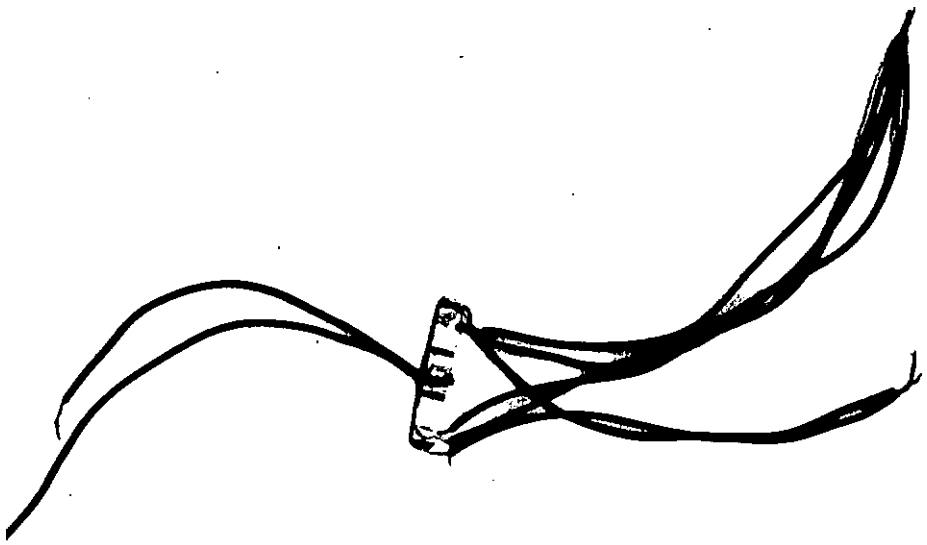

Fig .4.3. A photo of the length mode (k_{31}) MPT with the size of:

26 mm(Length) x 5 mm(Width) x 1.4 mm(Thickness)

4.3 Fabrication Procedure

Basically, most of the fabrication process of the length mode MPT is the same as that of the thickness mode MPT. The experimental conditions are shown in Table 4.1.

Table 4.1.The experimental conditions of the length mode (k_{31}) MPT

Thickness of the ceramic green sheet (By roll casting method)	700 μm
Hot-press condition	700 kg/cm^2, 150°C for 2 hours then natural cooling without removing the pressure till room temperature.
Sintering	1280°C for 1.5 hours
Poling	6~6.5 kV/mm, 120 °C for 20 min, then natural cooling to room temperature

4.4 Measurement and Analysis

4.4.1 Physical Properties of the Length Mode (k_{31}) MPT

Table 4.2 Physical properties of the length mode (k_{31}) MPT

k_{31}	0.3	k_{33}	0.55
d_{31}	50 (pm/V)	d_{33}	110 (pm/V)
S^E_{33}	1.5*E*-11 (m^2/N)	Density	7500 (kg/m^3)

Q_m	~130	Fundamental Frequency	~55 kHz
		Working Frequency	167 kHz
v^E_{33}	3300 m/s	Total thickness	~1.4 mm
Length	26 mm	Width	~5 mm

The mechanical quality factor Q_m reflects the internal loss of the material during the vibration. The mechanical quality factor is inversely proportional to the mechanical loss. The higher the Q_m, the less loss it has.

4.4.2 Lumped Equivalent Circuit of MPT

In order to stimulate the performance of the length mode (k_{31}) MPT, a simplified equivalent circuit based on the lumped equivalent circuit of Fig. 3.5 was used as shown in Fig.4. 4.[23]

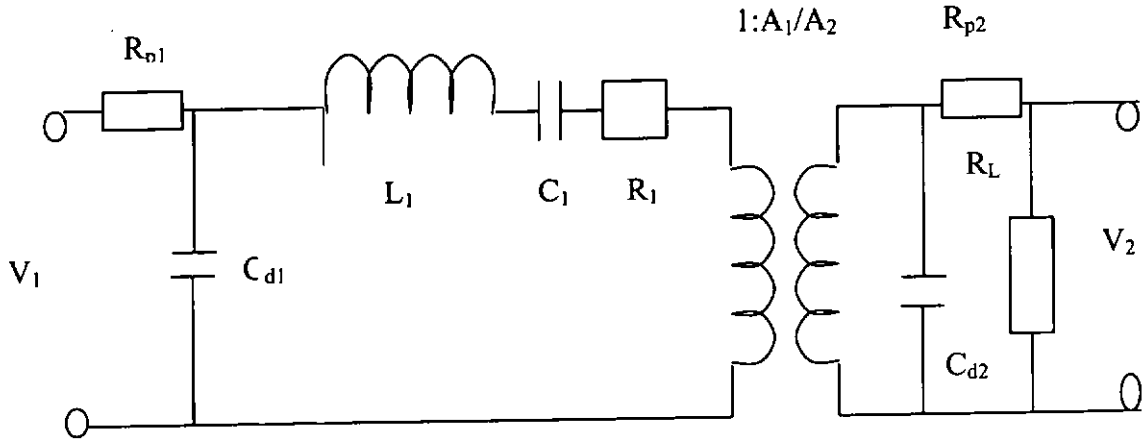

Fig. 4.4. A simplified equivalent circuit of the length mode (k_{31}) MPT

The equivalent circuit parameters of the MPT around the three half-wavelength resonant frequency are calculated and listed below:

C_{d1}= 102.6 pF	L_1= 213.8 mH	R_1= 642 Ω
C_1= 28.7 pF	C_{d2}=392.2 pF	Q_m= 130
R_{p1}= 5 Ω	R_{p2}= 5 Ω	A_1/A_2=2.7

Three half-wavelength resonance frequency = 167 kHz

$$\frac{V_2}{V_{1(\max)}} = \frac{A_1}{A_2}\frac{1}{2\pi f C_{d2} R_1} = 12$$

When R_L = 5 MΩ (nearly open-circuit). (4.1)

The theoretical performance properties of the MPT, as shown in Fig. 4.5, are calculated by using the program shown in Appendix 2 and using the measured parameters. The input voltage is 1V, and the loading impedance is 5 MΩ. It can be seen that the MPT has higher output voltages near the resonance frequency of 55 kHz,110 kHz and 167 kHz, which are the 1/2 λ, λ, 3/2 λ resonance frequencies.

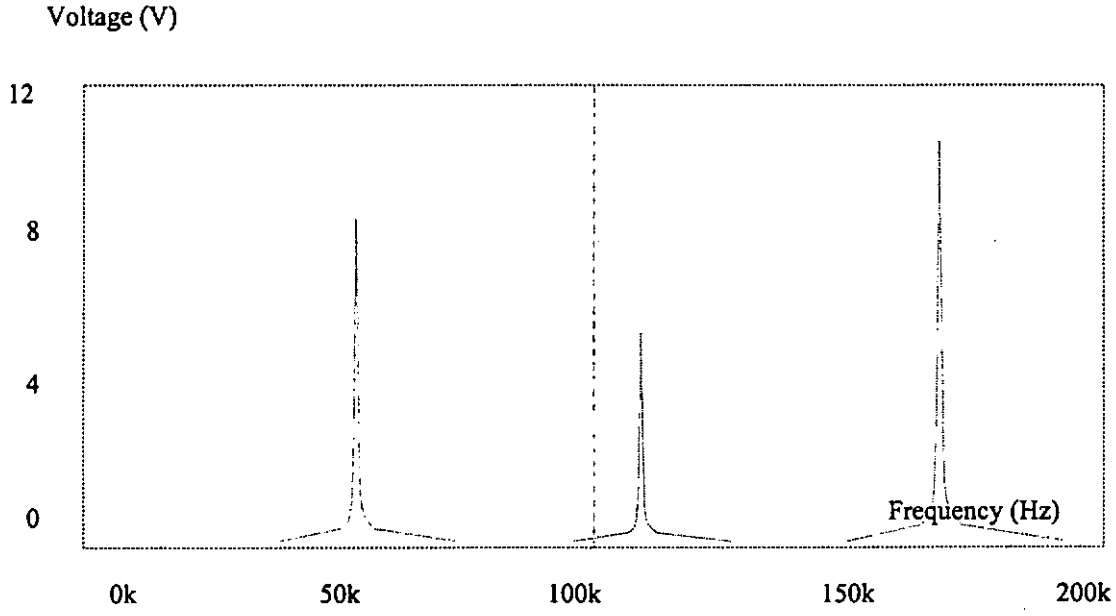

Fig. 4.5. Theoretical performance of the length mode (k_{31}) MPT : Output voltage as a function of driving frequency at an input voltage of 1V. Frequency range from 0 Hz to 200 kHz.

4.4.3 Measured Operating Performance of the Length Mode (k_{31}) MPT

Fig. 4.6 to Fig. 4.9 shows the voltage amplification results and power transmission characteristics of the length mode (k_{31}) MPT with different loading impedance and different input voltages. The input voltage is 1 V and 10 V, and the loading impedance (R_L) is 2 MΩ and 5MΩ, respectively.

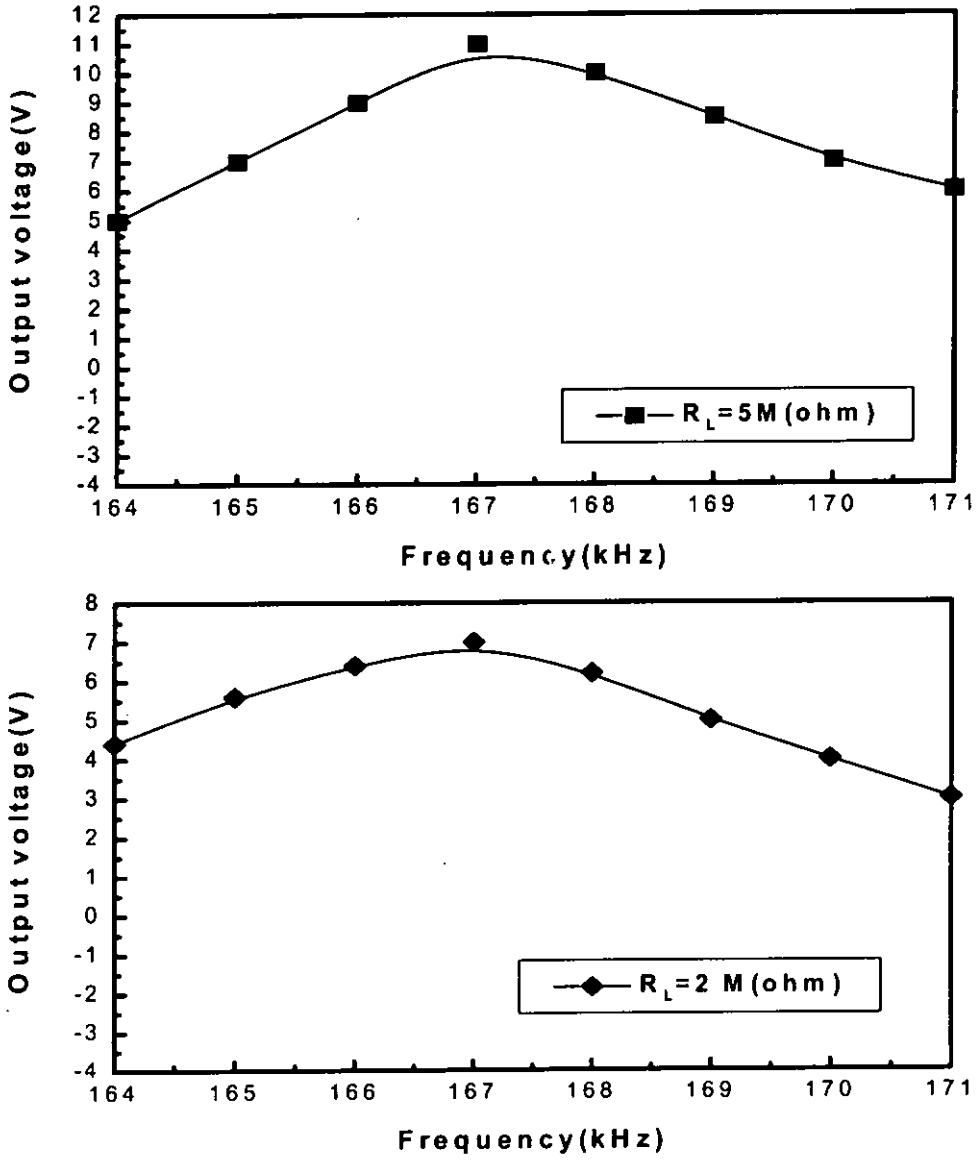

Fig. 4.6. Measured output voltage as a function of driving frequency at an input voltage of 1 V.

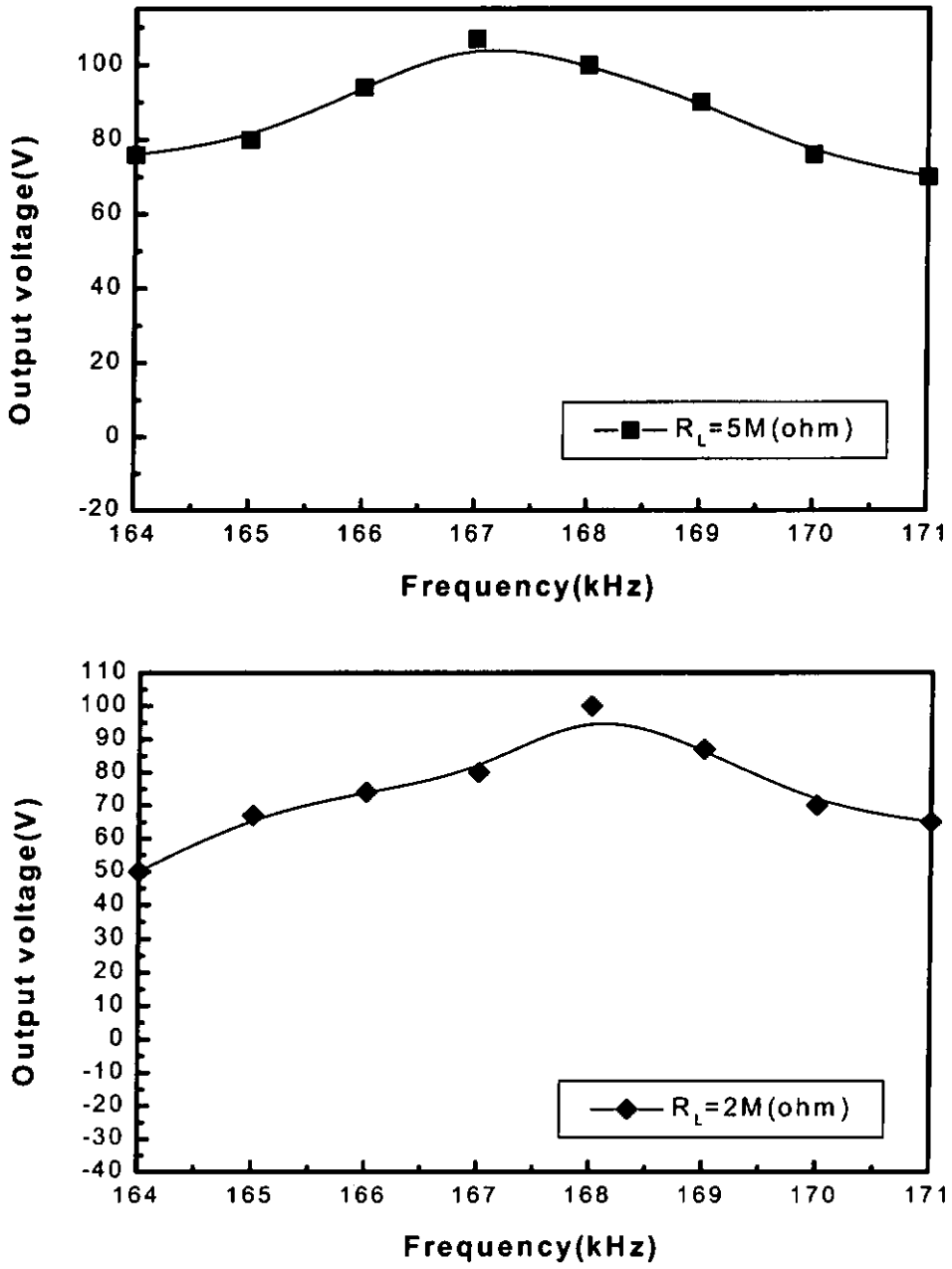

Fig. 4.7. Measured output voltage as a function of driving frequency at an input voltage of 10 V.

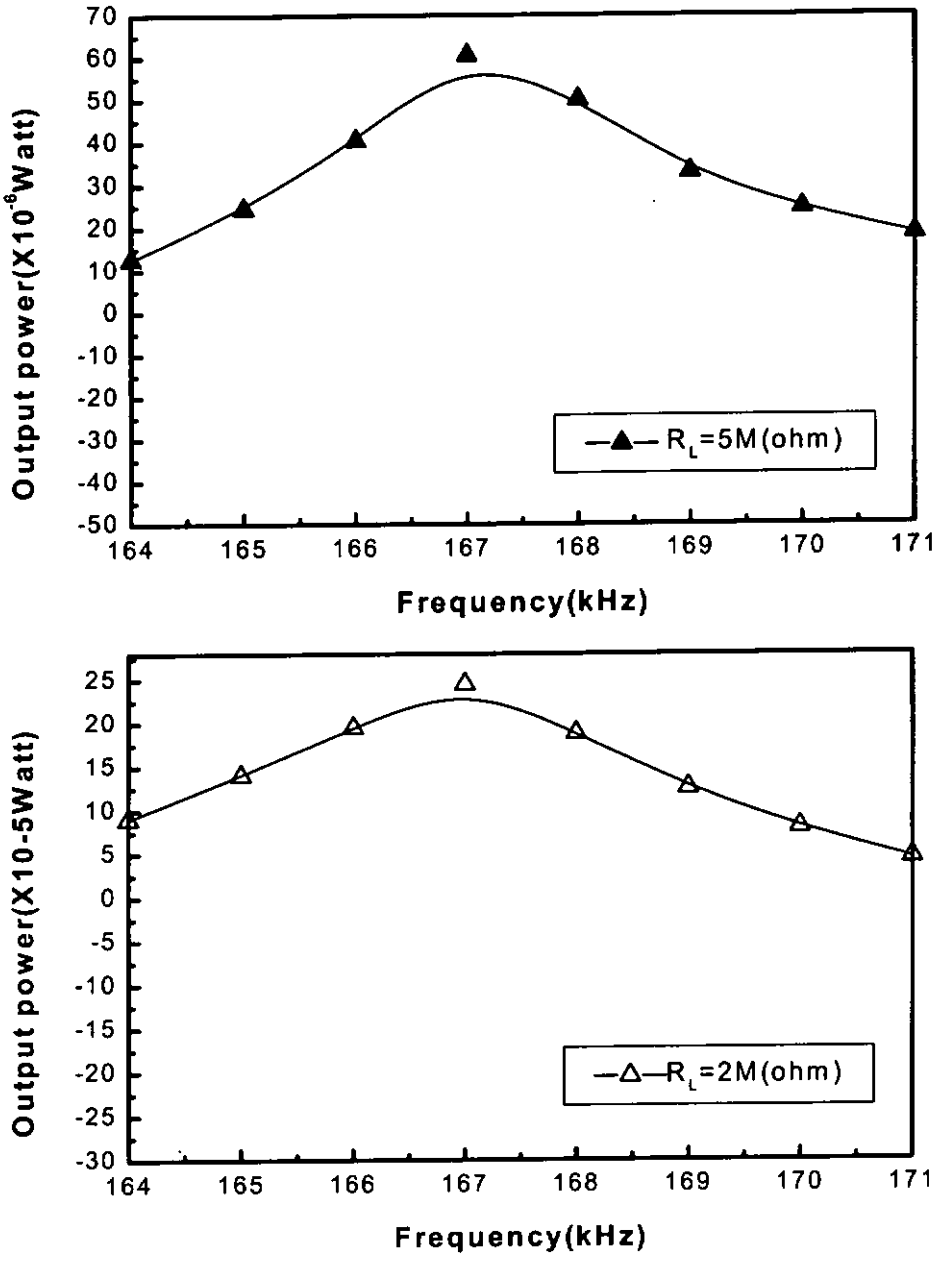

Fig. 4.8. Measured output power as a function of driving frequency at an input voltage of 1 V.

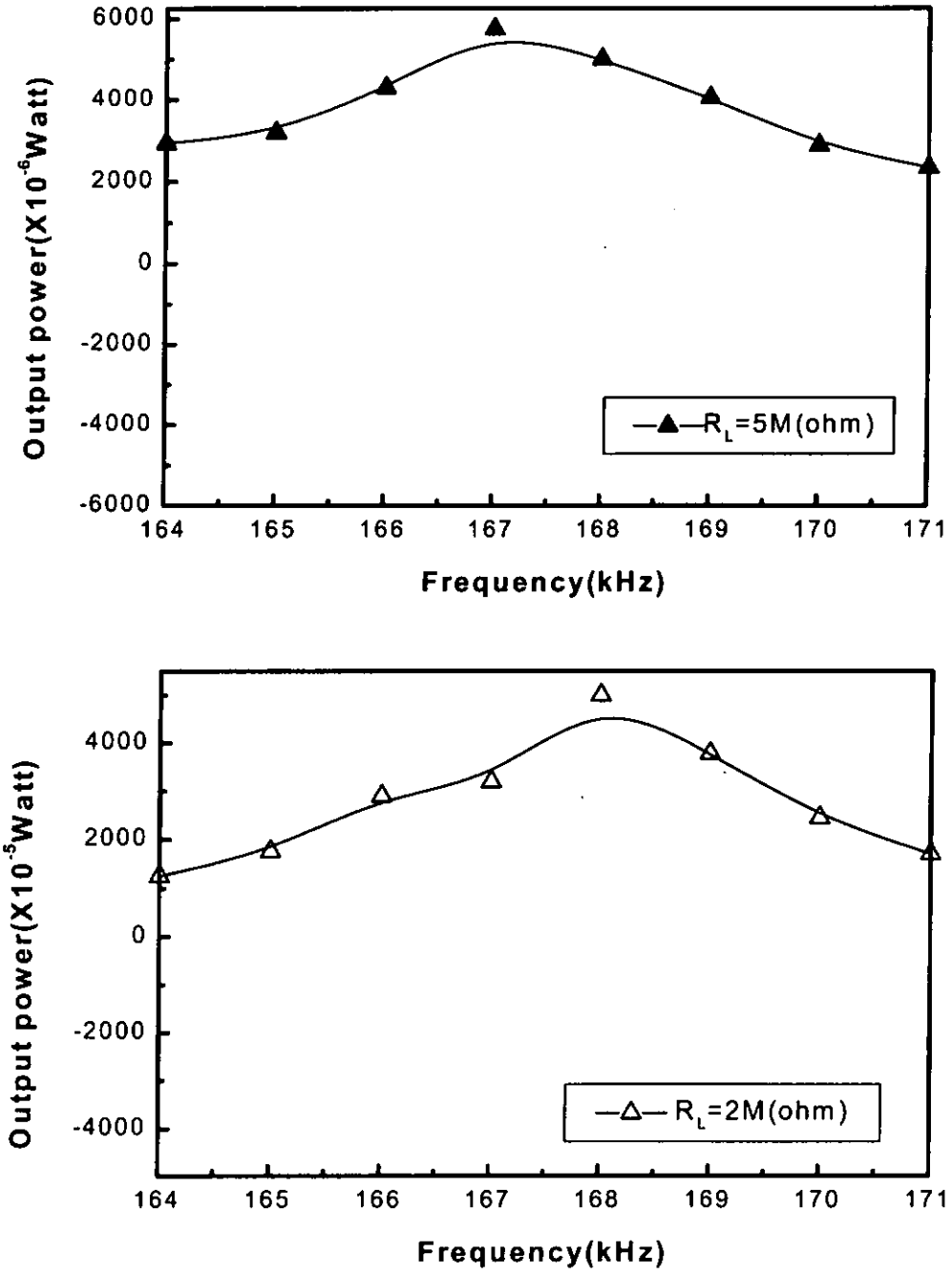

Fig. 4.9. Measured output power as a function of driving frequency at an input voltage of 10 V.

4.5. Conclusion

From the above analysis, when the driver section adopts the multilayer structure, a lower input electrical impedance is obtained, which makes the driving circuit simpler. The length mode (k_{31}) MPT fabrication can still be further optimized. By choosing a PZT ceramic powder with higher Q_m value, Q_m value of the MPT can also be improved. This is a way to increase the power transmission efficiency and voltage amplification of the MPT. The nonuniformity of the internal electrode and the external electrode's painting result will also need to be further improved. Besides that, more research about the testing method needed to be done. For example: the phase difference between the input voltage and current fluctuates during measurement, which makes the result rather inacurate. How to stabilize the phase difference between the input voltage and current is very important for the measurement of the input power and the power transmission efficiency.

Chapter Five

Two-step Sintering Process for Reducing the Sintering Temperature of a Multilayer Structure with Pd/Ag Interleaving Electrodes

5.1 Introduction

The co-fire technology has been used extensively in the fabrication of multilayer actuators[1,2]. In order to use less expensive metal such as Pd/Ag (40/60 wt %), which has a lower melting temperature compared to Pt, as the interleaving electrodes to reduce the manufacturing cost, it is desirable to develop a low-temperature sintering process. Two-step sintering is a useful technique in reducing the duration of the ceramic sintered at a much higher temperature. Various stages exist in the sintering process. The first stage occurs when the particles come into contact under high temperature and is characterized by a rapid growth in the inter-particle necks. This stage actually continues for several minutes at a high temperature at which the thermal energy is high enough to drive the mass transportation in the solid state sintering [2]. In the two-step sintering technique, the highest temperature was applied at the first stage of sintering for only a few minutes, just long enough to induce a rapid growing speed in the inter-particle necks and causes a great effect on the final sintering results[1,3]. The sintering temperature was then decreased by 130°C to 1150°C and held for 1.5 hours to prevent excess diffusion of the metal into PZT.

5.2 Sintering Procedure of the Multilayer Structure with Pd&Ag Interleaving Electrodes

There are two steps in the sintering procedure. The first step is the high temperature step, which lasts for a few minutes. Then the temperature is quickly decreased at a rate of 10 degree per minute to 100°C ~ 150°C below the original sintering temperature, and lasts for a period longer than the conventional sintering procedure.

After finishing the fabrication process, the green multilayer structure was buried in annealed PZT powder. Then Al_2O_3 fire bricks were placed on the top of the MPT to apply pressure during sintering. Starting from room temperature, a heating rate of 5°C per minute was used to increase the temperature to 300°C and dwelt for 1 hour to evaporate the organic contents. Second, the heating rate was set at 3°C per minute and the temperature was increased to 1150°C and the temperature was immediately raised to 1250°C with a heating rate of 10°C per minute and kept at 1250°C for 5 minutes. The temperature was decreased to 1150°C at a rate of 5°C per minute and was kept at 1150°C for 2 hours. Then the temperature was decreased to room temperature slowly. The whole procedure is shown in Fig. 5.1:

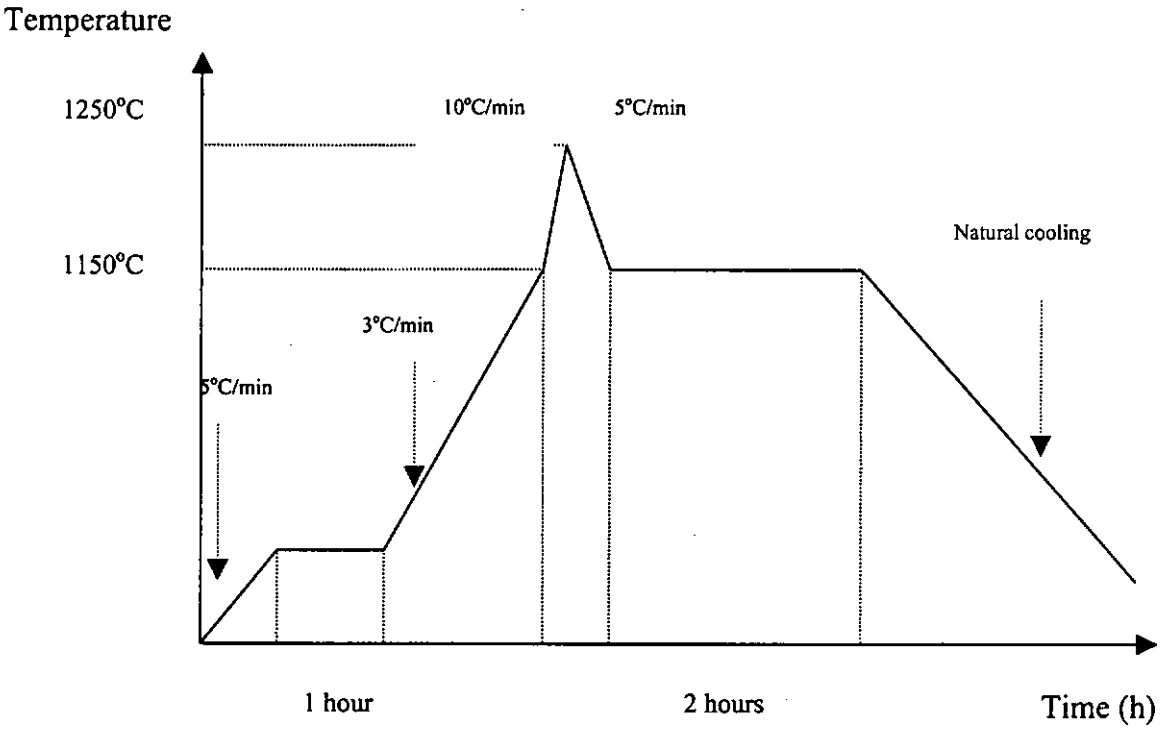

Fig. 5.1. Schematic diagram of the two-step sintering procedure

5.3 Characterization of the Multilayer Transformer prepared by Two-step Sintering process

5.3.1 XRD Measurement and SEM Measurement

As shown in the XRD pattern in Fig. 5.2, in the PZT powder sintered with conventional method at a sintering temperature of 1150°C and kept for 2 hours, no clear XRD peaks can be seen which indicates that the PZT has not crystallized. But when we use the two-step sintering procedure, the XRD pattern shows clear PZT crystallization peaks which means the PZT ceramic has better crystallization. The same results can also be seen from the SEM result as shown in Fig. 5.3 (a. conventional sintering process; b. two-step sintering process). From the SEM image we also noticed that when the specimen was only sintered at 1150°C for two hours, the ceramic grain has not grown[2-5,29]. Fig. 5.4 shows the SEM micrographs of the cross sectional view of the PZT multilayer structure with Pd/Ag interleaving electrode (a) by conventional sintering method at 1250°C for 2 hours, (b) by the two-step sintering process. From Fig. 5.4.(a), we can see that when the multilayer structure was sintered by the two-step sintering procedure, a clear multilayer structure can be seen. This indicates that the Pd/Ag electrodes have not diffused extensively. But by using the conventional sintering process, and lift the sintering temperature to 1250°C for 2 hours, the Pd/Ag electrodes disappeared, as shown in Fig. 5.4 (b).

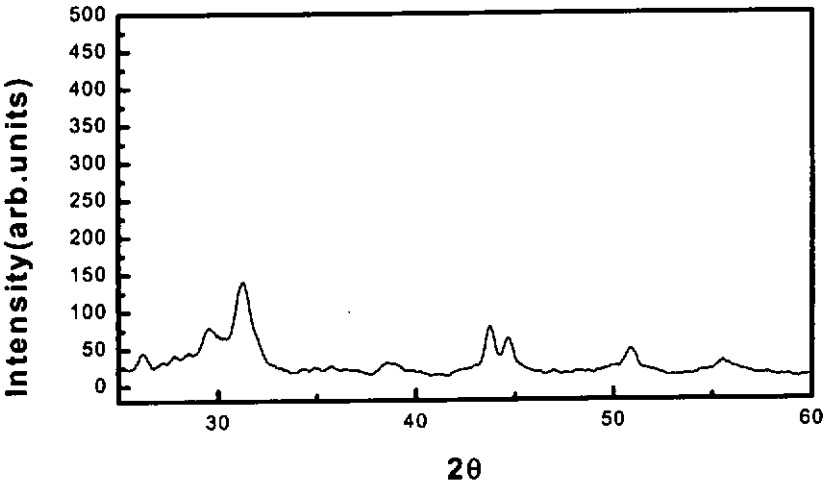

(a)

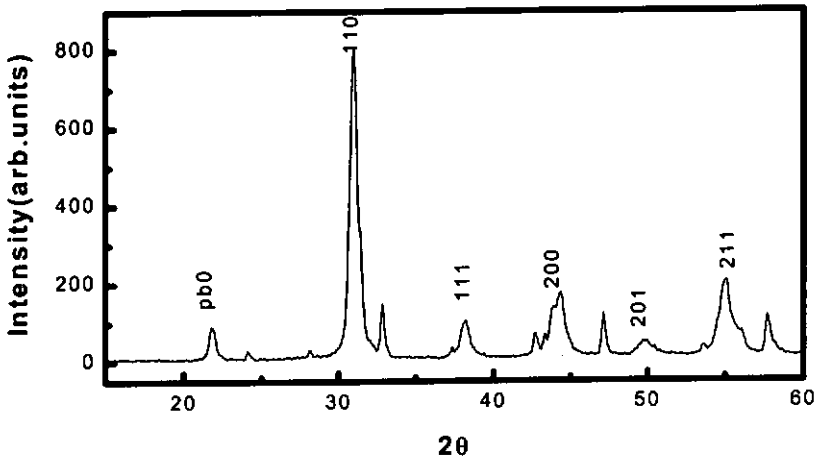

(b)

Figure. 5.2. XRD patterns of PZT sample sintered with (a)conventional method at a sintering temperature of 1150°C for 2 hours, (b) the two-step sintering process.

(a)

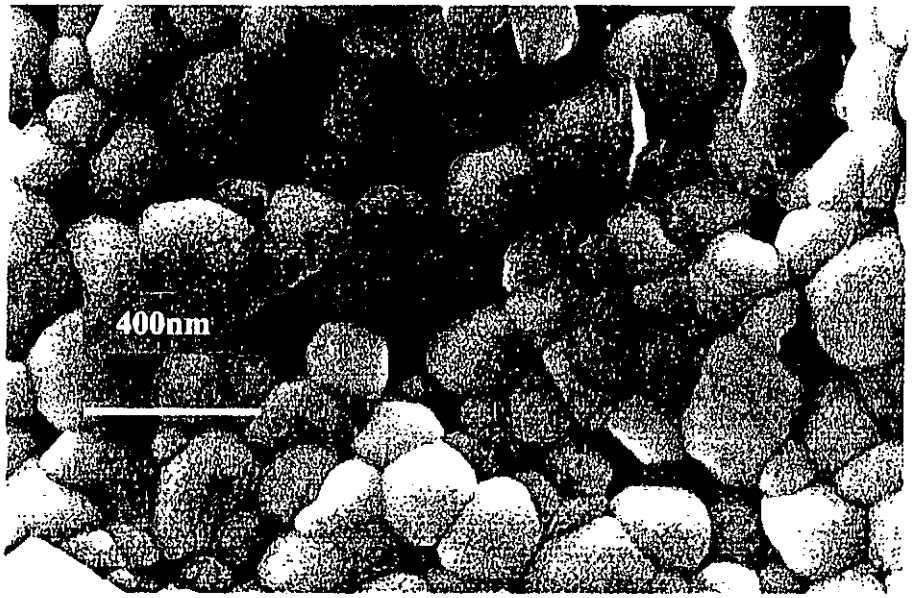

(b)

Figure. 5.3. SEM micrographs of PZT sample sintered with (a)conventional method at a sintering temperature of 1150°C for 2 hours, (b) the two-step sintering process

(a)

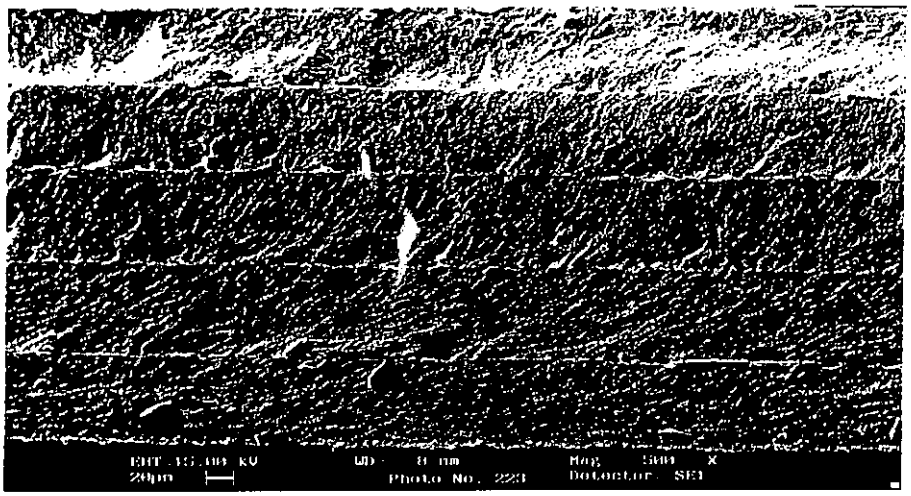

(b)

Fig. 5.4. SEM micrographs of cross sectional view of the PZT multilayer structure (a)by conventional sintering method at 1250°C for 2 hours, (b) by the two-step sintering process

5.3.2. Piezoelectric Constant d_{33} and Mechanical Quality Factor Q_m

The piezoelectric d_{33} coefficient of the PZT sample sintered by the two-step process is measured by a d_{33} meter (from Beijing Institute of Acoustics, China) and data obtained are shown in Table. I. It is seen that after the 5 min. sintering at 1280°C, as the dwelling time at 1150°C increases from 1 hour to 2 hours, the d_{33} coefficient increases from 181 pC/N to 241 pC/N and becomes stable after that. Mechanical quality factor Q_m, measured by finding the equivalent circuit parameters around the sample resonance (1.26 MHz) also shows the highest value at 2 hours dwelling time. Comparing the data with those of the conventional sintering process of the single layer PZT ceramic and results are shown in Table 5.1

Table 5.1 Piezoelectric Coefficient d_{33} and Q_m of the PZT.

	Piezoelectric coefficient d_{33}(pC/N)			Q_m Factor		
Dwelling time(hour)	1	1.5	2	1	1.5	2
Conventional sintering at 1150°C	0	0	10	0	0	0
Two step sintering process	181	240	241	91	124	153

5.3.3. P-E hysteresis loop measurement

Figure 5.5 shows the hysteresis loops of PZT samples as measured by a Sawyer-Tower circuit. The sample sintered by the conventional process at 1150°C for 2 hour (Figure 5.5 a) does not have a P-E loop and cannot withstand high electric field as it breaks down easily. P-E loop of the multilayer prepared by the two-step sintering has good ferroelectric properties. It has a coercive field of 0.85 kV/cm and a remnant polarization of 50 $\mu C/cm^2$.

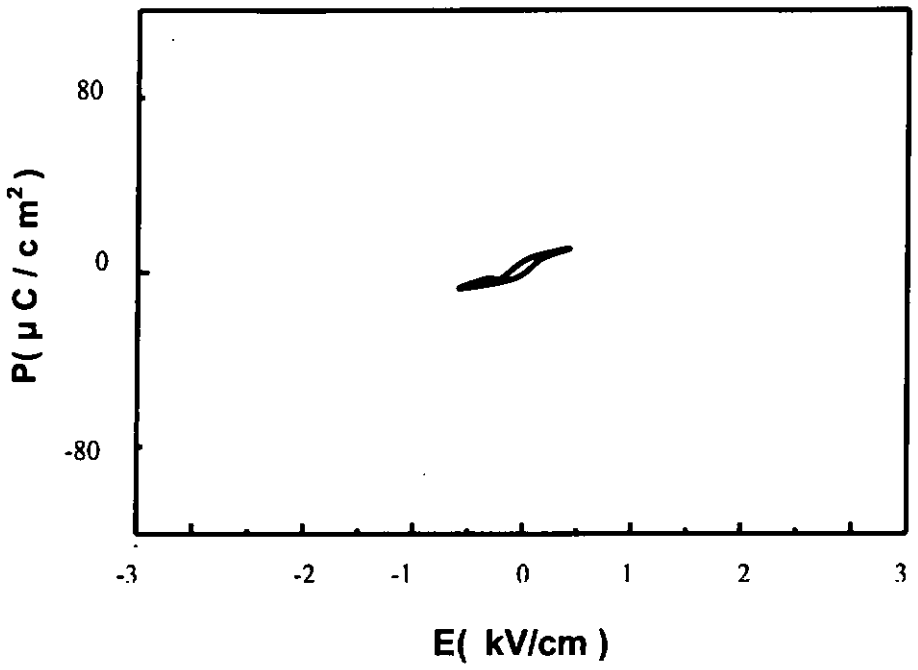

(a)

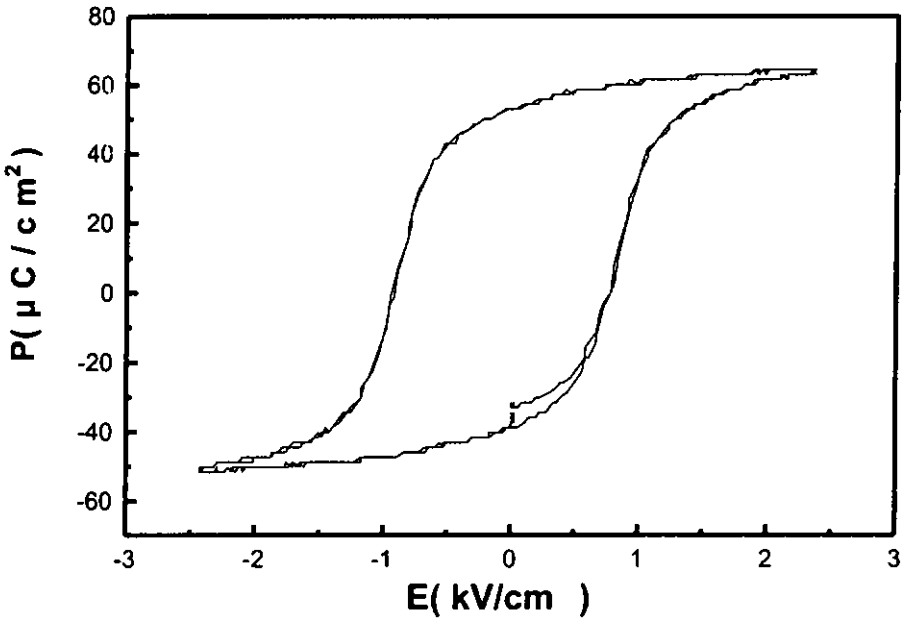

(b)

Figure 5.5. PE hysteresis loop of the same PZT sample sintering with (a) conventional method at a sintering temperature of 1150°C for 2 hours, (b) the two-step sintering process

5.5 Experimental Analysis

From the experimental results, we can see that the two-step sintering process can be used to reduce the duration at a high sintering temperature of selected PZT (from Ferroton LTD. Shenzhen, China) ceramic. The resulting PZT has good ferroelectric properties. Especially, this technology can be used in fabricating multilayer device with a more cost-effective material Pd/Ag instead of the expensive Pt as the interleaving electrodes which greatly reduces the manufacturing cost.

Chapter Six

Fabrication of PZT/LNO Multilayer Structure

6.1 Introduction and background review

In this chapter, the fabrication process of lead zirconate titanate / lanthanum nickel oxide (PZT/LNO) multilayer structure was described. The PZT films were produced by a modified sol-gel method, then , a LNO film prepared by a metal-organic deposition method was spin-coated onto the PZT film. The sandwich structure was sintered by rapid thermal annealing technology at various temperatures. A buffer layer consisting of a mixture of PZT and LNO was introduced to enhance the adhesion between the LNO and the PZT layer. The electrical resistivity of the LNO films was measured as a function of temperature, and 750°C was found to be the optimum sintering temperature. The microstructures of the PZT/LNO films were studied in a scanning electron microscope (SEM).

In the fabrication of multilayer ceramic devices, metallic alloys such as Pt and Pd/Ag are often used as electrodes, but this leads to mechanical weakness at the ceramic-alloy junction and possibly delamination. Ideally, if a conducting ceramic with (1) sintering temperature and shrinkage close to the ceramic (e.g. lead zirconate titanate, PZT), (2) good adhesion to PZT and (3) slow diffusion into PZT during sintering can be found, then the delamination problem in multilayer devices can be alleviated.

LNO is a conducting ceramic [34-36] which has good potential for use as electrodes in multilayer devices. It has a pseudo-cubic perovskite structure with a lattice parameter of 0.384 nm. However, it is difficult to co-fire LNO with PZT prepared by conventional mixed oxide technique as the sintering temperature is higher than 1100°C and LNO will disintegrate at such a high temperature. To alleviate this problem, a modified sol-gel method is used to prepare thick PZT films [37] on stainless steel substrates. The LNO films are deposited on the PZT films as electrodes and they can be co-fired at a much lower temperature.

6.2 Materials Preparation

6.2.1 Modified Sol-Gel Method for Fabricating PZT Film

The PZT films were prepared on stainless steel substrates (10 mm × 10 mm) using a modified sol-gel method. Nanosized sol-gel PZT powder [38] with a crystallite size of ~28 nm, which had been previously annealed at 550°C, was dispersed in a PZT (Zr/Ti = 48/52) sol-gel solution under ultrasonic agitation. The nanosized powder content is about 30 wt%. Glycerin and deionized water were added to adjust the viscosity. The PZT films were prepared by spin-coat the sol-gel solution onto stainless steel substrates. After deposition of each layer, the wet film was dried in a rapid thermal processor (RTP) at 150°C for 6 min, 300°C for 6 min and 550°C for 10 min, with a heating rate of 1800°C/min.. The spin-coating procedure was repeated to produce the required film thickness. The PZT film used in the present experiment was ~ 1.5 μm thick.

6.2.2 Organic Decomposition Method for Fabricating LNO Films

The LNO films are prepared by a metal-organic deposition (MOD) method [35,36] with lanthanum nitrate [$La(NO_3)_3.24H_2O$] and nickel nitrate [$Ni_2O_3.6H_2O$] as the starting materials. [$Ni_2O_3.6H_2O$] and [$La(NO_3)_3.24H_2O$] were dissolved in HNO_3 and deionzed water, respectively, to form solutions. The two solutions were mixed with a La:Ni = 1:1 molar ratio and polyvinyl alcohol (PVA) and glycerin were added to adjust the viscosity. A clear and stable solution of 1 M concentration was obtained and was spin-coated onto PZT films to form electrodes.

6.3 Fabrication of a PZT/LNO Multilayer Structure

Initially, the LNO was spin-coated onto the PZT and both films were co-fired at various temperatures. Adhesion of the LNO to the PZT was very poor due to the mismatch in thermal expansion. A buffer layer was introduced by spin-coat a thin layer (~50 nm) of the mixture of the PZT sol-gel solution and the LNO solution (in a volume ratio of 70% : 30%). With the buffer layer, the adhesion of LNO to the PZT was

significantly improved. When the PZT/LNO films were co-fired, the mixed powders of PZT and LNO can react to form an intermediate compound, this reaction mainly happens inside the buffer layer, which serves as a bonding structure between PZT and LNO layers.

6.4 Measurement and Analysis

6.4.1 Characterization

The crystallization of the PZT/LNO film (with a buffer layer) was examined using an x-ray diffractometer (Phillips X'pert XRD system). The x-ray diffraction (XRD) patterns were recorded at a rate of 1°C/min in the 2θ range of 20° - 60°. The microstructures of the films were studied using a scanning electron microscope (SEM, Steroeoscan 440). The resistivity per unit area ρ/A = R/L (in Ω/cm) of the LNO film was found by using a multimeter to measure the electrical resistance R across different points on the top surface of the LNO film and then divided by the separation between the two points L.

6.4.2 Results and Discussions

A multilayer film with ~1.5 μm PZT on a stainless steel substrate, a 50 nm buffer layer and a 0.7 μm LNO film was sintered using RTP at different temperatures. Figs.6.1(a) - (d) show the XRD patterns of the multilayer film annealed at 600°C, 700°C, 750°C and 800°C, respectively. In Fig. 6.1 (a), the film sintered at 600°C exhibits the crystalline peaks and the pyrochlore phase of PZT while the LNO crystalline peaks are relatively weak, indicating that LNO is starting to crystallize but the grain size is small. When the film was sintered at 700°C (Fig. 6.1.(b)), crystalline peaks of LNO appeared and as sintering temperature increased (Figs. 6.1.(c) and (d)), the LNO peaks became more prominent. For information, the XRD patterns of (a) a PZT film sintered at 750°C [7], (b) a LNO film sintered at 750°C, (c) lanthanum oxide and (d) nickel oxide are

shown in Figs. 6.2.(a) -(d)). Some small XRD peaks which belong neither to the PZT nor to the LNO films may be ascribed to the residual lanthanum oxide.

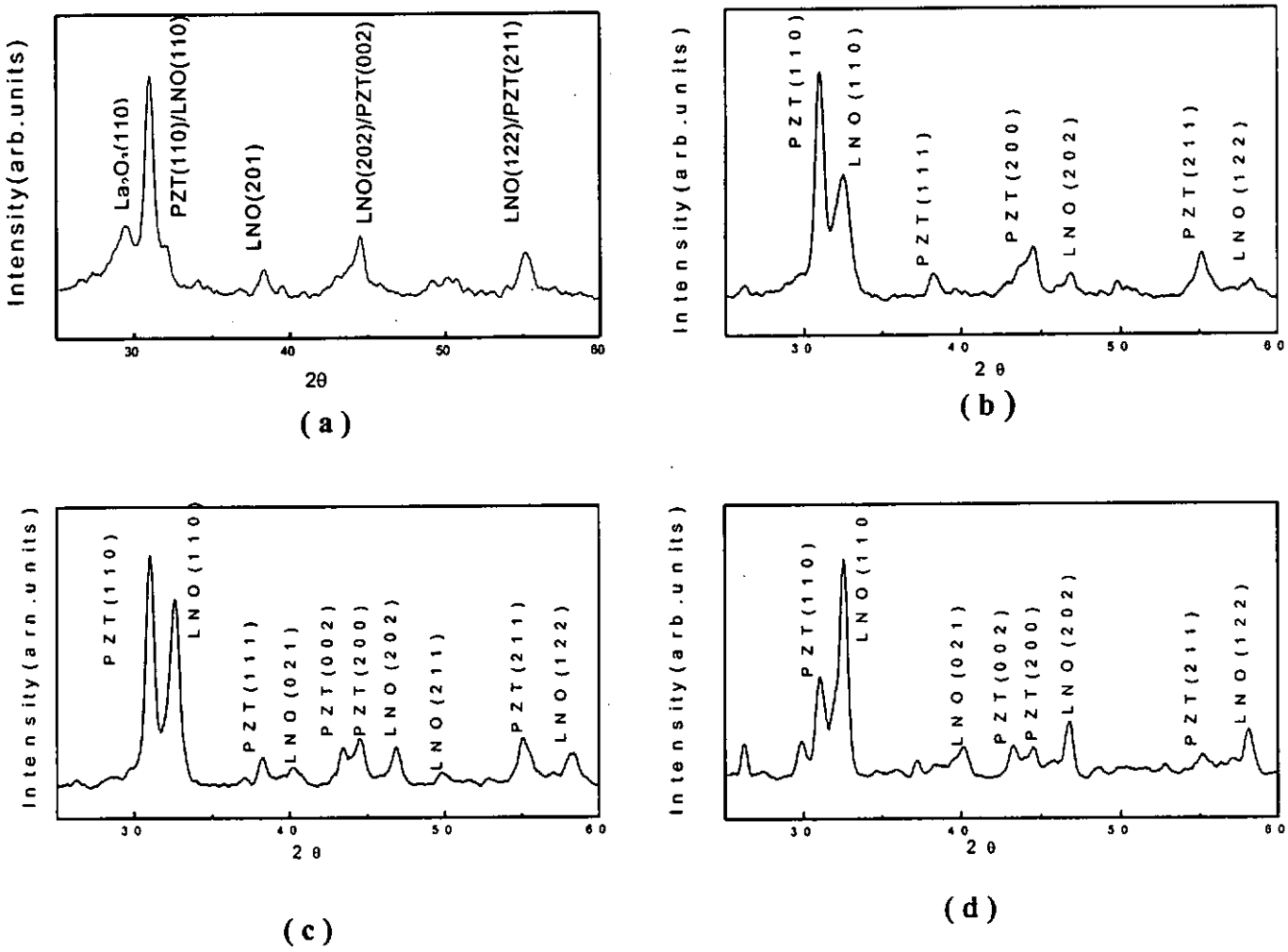

Fig.6.1. The XRD patterns of the multilayer film annealed at (a) 600°C, (b)700°C, (c)750°C and (d)800°C

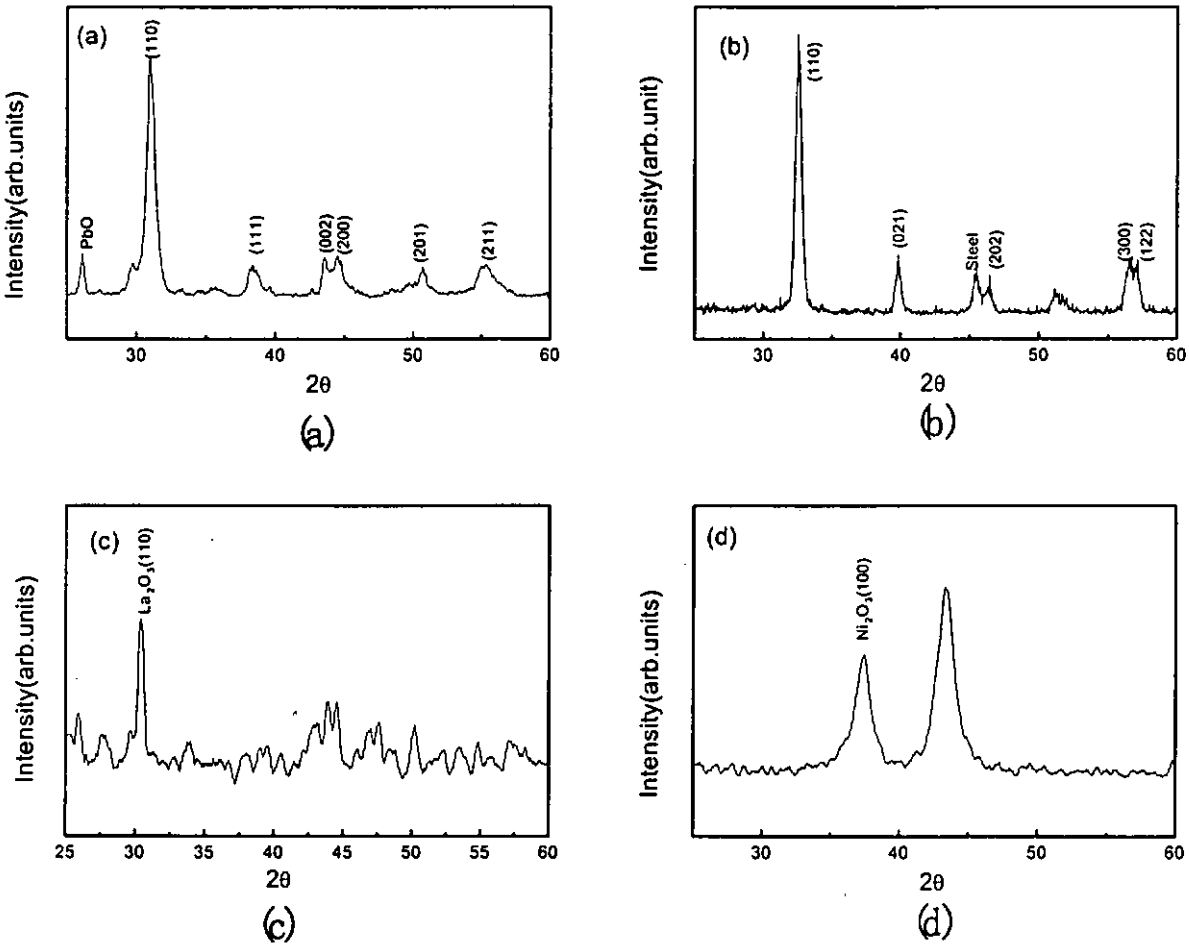

Fig. 6.2. XRD patterns of (a) a PZT film sintered at 750°C [7], (b) a LNO film sintered at 750°C, (c) lanthanum oxide and (d) nickel oxide

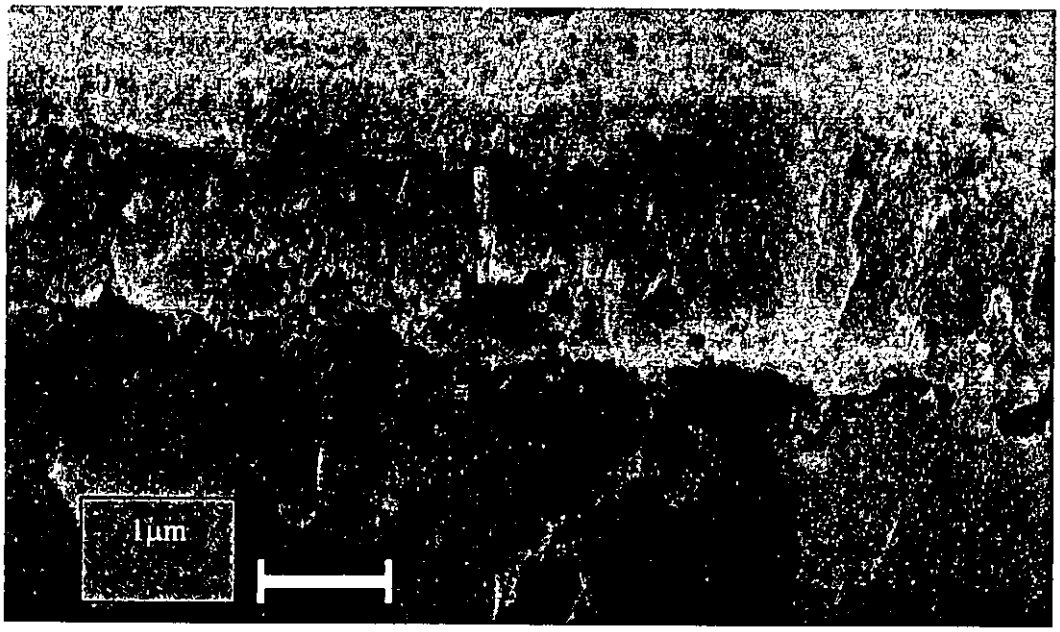

(a)

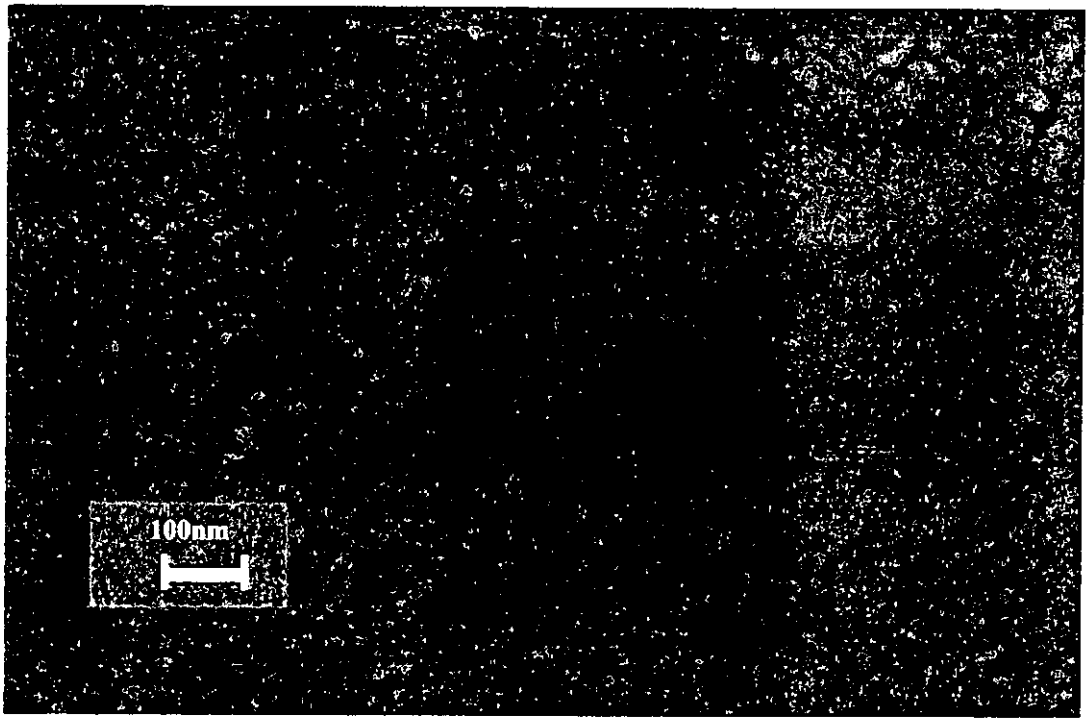

(b)

Fig. 6.3. SEM micrographs of the multilayer film sintered at 750°C
(a) cross section view, (b) top view

The SEM micrographs of the multilayer film sintered at 750°C are shown in Figs. 6.3 (a) and 6.3 (b). The LNO and the PZT films are about 0.7 μm and 1.5 μm thick, respectively (Fig. 6.3.a). As the buffer layer has a high PZT content, it has merged with the PZT film and thus is not visible in the micrograph. The grain size in the LNO film is ~100 nm as seen in Fig. 6.3 (b).

To determine the optimum thickness and sintering temperature of the LNO electrode, the resistivity per unit area (ρ/A) of the LNO was measured as a function of sintering temperature and film thickness and results are shown in Figs. 6.4 and 6.5, respectively. From Fig. 6.4 (a), it can be seen that the resistivity has a significant increase when the sintering temperature is higher than 800°C due to thermal degradation of the LNO. Between 700°C and 750°C (Fig. 6.4.(b)) , the LNO film has the lowest ρ/A. As the XRD results (Figs. 6.2. b and c) show that both the PZT and LNO have good crystalline peaks when sintered at 750°C, hence, 750°C will be used as the optimum sintering temperature in subsequent work. From Fig. 6.5, we can see that the LNO film has to be thicker than 500 nm in order to obtain good conductivity (low resistivity).

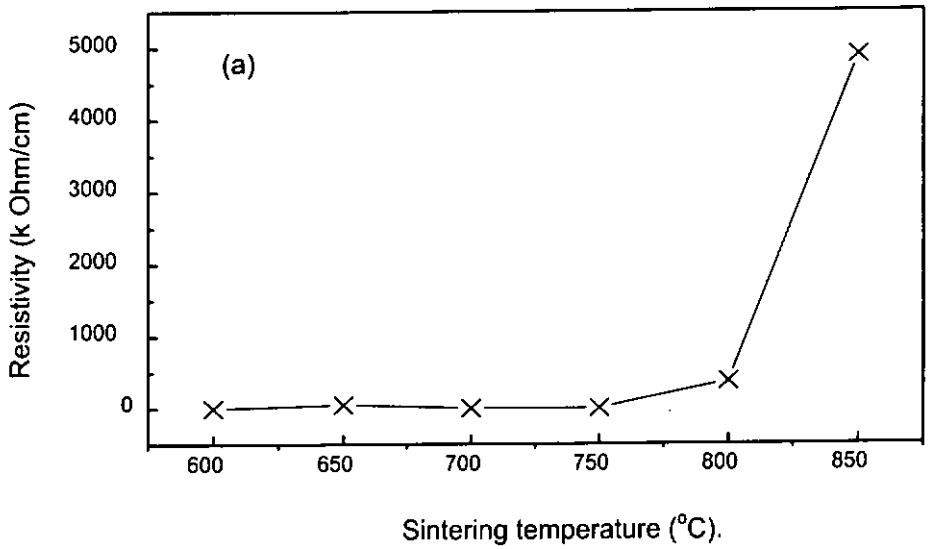

(a)

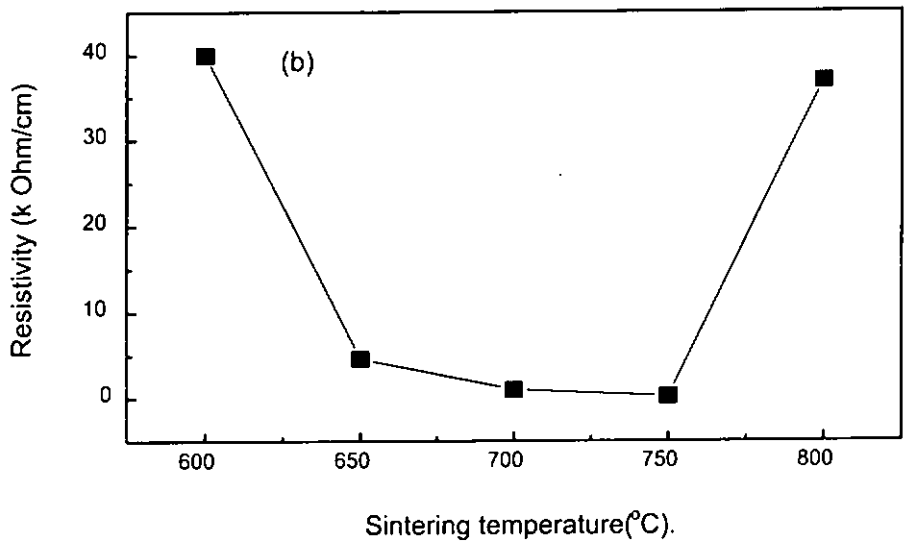

(b)

Fig. 6.4. Resistivity per unit area (ρ/A) of the LNO measured as a function of sintering temperature

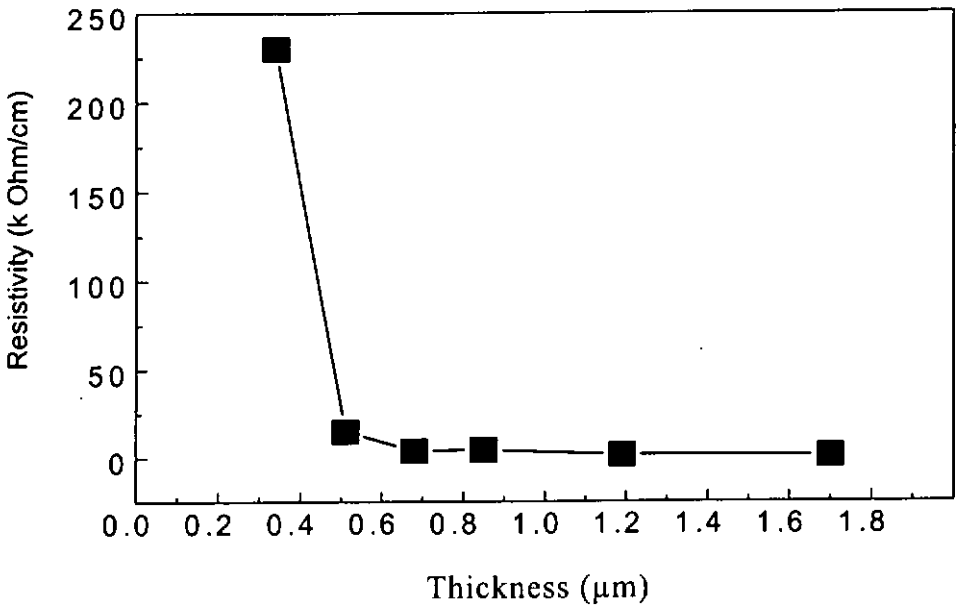

Fig.6.5. Resistivity per unit area (ρ/A) of the LNO measured as a function of film thickness

6.5 Conclusions

LNO has been successfully cofired with PZT to form electrodes. A buffer layer is required to enhance the adhesion of the LNO to the PZT. The optimum sintering temperature of the LNO/PZT film is 750°C using RTP. The resistivity of the LNO electrode decreases as the thickness of the film increases and a minimum thickness of the LNO to give good conductive property is ~ 500 nm.

Chapter Seven

The Seeding Effect of Lanthanum Nickel Oxide Ceramic/Ceramic Nanocomposite Thin Films Prepared by the MOD Method

7.1 Introduction

Nanosized particles are of interest in fundamental as well as applied research because many material properties change drastically when the crystallite size reaches the nano/submicrometer range [41]. Since nano-scaled particles have relatively larger surface areas, they tend to agglomerate to minimize the total surface energy. Agglomeration adversely affects their properties [42,43], for example: different reaction temperature, faster grain growth speed, higher density and more uniform film quality, etc.

Recently, it has been reported that the formation of PZT thin films may be controlled by seeding with PZT powder[41-46]. Applying the seeding effect in order to enhance the transformation kinetics and to control the development of a desired phase has been successfully investigated.

Lanthanum nickel oxide (LNO) is a conductive ceramic material that can be used in fabricating interleaving electrodes in PZT multilayer devices[45-48]. In this work, new investigation of using seeding effect to reduce the annealing temperature of LNO films is presented. Various weight percentages of nanosized lanthanum nickel oxide (LNO) powder fabricated by MOD method were added into a 0.5M LNO solution [49,50,51] as seeds. Then the LNO film was spin-coated onto a $Pt/Ti/SiO_2/Si$ multilayer substrate. Using rapid thermal annealing process (RTA) and by changing the annealing temperature and annealing time, samples with different properties were obtained.

7.2 Experiments

Lanthanum nickel oxide (LNO) powder has been produced by using a MOD method [49-52] and annealed at 700°C for 60 minutes. The crystallization process of LNO was studied by X-ray diffraction (XRD, Philips x'pert XRD system), differential thermal analysis (DTA, Perkin-Elmer 1700) and thermo-gravimetry analysis (TGA, perkin-Elmer TGS2).

The LNO metal-organic decomposed solution was produced by combining the $La(NO_3)_3$ and $Ni(NO_3)_3$ solutions in a molar ratio of 1:1. The concentration of the final solution was about 0.5 M. Polyvinyl alcohol (PVA) with a weight percentage of about 5% was added as a binder. A small amount of glycerin was also added to increase the viscosity of the solution [46,48-55].

Nanosize LNO powder was added as seeds to the pure LNO solution in different amounts, including 2%, 4%, and 10% by weight. After stirring and powder dispersion in an ultrasonic bath, a uniform suspension was formed.

The nanocomposite LNO solution was then spin-coated onto the $Pt/Ti/SiO_2/Si$ substrate. The spinning speed was 100 rpm for the first 6 seconds then 3500 rpm for the next 30 seconds. The spin-coated nanocomposite film was heat-treated by the rapid thermal annealing process (RTA) in order to evaporate the water and organic solvent inside the film. The heat-treat procedure is 150°C for 10 min, then 350°C for 15 min. This whole process was repeated three times in order to get the final nanocomposite LNO thin film with a thickness of ~400nm. The sample was then annealed for 30 minutes at various temperatures, ranging from 550°C to 700°C. The crystallization of the film was monitored by X-ray diffraction [43,46] and the crystallite size in the LNO film was estimated through the width of the diffraction peaks.

Scanning electron microscope (SEM) was used to study the morphology of the LNO films, and to observe the grain growth. The DTA and TGA methods were also used to study the change in the phase transition temperature in the LNO film with and without seeding in order to reveal its effect.

The whole experimental process is shown in Fig.7.1.

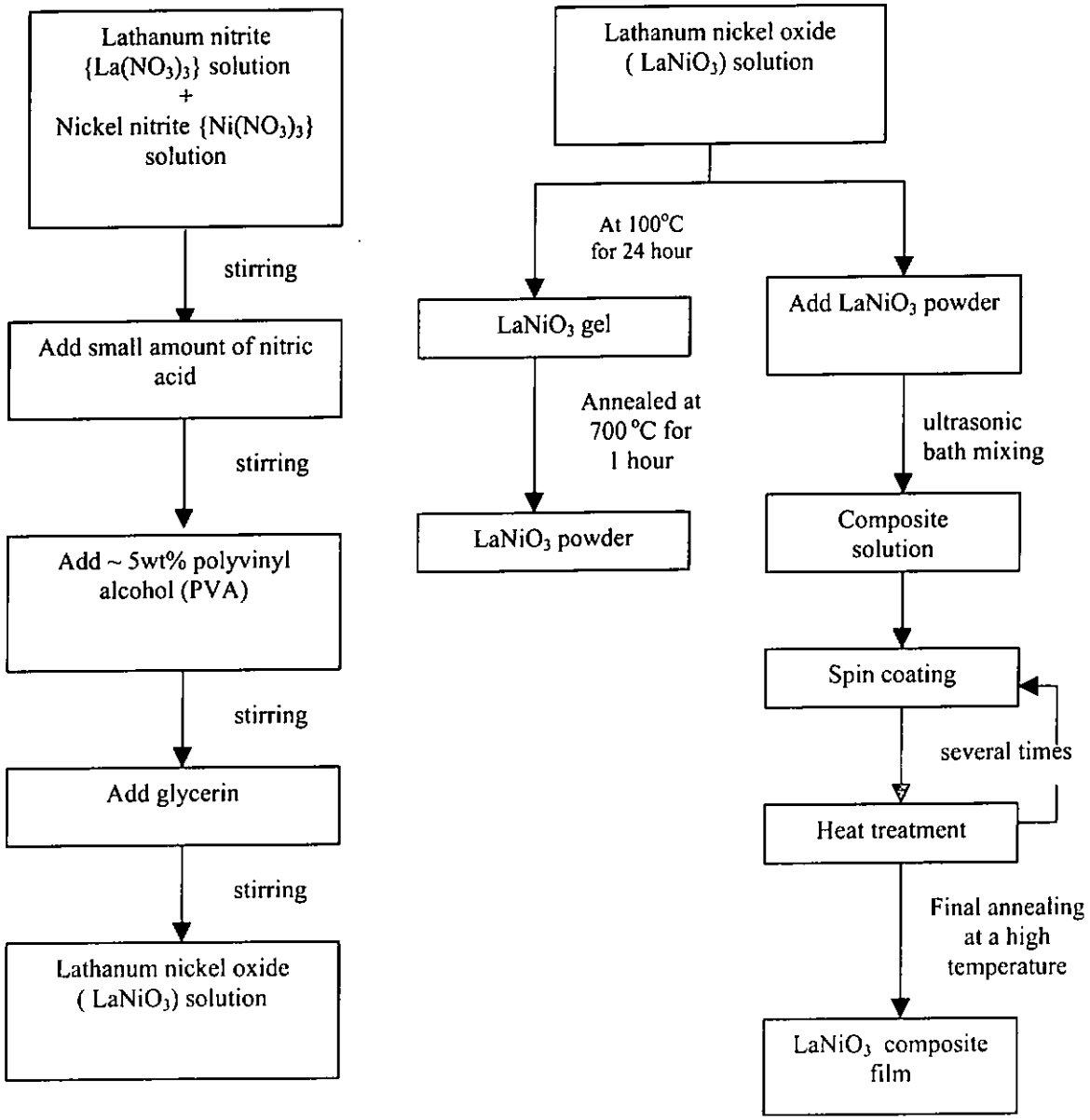

Fig. 7.1. Schematic illustration of the whole fabrication procedure of LNO nanocomposite film

7.3 Results and discussions

The XRD patterns in Fig. 7.2 show that the LNO powder annealed below 450°C has an amorphous structure. When the annealing temperature increased to 700°C, crystalline peaks of LNO become clear. Then Fig.7.3 shows the XRD patterns of LNO thin film. It is seen that crystalline LNO phase was formed at ~700°C.

Fig. 7.4 shows the XRD patterns of LNO nanocomposite films made by the metal organic decomposition (MOD) method after they were annealed at different temperatures. This pattern shows that the nanocomposite LNO film has ~80°C lower crystallization temperature compared to the pure LNO film (Fig. 7.3). This is consistent with the thermal data. Fig. 7.5 is the DTA (Fig.7.5.(a)) and TGA (Fig.7.5.(b)) graphs of the pure LNO film. Fig. 7.6 shows the DTA (Fig.7.6.(a)) and TGA (Fig.7.6.(b)) graphs of the composite LNO films with different amount of LNO powder (including 2%, 4%, 10% by weight) added as seeds. Comparing these patterns, clear differences in the DTA and TGA curves can be observed. In the pure LNO film, DTA curve shows a prominent peak at around 587°C. In the LNO composite films, peaks are observed at ~578°C for the film with 2 wt% LNO powder, and as the amount of powder increases to 4 wt% and 10 wt%, the peak shifts to ~570°C and ~511°C, respectively. This indicates that the crystalline grain growth temperature is progressively lowered as the amount of seeding increases.

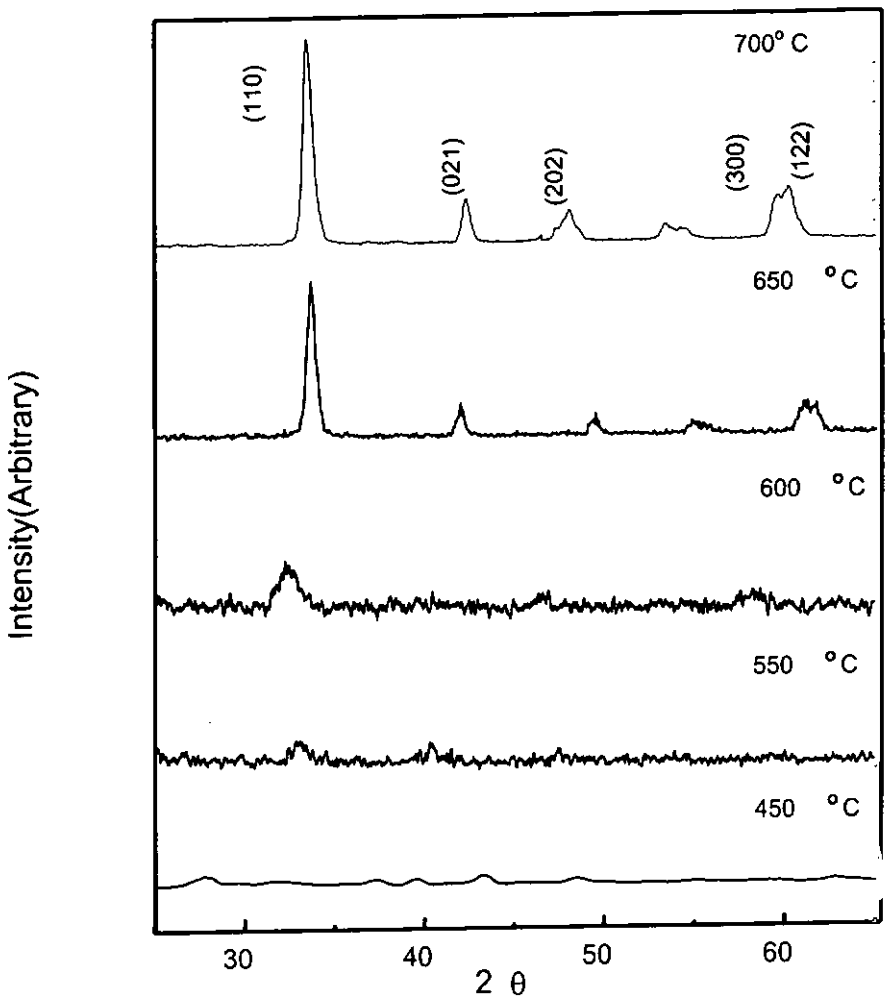

Fig. 7.2. XRD patterns of LNO powder annealed at different temperatures

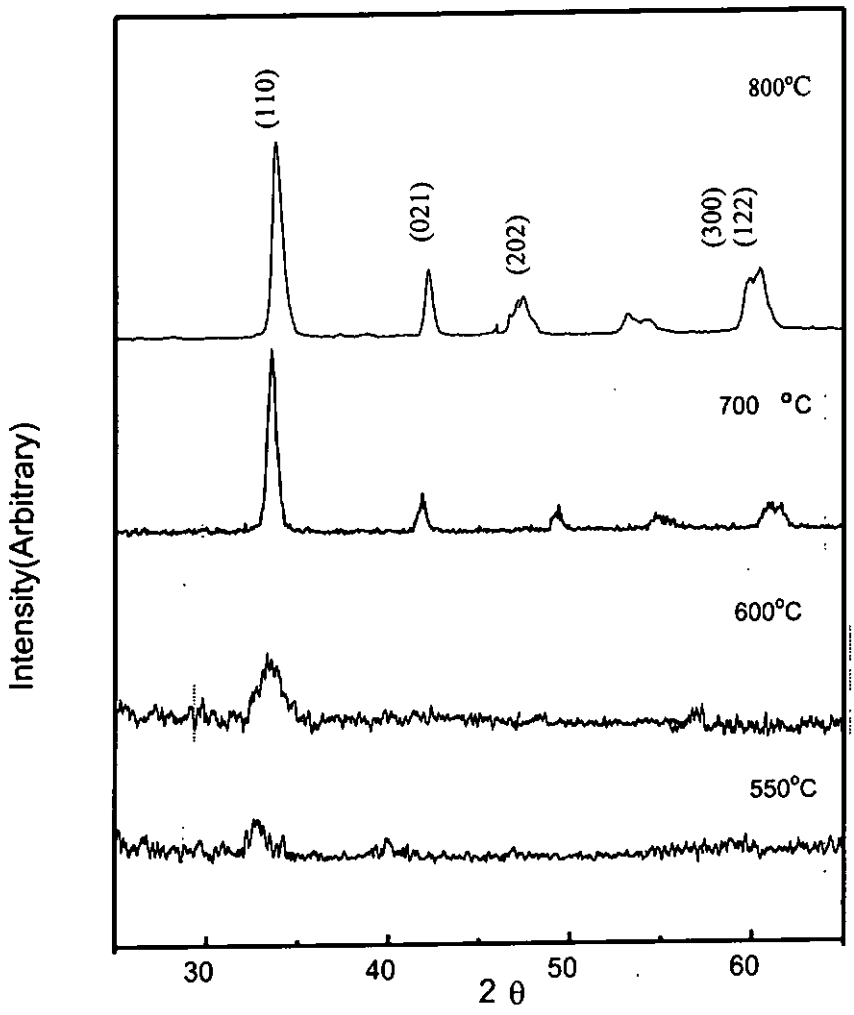

Fig. 7.3 XRD patterns of LNO films made by the metal organic decomposition (MOD) method annealed at different temperatures

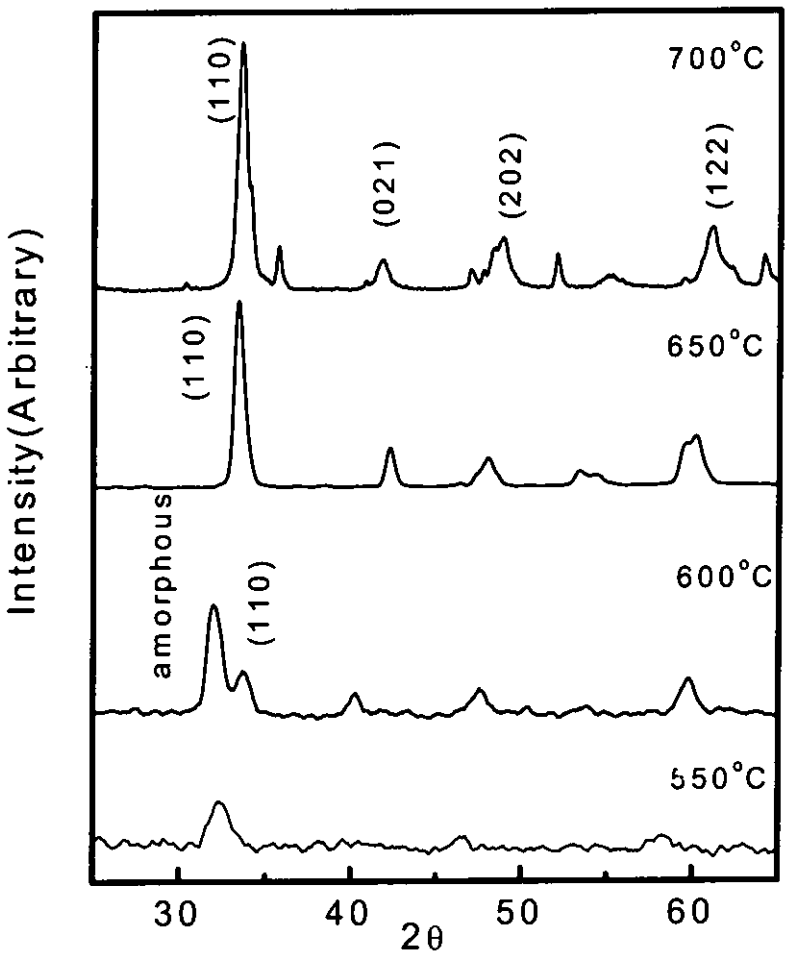

Fig. 7.4. XRD patterns of LNO nanocomposite films with 10% LNO powder made by the metal organic decomposition (MOD) method annealed at different temperatures

Table 7.1 shows the crystallite size of the LNO nanocomposite films annealed at various temperature, which are calculated from the full width at half maximum (FWHM) of the (110) XRD peaks using the Scherrer's equation [47]:

$$\tau = \frac{K\lambda}{\beta_r \cos\theta}$$

where β_r is the line broadening due to the effect of small crystallite, τ is the mean crystallite dimension, K is a constant (=0.8), θ is the angle where x-ray diffraction peaks occur.

Table 7.1. Crystallite size of the LNO nanocomposite films annealed at various temperatures.

Annealing temperature(°C)	550	600	650	700
Crystallite size(nm)	16.2	18.4	19.5	26.4

Fig. 7.7 shows the surface morphology of composite films heat-treated for 30 minutes at 450°C and 600°C, respectively. For the film annealed at 450°C, it is easily seen that the powder is uniformly dispersed in an amorphous matrix. After annealing at 600°C, the matrix has crystallized and the powder disappeared into the crystalline grains of the matrix. We can see that the nanocomposite LNO film is denser and has better uniformity compared to the surface morphology of LNO film without seeding and heat-treated at 600°C (c/f Fig. 7.7 (b) and Fig. 7.8).

Fig. 7.9 shows the conductivity of the LNO composite film as a function of the annealing temperature. From this graph we can see that when annealed at 600°C~650°C, the film has the highest conductivity, and as the annealing temperature increases, the conductivity decreases rapidly, which may be caused by the decomposition of the LNO into La_2O_3 and Ni_2O_3[45,48,49].

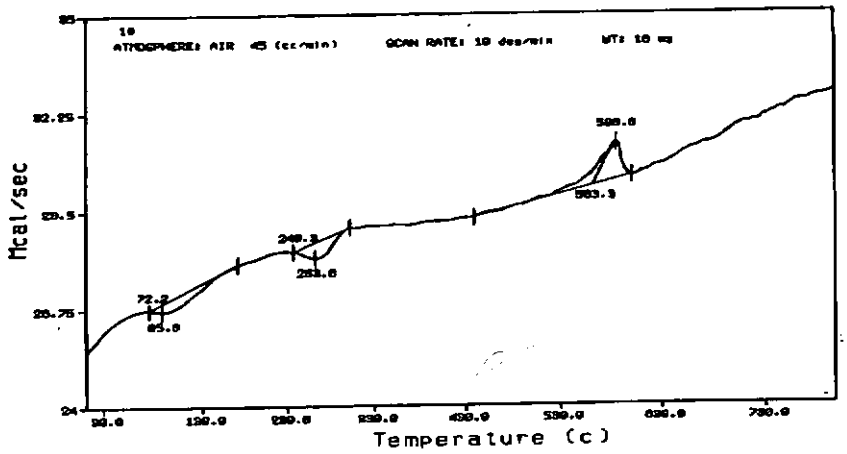

(a)

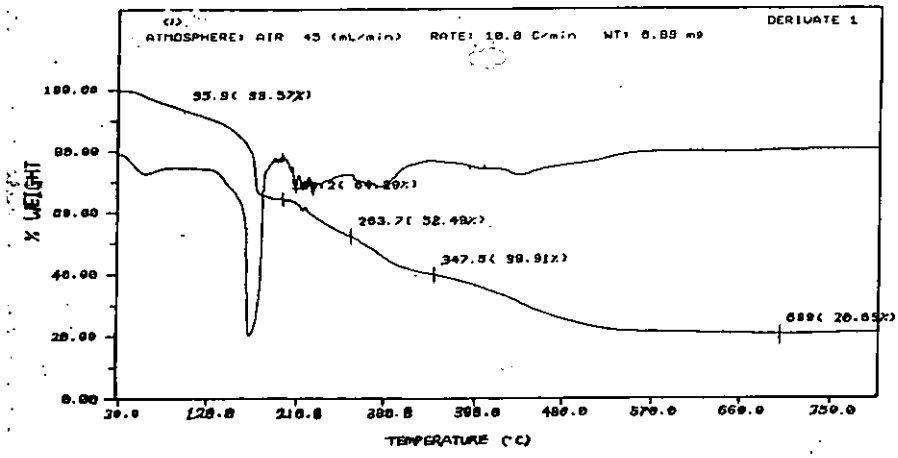

(b)

Fig. 7.5. DTA (a) and TGA (b) graphs of the pure LNO film

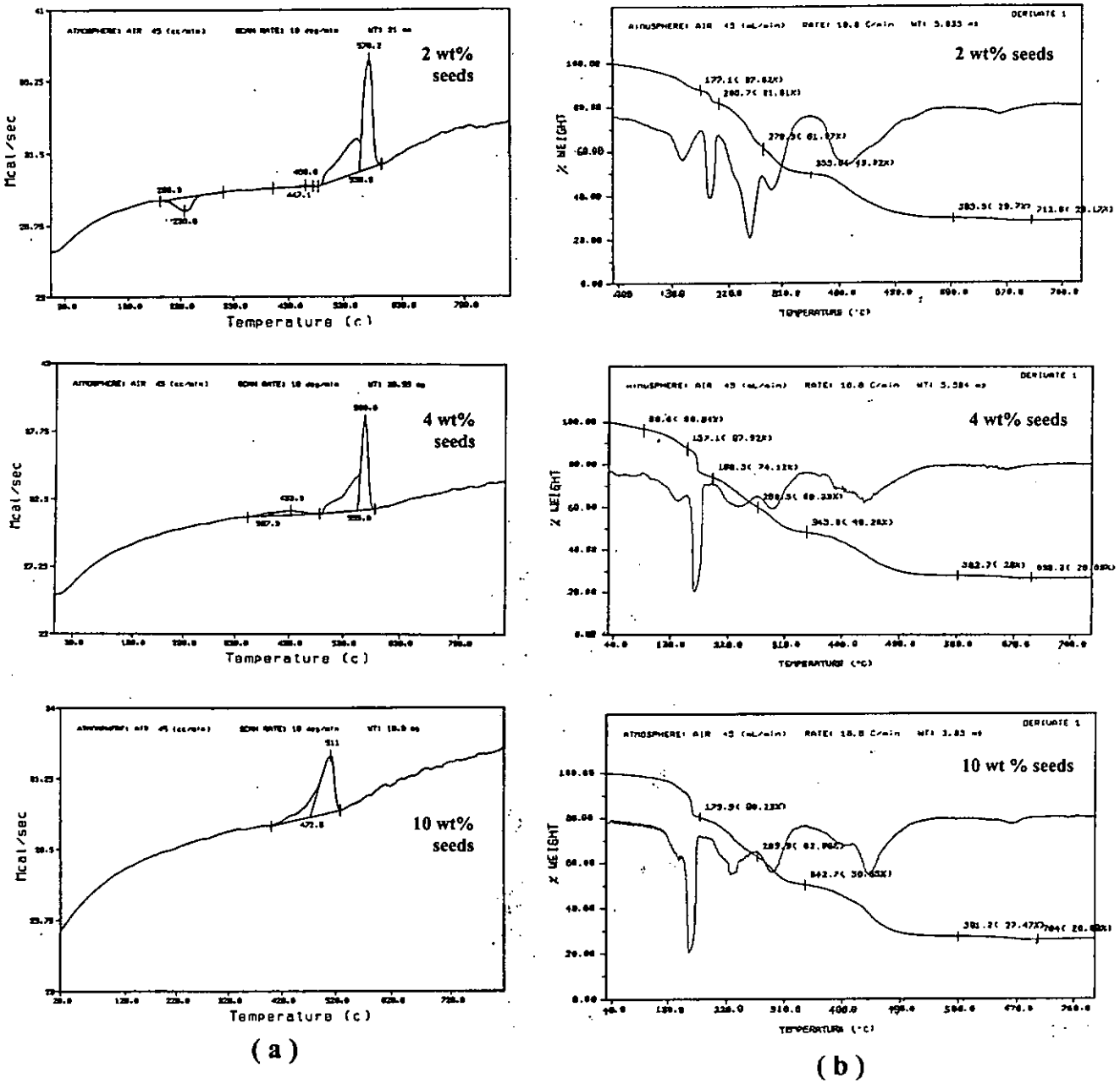

Fig. 7.6. DTA (a) and TGA (b) graphs of the composite LNO films with different amounts of LNO (2 wt%, 4 wt%, 10 wt%) seeds

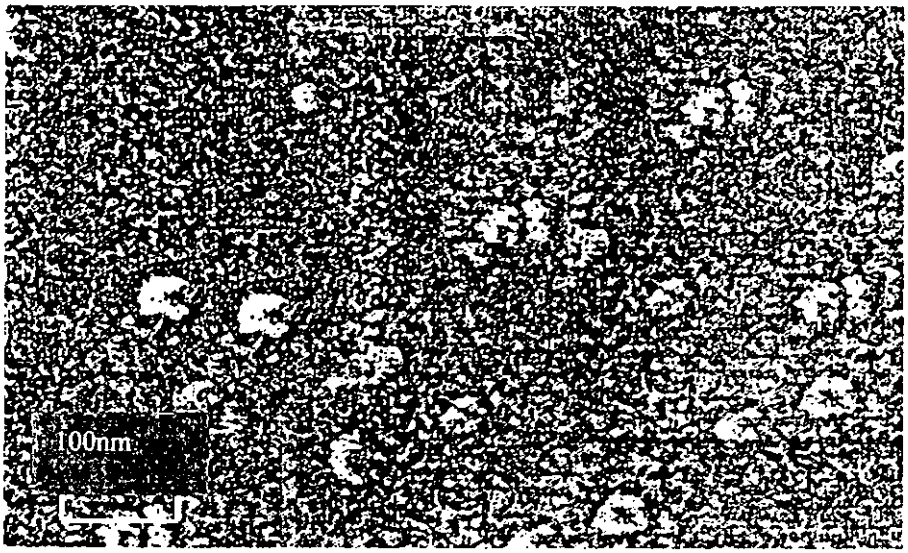

(a)

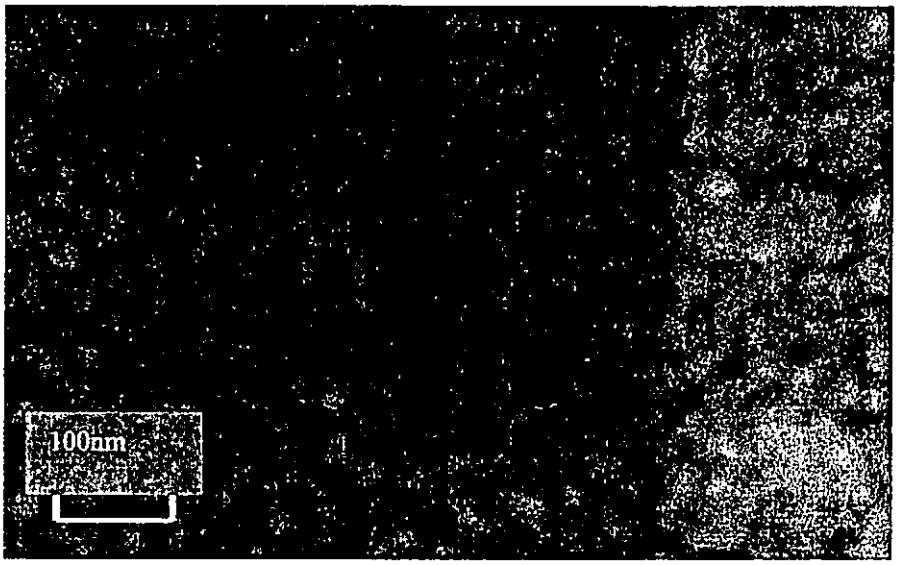

(b)

Fig. 7.7. Surface morphology of LNO composite films heat-treated for 30 minutes at (a) 450°C and (b) 600°C

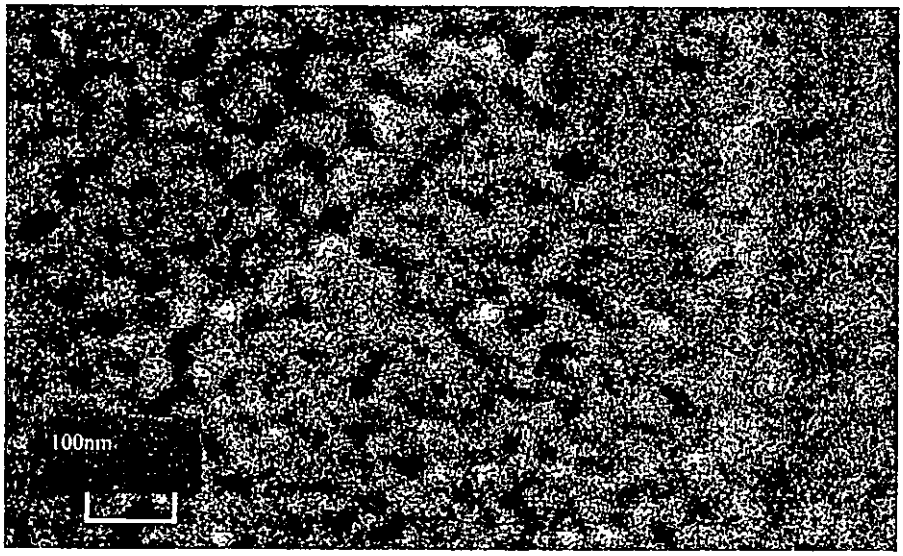

Fig. 7.8. Surface morphology of LNO film without seeds, heat-treated at 600°C

7.4 Conclusion

Lanthanum nickel oxide (LNO) ceramic/ceramic nanocomposite thin films with a thickness of ~400 nm were fabricated by MOD method with various amounts of LNO powder added as seeds to induce nucleation of the crystalline phase. Depending on the amount of LNO powder added, the crystallization temperature can be lowered from 590°C to 510°C.

Experimental results show that LNO composite film has faster grain growth and the grains are more densely packed. The film uniformity can also be improved due to this seeding effect and the crystallization of pure perovskite phase was induced at lower temperature. The conductivity of the LNO composite thin film annealed at 550°C, 600°C, 650°C, 700°C, and 750°C has been measured at room temperature, respectively. The LNO composite film annealed at 600~650°C has the highest conductivity.

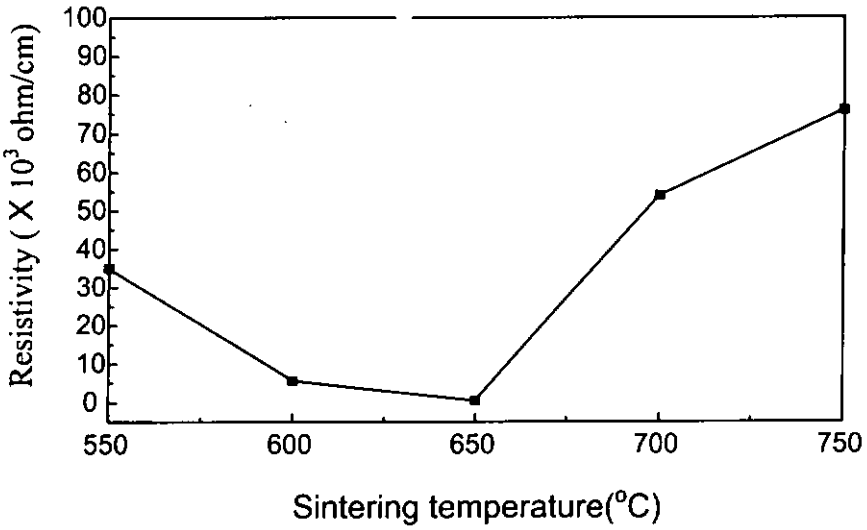

Fig. 7.9. The conductivity of the LNO composite film as a function of the annealing temperature

Chapter Eight

Conclusion and Suggestions for Future Work

8.1 Conclusions

This thesis presents a study on multilayer piezoelectric transformer (MPT) which has potential to be used in switching power supply. After an introduction in Chapter 1, Chapter 2 described the fabrication process of MPT, the hot-press lamination process and the behavior of high temperature sintering process was discussed. In Chapter 3 and Chapter 4, two types of PZT multilayer transformer with Pt metallic interleaving electrode have been investigated. 40~400μm thick PZT green sheets were fabricated by the roll-casting method. Thickness mode vibration and length mode device have been introduced. In Chapter 5, a two-step sintering process was described. This process can lower the MPT sintering temperature by about 100~150°C. This process was useful in the fabrication of multilayer piezoelectric device using palladium/silver (Pd/Ag) interleaving electrodes instead of Pt interleaving electrode, which can greatly reduce the production cost of MPT.

This thesis also presented a second type of multilayer PZT structure fabricated by a sol-gel technique. A conductive oxide, lanthanum nickel oxide (LNO), was used as the interleaving electrodes and the PZT/LNO multilayers were co-fired at below 650°C to make the process compatible with the integrated circuit (IC) technology. Sol-gel prepared PZT/LNO multilayer structures were studied, a buffer layer consisting of a mixture of PZT and LNO was introduced at the interface to enhance the adhesion between the PZT and LNO. To fabricate LNO films thick enough to be used as electrodes, a modified sol-gel process has been used. LNO powder was introduced into the LNO sol-gel solution to induce a seeding effect in the film formation process and the annealing temperature has been reduced. This study was an initial exploration of using the piezoelectric ceramic co-fired with conductive ceramic to fabricate micro-multilayer piezoelectric device on Si substrate.

8.2 Suggestions for Future Work

The study on multilayer piezoelectric transformer is on-going, especially for the application of high power transmission circuit and high frequency DC circuit that can be used in LCD(Liquid Crystal Display) of notebook computer. The studies of the design and fabrication process of the device are still improving and will be further pursued. First, some new structure of MPT should be investigated. For example: radial mode multilayer transformer which can bear high transmission power and can work at low energy losses, as shown in Fig. 8.1; bending mode multilayer transformer which can work at low resonance frequency with high Q_m factor, as shown in Fig. 8.2. Second, more elaborate equivalent circuit analysis and finite element analysis should be used to simulate the device performance.

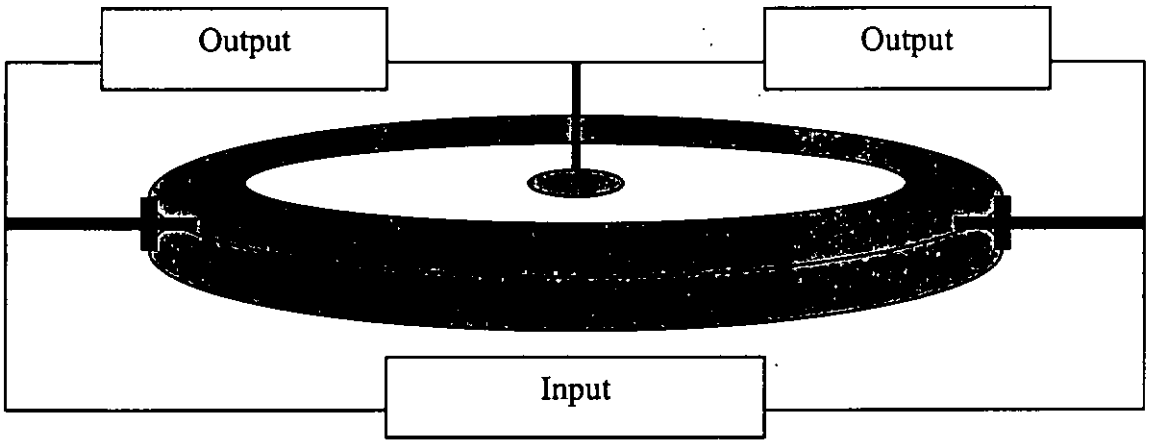

Fig. 8.1. Radial mode multilayer transformer

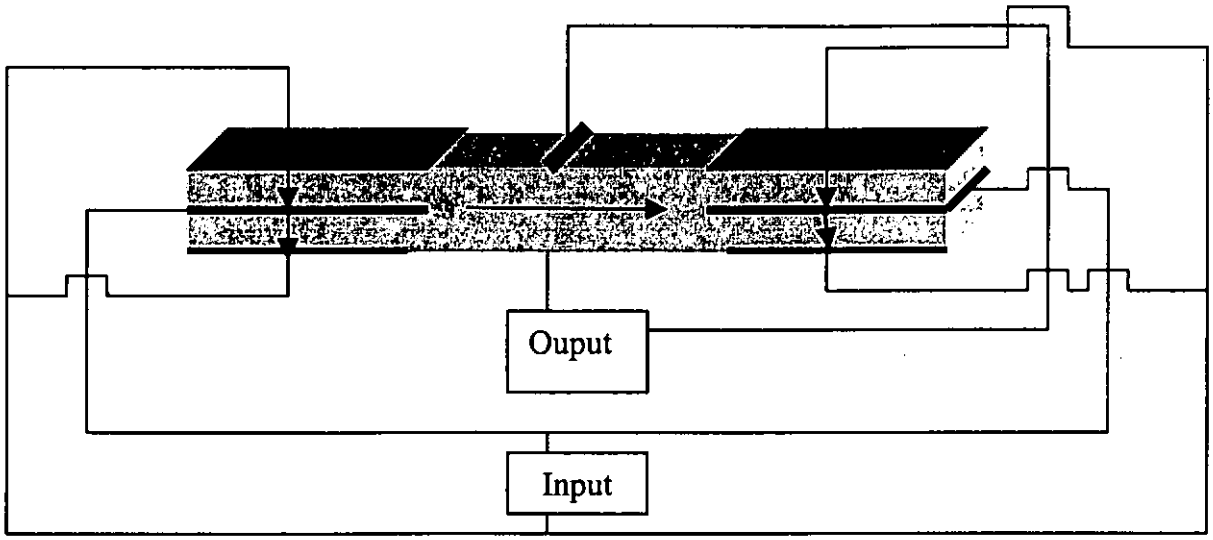

Fig. 8.2.Bending mode multilayer transformer

We have carried out some work in the radial mode multilayer transformer. A special feature in our work is the ring-shaped electrode at the boundary of the input and output sections, as shown is Fig. 8.3. This structure is used to connect parts of the interleaving electrode layers, and also used as a vertical electrode where the output portion of the whole multilayer transformer is connected. The outside part of the ring with several laminate ceramic and interleaving electrodes is the input portion of the device. Some measurement have been carried out and the prelinimary results are given in Appendix. 3. We plan to pursue this work in the near future.

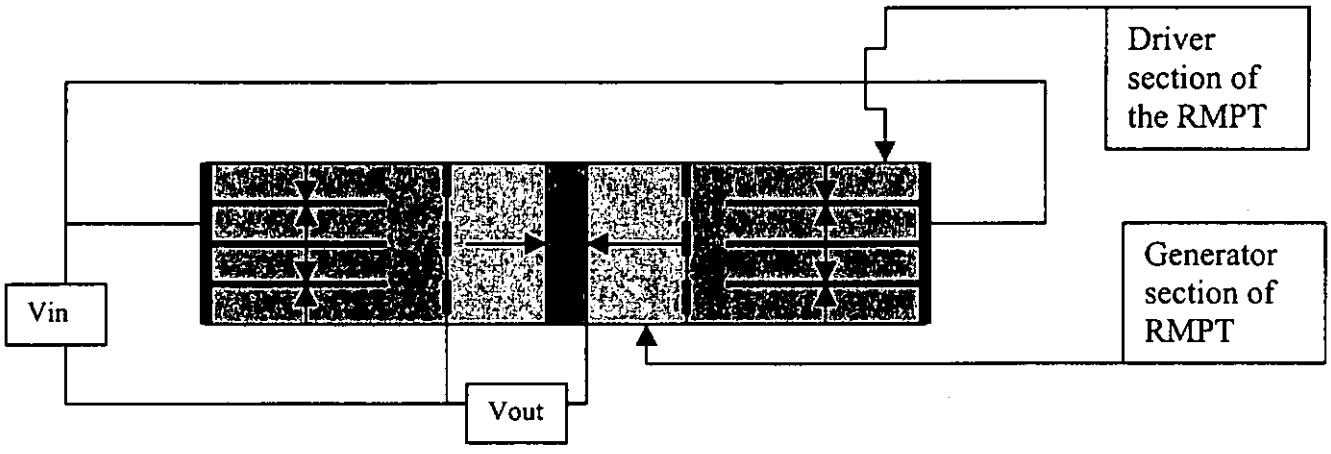

Fig.8.3. Cross section view of radial mode multilayer piezoelectric transformer (RMPT)

Another approach to extend our research work is to study the fabrication of micro-sized piezoelectric device on Si substrate by using conductive ceramic as electrode and co-fire with PZT thin film. The first step is using the co-fire method and modified sol-gel method to fabricate a sandwich structure LNO/PZT/LNO film onto the Si substrate. Our early result can be used as reference, for example, the seeding effect to reduce the LNO sintering temperature and a buffer layer to match the thermal expansion condition with PZT. After the fabrication work, some measurement should be made on this multilayer structure device, e.g. dielectric and piezoelectric properties, electrical conductivity of the LNO ceramic electrode, aging problem, etc. These will be left for future work.

List of Publications

1. "Conducting LNO as electrodes of PZT films"

   By Yu. Zhang, Q. F. Zhou, H. L. W. Chan, C. L. Choy.

   Thin Solid Films, V.375, P.87-90, (2000).

2. "The seeding effect of lanthanum nickel oxide ceramic/ceramic nanocomposite thin films prepared by the MOD method"

   By Yu. Zhang, Q. F. Zhou, H. L. W. Chan, C. L. Choy.

   Proceeding of MRS 2000 Spring Conference in San Francisco, USA

3. " Two-step sintering process for reducing the PZT multilayer structure's sintering temperature"

   By Yu. Zhang, H. L. W. Chan, C. L. Choy.

   Submitted to 3rd Asian meeting on Ferroelectrics, Hongkong, China, December, 2000.

4. 多层一体化共烧结构之弯曲振动模式压电陶瓷升压变压器

   Chinese Patent, Pending

Reference

[1]. IEEE standard on Piezoelectricity.

[2]. Orlando Auciello, J. Engemann, "Multicomponent and Multilayered Thin films for advanced Microtechnologies: Techniques, Fundamentals and Devices" Series E: Applied Sciences-Vol.234.

[3]. A.M. Flymn, S.R.Sanders, "Fundamental Limits on Energy Transfer and Circuit Considerations for Piezoelectric Transformers", IEEE PESC'98 RECORD, Pages 1504-1510, 1998.

[4]. Randall M.German, "Sintering Theory and Practice", 1996.

[5]. Toshiyuki, ZAITSU, Tamotsu NINOMIYA, Masahito SHOYAMA, "Piezoelectric Transformer Converter with PWM Control" Journal of Japanese Physics, Vol.E80-B No.7 Pages 1035-1044, 1997.

[6]. PIEZO KINETIC INCORPERATED product cataloge, July, 10, 1988.

[7]. J.Emsley, "The Elements", Clarendon Press, Oxford, UK, 1989.

[8]. R.M.German, "Power Metallury Science", second edition, Metal Power Industries Federation, Princeton, NJ, 1994.

[9]. H.Jones, "The Surface Energy of Solid Metals", Metal Sci. J. 1971, Vol. 5, Pages 15-18.

[10]. NEC Patent of "thickness mode Multilayer Piezoelectric Transformer, design and fabrication skill". Japanese Patent No. 09059969.

[11]. R. Morrell, " Handbook of Properties of Technical and Engineering Ceramics", revised edition, Her Majesty's Stationary Office, London, 1989.

[12]. J.F.Shackelford, "Materials Science of Engineering", Macmillan, New York, 1988.

[13]. Z.M.Zhao, "Handbook of Piezoelectric Transformer", ZheJian University, China, 1984.

[14]. Y.Fuda, K.Kumasaka, M.Katsuno, H.Sato, Y. Ino," Piezoelectric Transformer for cold Cathode Fluorescent Lamp inverter", Jpn.Journal of Applied Physics, Vol. 36, Pages 3050-3052, 1997.

[15]. O.Ohnishi, H.Kishie, A.Iwamoto, Y.Sasaki, T.Zaitsu, T.Inoue," Piezoelectric Ceramic Transformer Operating in Thickness extensional Vibration Mode for Power Supply", IEEE Ultrasonic Symposium, Pages 483-488, 1992.

[16]. J. H. Yoo, J. I. Hong , S. Suh," Effect of MnO2 impurity on the modified PbTiO3 system ceramics for power supply", Sensors and Actuators A: Physical, Volume 78, Issues 2-3, 14 December 1999, Pages 168-171.

[17]. Yeong-Ho Jeong, Su-Ho Lee, Ju-Hyun Yoo, Chang Yub Park," Voltage gain characteristics of piezoelectric transformer using PbTiO3 system ceramics", Sensors and Actuators A: Physical, Volume 77, Issue 2, 12 October 1999, Pages 126-130.

[18]. J.H.Hu, G.R.Li, H.L.W.Chan, C.L.Choy, "An improved method for analyzing the performance of multilayer piezoelectric transformers", 1999 IEEE Ultrasonics Symposium-943.

[19]. A. Vázquez Carazo, R. Bosch," Piezoelectric non-resonant transformer to measure high voltage", Journal of the European Ceramic Society, Volume 19, Issues 6-7, June 1999, Pages 1275-1279.

[20]. Basak, Amitava," Condition monitoring of power transformers", Engineering Science and Education Journal, Volume 8, Issue 1, February 1999, Pages 41-46.

[21]. Imori, Masatosi; Taniguchi, Takashi; Matsumoto, Hiroshi," Photomultiplier high-voltage power supply incorporating a ceramic transformer driven by frequency modulation", IEEE Transactions on Nuclear Science, Volume 45, Issue 3 Part 1, June 1998, Pages 777-788.

[22]. Fisher, N.E.; Henderson, P.J.; Jackson, D.A," Interrogation of a conventional current transformer using an in-fibre Bragg grating", Measurement Science & Technology, Volume 8, Issue 10, October 1997, Pages 1080-1084.

[23]. Karlash, V.L," Planar-thickness oscillations of circular piezo-ceramic rings and discs", Prikladnaya Mekhanika, Volume 33, Issue 7, July 1997, Pages 72-78.

[24]. Imori, Masatosi; Taniguchi, Takashi; Matsumoto, Hiroshi; Sakai, Toshiyuki," Photomultiplier high voltage power supply incorporating a piezoelectric ceramic transformer", IEEE Transactions on Nuclear Science, Volume 43, Issue 3 Part 2, June 1996, Pages 1427-1431.

[25]. Farosz B.J," FEASIBILITY OF ULTRASOUND HYPERTHERMIA WITH WAVEGUIDE INTERSTITIAL APPLICATOR", IEEE Transactions on Biomedical Engineering, Volume 43, Issue 11, 1996, Pages 1106-1115.

[26]. Antaki, James F., Bertocci, Gina E., Green, Elizabeth C., Nadeem, Ahmed, Rintoul, Thomas, Kormos, Robert L., Griffith, Bartley P," Gait-powered autologous battery charging system for artificial organs", ASAIO Journal, Volume 41, Issue 3, July - September 1995, Pages M588-M595.

[27]. Kim, Jung-Hyun; Han, Deuk-Young; Nam, Moon-Hyon; Kang, Sung-Mo," Analysis of a three-layered piezoelectric ceramic transformer filter", IEEE Transactions on Circuits and Systems I: Fundamental Theory and Applications, Volume 42, Issue 6, June 1995, Pages 307-313.

[28]. Lee, Fu-Shin, Moon, Tess J., Masada, Glenn Y," Extended bond graph reticulation of piezoelectric continua", Journal of Dynamic Systems, easurement and Control, Transactions of the ASME, Volume 117, Issue 1, March 1995, Pages 1-7.

[29]. Jaeger, Nicolas A.F., Rahmatian, Farnoosh," Integrated optics pockels cell high-voltage sensor", IEEE Transactions on Power Delivery, Volume 10, Issue 1, January 1995, Pages 127-134.

[30]. Kemp, I.J.," Partial discharge plant-monitoring technology: Present and future developments", IEE Proceedings: Science, Measurement and Technology, Volume 142, Issue 1, January 1995, Pages 4-10.

[31]. Won, C. Chung," Piezoelectric transformer", Journal of Guidance, Control, and Dynamics, Volume 18, Issue 1, January - February 1995, Pages 96-101.

[32]. Wallace, John L.," Extremely low-cost interface between an inchworm piezoelectric motor and a personal computer, Measurement Science & Technology, Volume 5, Issue 7, July 1994, Pages 861-863.

[33]. Leach, W. Marshall Jr.," Controlled-source analogous circuits and SPICE models for piezoelectric transducers", IEEE Transactions on Ultrasonics, Ferroelectrics, and Frequency Control, Volume 41, Issue 1, January 1994, Pages 60-66.

[34]. Craig A. J. Fisher, Hideaki Matsubara,"The influence of grain boundary misorientation on ionic conductivity in YSZ", Journal of the European Ceramic Society, Vol 19, Issue 6-1, (1998), Pages 703-707.

[35]. Slavko Bernik, Petra Zupancic, Drago Kolar," Influence of Bi_2O_3/TiO_2, Sb_2O_3 and Cr_2O_3 doping on low-voltage varistor ceramics", Journal of the European Ceramic Society, Vol 19, Issue 6-1, (1998), Pages 709-713.

[36]. Shigeru Tanaka, Ken Takahashi," Direct measurements of voltage/Current characteristics of single grain boundary of ZnO varistors", Journal of the European Ceramic Society, Vol 20, Issue 6-3, (1998), Pages 727-730.

[37]. Carlos Navas, Harry L. Tuller, Hans-Conrad zur Loye," Electrical conductivity and nonstoichiometry in doped Sr3Ti2O7", Journal of the European Ceramic Society, Vol 29, Issue 6-2, (1998), Pages 737-740.

[38]. K. Sasaki, J. Maier," Low temperature defect chemistry of oxides", Journal of the European Ceramic Society, Vol 19, Issue 6-1, (1997), Pages 741-745.

[39]. Enrico Traversa, Manuela Baroncini, Elisabetta Di Bartolomeo, Gualtiero Gusmano, Plinio Innocenzi, Alessandro Martucci, Andrea Bearzotti," Electrical humidity response of sol-Gel processed undoped and alkali-doped TiO2/Al2O3 thin films", Journal of the European Ceramic Society, Vol 19, Issue 6-1, (1996), Pages 753-758.

[40]. Y.Ling, W.Ren, X.Q.Wu, L.Y.Zhang, X.Yao. Thin Solid Films. Vol 128 (1997) pages 311.

[41]. C.R.Cho, David.A.Payne. Applied Physics Letter. Vol 71(20) (1997) pages 3013.

[42]. A.Li, C.Z.Ge, P.Lu. Applied Physics Letter. Vol 68(10) (1996) pages 347.

[43]. K.Sceedhar, J.M.Honig. Physics Review B. Vol 46(10) (1992) pages 6382.

[44]. M.S.Chen, T.B.Wu, J.M.Wu. Applied Physics Letter. Vol 68(10) (1996) pages 1430.

[45]. A.Li, C.Z.Ge, P.Lu, D.Wu, S.B.Xiong. Applied Physics Letter. Vol 70(12) (1997) pages 1616.

[46] Q.F. Zhou, H.L.W. Chan and C.L.Choy, Submitted to Thin Solid Films.

[47]. Q.F.Zhou, H.L.Chan and C.L.Choy. J. Mater. Process. Tech. Vol 63 (1997) pages 281.

[48]. C.R.Cho, David.A.Payne. Applied Physics Letter. Vol 71(20) (1997) pages 3013

[49]. Q.F.Zhou, H.L.Chan and C.L.Choy. J. Mater. Process. Tech. Vol 63 (1997) pages 281.

[50]. Y.Zhang, Q.F.Zhou, H.L.W.Chan and C.L.Choy. Thin Solid Films, Vol.375, (2000) Pages 87-90.

[51]. Pramod K.Sharma, M.H.Jilavi, R.Nab, H.Schmidt. Journal of Materials Research Letters. Vol 17(1998) pages 823

[52]. A.Li, C.Z.Ge, P.Lu. Applied Physics Letter. Vol 68(10) (1996) pages 1347.

[53]. A.Li, C.Z.Ge, P.Lu, D.Wu, S.B.Xiong. Applied Physics Letter. Vol 70(12) (1997) pages 1616.

[54]. A.Wu, P.M.Vilarinho, I.M.MirandaSalvado and J.L.Baptista. Material Research Bulletin. Vol 33(1998) pages 59

[55]. H.B. Sharma and A.Mansingh, Ferroelectric Letter. Vol 22 (1997) pages 75

Appendix 1
Preliminary Design of PT Based on the Equivalent Circuit Analysis

It is seen from the analyses in Chapter 3 and Chapter 4 that the configuration (related to vibration model), material properties and dimensions have effects on the properties of piezoelectric transformer. After the operating vibration mode and the piezoelectric material are chosen according to the given specification, the availability to the design is mainly on the geometry. Temporary dimensions are obtained from the preliminary design based on the equivalent circuit. For this purpose, the equivalent circuit and the relation equations are first derived. In the following section, preliminary design for the Rosen-type PT is described as an example.

1. Related Equations for Design

The lumped equivalent circuit has already been obtained in Chapter 3 and some related equations are also derived in the foregoing chapters. From the viewpoint of gaining high efficiency, the voltage amplification Am for the maximum efficiency is then derived from the obtained equations. Most of the symbols inside the equations are defined like Chapter 1 & 2.

$$A = \left|\frac{\phi}{\psi}\right| \left| \frac{R'_L - j\dfrac{1}{wC_{22}'}}{R' + R_L'} \right| = \frac{4\phi\psi R_L \sqrt{1 + w_r^{\,2} C_{22}^{\,2} R_L^{\,2}}}{R(1 + w_r^{\,2} C_{22}^{\,2} R_L^{\,2}) + 4\psi^2 R_L} \qquad (1.1)$$

$$A_\infty = \frac{4 d_{31} g_{33} c_{11}^{\,E} Q_m l}{\pi^2 (1 - k_{33}^{\,2}) t} \qquad (1.2)$$

$$R_L = \frac{1}{wC_{22}} \qquad (1.3)$$

$$\eta_m = \frac{2\psi^2}{wC_{22}R + 2\psi^2} = \frac{1}{1+(\pi^2(1-k_{33}^{\ 2})/2k_{33}^{\ 2}Q_m)} \tag{1.4}$$

A is the voltage ratio for the general case, and A_∞ is open-circuit voltage ratio. Equation 1.4 is the maximum efficiency, and equation 1.3 is the condition for η_m. Inserting equation 1.3 into equation 1.1, there is

$$A_m = \frac{2\sqrt{2}R_L\psi\phi}{R + 2\psi^2 R_L} \tag{1.5}$$

The relation of A_m and A_∞ can be derived as:

$$\frac{A_m}{A_\infty} = \frac{1}{\sqrt{2}(1 + 2\psi^2 R_L / R)} \tag{1.6}$$

Expanding $\frac{\psi^2 R_L}{R}$ in fundamental quantities with the same way of derivation of A_∞ in Chapter 3:

$$\frac{\psi^2 R_L}{R} = \frac{k_{33}^{\ 2}Q_m}{\pi^2(1 - k_{33}2)} \tag{1.7}$$

$\frac{A_m}{A}$ can be obtained

$$\frac{A_m}{A_\infty} = \frac{1}{\sqrt{2}(1 + 2k_{33}^{\ 2}Q_m / \pi^2(1 - k^2{}_{33}))} \tag{1.8}$$

where

$$k_{33}^{\ 2} = \frac{d_{33}}{\sqrt{\varepsilon_{33}^{\ T} s_{33}^{\ E}}} \tag{1.9}$$

The design may also be considered from the point of gaining more power transfer. In this case, the voltage ratio for maximum power transfer is approximately one half the open-circuit one.

2. Preliminary Design Steps for PT

The steps of the preliminary design are as follows:

1. Determine the vibration mode and structures for the piezoelectric transformer according to the specification.

2. Choose a suitable piezoelectric material, for example, select material with high Q_m and high electromechanical coupling factor if high efficiency is desired.

3. Check the limitations. There is a limitation of how high an electric field can be applied because of the non-linear characteristics of the material. Hence, the working field in the generator section should not surpass the limitation value for safety. Thus the minimum half-length is limited by the output voltage and the limited field specified.

4. The length is set by the operation frequency range which is given or selected, for the frequency constant is almost a constant as analysed in Chapter 4. In the case of one-wavelength, there is

$$2l = v/f = \frac{\sqrt{\frac{1}{\rho s^{E}_{11}}}}{f} \tag{2.1}$$

5. Estimate the thickness t of PT.

The open-circuit voltage amplification A_∞ is needed first, then use equation 1.2 to calculate t. If the maximum efficiency is required, then use the equations below to calculate the thickness.

$$A_{\infty} = A_V \sqrt{2}\{1 + [2K^2{}_{33}Q_m / \pi^2(1 - K^2{}_{33})]\} \tag{2.2}$$

$$t = \frac{4Q_m C_E{}^{11} g_{33} d_{31}}{\pi^2(1 - K^2{}_{33})} \frac{l}{A_{\infty}} \tag{2.3}$$

Since the values of l, A_{∞} are always known, t can be obtained.

Appendix 2

Program for Calculating the Theoretical Performance of the Thickness Mode MPT

(This program can only work under the software of Matlab environment.)

```
clear; % clear all variables

close all; % close all graph windows

----------

step=200;  % number of step will be used for calculation

range=5;  % number of delf will be calculated

% Circuit parameters


Rp1=3;

Cd1=43e-12;

L1=7.78e-3;

C1=39.75e-12;

R1=560;

N=1.9;

Cd2=0.78e-12;

Rl=10e6;
```

```
fr=1.26e6;

fa=1.41e6;

fo=sqrt(fr*fa);


delf=abs(fa-fr);

fl=fo-delf*range/2;  % lower frequency for calculation

fu=fo+delf*range/2;  % upper frequency for calculation


f=fl:range*delf/(step):fu;  % frequency range for calculation

nstep=size(f,2);

w=f.*2*3.1416;


for n=1:nstep


% calculate impedance for all reactive components

  Xcd1(n)=1/(i*w(n)*Cd1);

  Xcd2(n)=1/(i*w(n)*Cd2);

  Xc1(n)=1/(i*w(n)*C1);

  Xl1(n)=i*w(n)*L1;
```

```
% calculate the input impedance

  Z1(n)=1/(1/Xcd2(n)+1/Rl);

  Zin(n)=Rp1+1/(1/Xcd1(n)+1/(Xl1(n)+Xc1(n)+R1+Z1(n)/N^2));

  Yin(n)=1/Zin(n);


% calculate the output impedance

  Z2(n)=1/(1/Rp1+1/Xcd1(n));

  Zout(n)=1/(1/Xcd2(n)+1/((R1+Xc1(n)+Xl1(n)+Z2(n))*N^2));


% calculate the ratio of the output voltage over the input voltage at no load

% note that the size of Rp1 has great impact on the output voltage

% for ideal case Xcd1>>Rp1, ie, Vo~Vi*N at no load

Vo(n)=(Xcd1(n)/(Rp1+Xcd1(n))*N)*(Xcd2(n)/(Xcd2(n)+(R1+Xc1(n)+Xl1(n)+Z2(n))*N
^2));


% calculate the ratio of the output voltage over the input voltage at Rl

  Vol(n)=Vo(n)*Rl/(Rl+Zout(n));

  Pin(n)=real(Yin(n)); % for vin=1V

  Pout(n)=abs(Vol(n))^2/Rl;

  eff(n)=Pout(n)/Pin(n);
```

```
end


figure
plot(f./fo, abs(Vol));
title('output load voltage with input at 1V and load=10Momh');
xlabel('f/fo');
ylabel('Vo, volts');
figure(2)
plot(f./fo,Pin);
title('power in with input at 1V and load=10Momh');
xlabel('f/fo');
ylabel('Pin, W');
figure(3)
plot(f./fo,Pout);
title('power out with input at 1V and load=10Momh');
xlabel('f/fo');
ylabel('Pout, W');
figure(4)
plot(f./fo,eff*100);
xlabel('f/fo');
```

```
ylabel('efficiency, %');

title('efficiency with input at 1V and load=10Momh');

figure(5)

plot(f./fo,abs(Zout));

xlabel('f/fo');

ylabel('Zout, ohms');

title('Zout');

figure(6)

plot(f./fo,abs(Zin));

title('Zin with input at 1V and load=10Momh');

xlabel('f/fo');

ylabel('Zin, ohms');
```

Appendix .3

Preliminary Experimental Result of the Radial Mode MPT

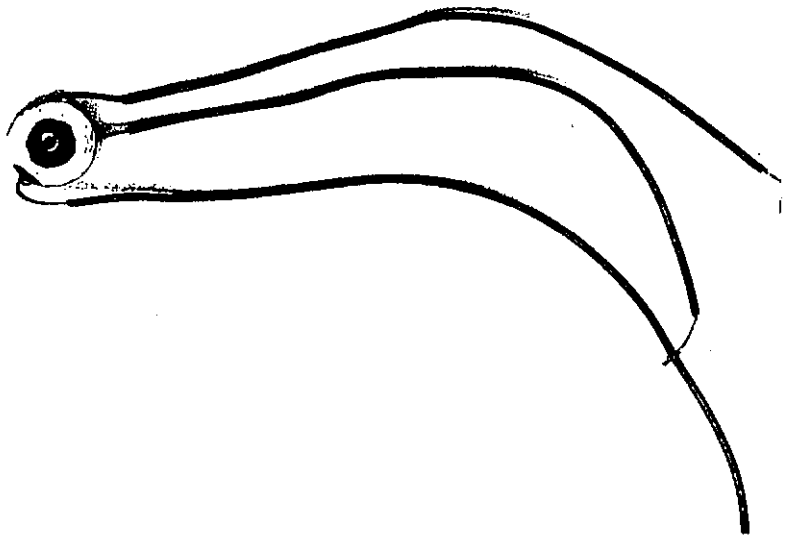

Fig. A.1. Photo of ring-shaped MPT

Basically, most of the fabrication process of the radial mode MPT is the same as those other MPT structures, e.g. the thickness mode MPT. But there are two major different steps that are unique to the radial mode structure. First, the drill slurry process in order to build a ring shaped electrode at the boundary of the input and output sections. Second, the poling process of the driver section and the generator section, which we need to pole the ceramic in two different directions.

In the first step, we need to dig small holes through each ceramic green sheet. As shown in Fig. A.2. This structure is used for poling the generator section in the radial direction. Also the interleaving electrode that was painted on alternate ceramic sheets has two different patterns (a) & (b) shown in Fig. A.2. This structure is used for connecting

the interleaving electrodes to two different external wires that can be used in subsequent poling.

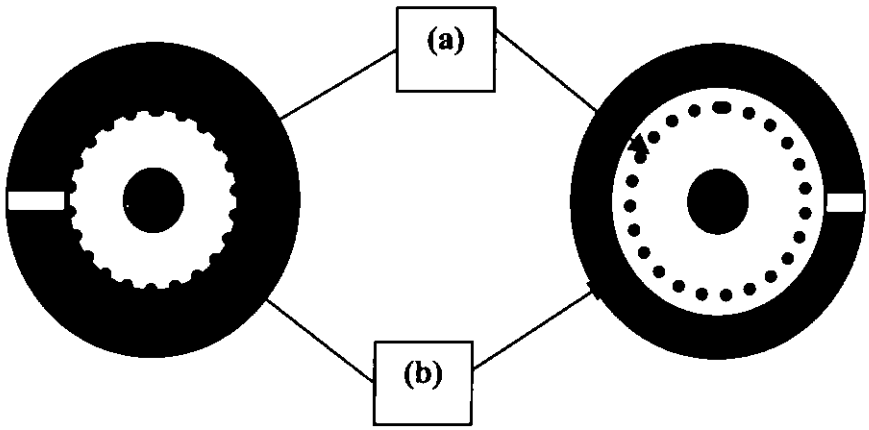

Fig. A.2. Top view of each ceramic sheet (a) Small holes through the ceramic sheets for the ring-shaped electrode, (b) different shapes of the interleaving electrode painted on the ceramic sheets.

In order to pole the radial mode MPT, we need .o separate the driver section and generator section clearly, a schematic of the cross section structure of RMPT is shown in Fig. 8.3. From the figure we can see, the driver section was laminated by several ceramic layers, with the interleaving electrode fabricated between those ceramic sheets. The inner ring (the output section) was poled radially while the multilayered outer part was poled vertically, as shown by the arrows.

In this structure, the driver input section of transformer can introduce radial movement by the k_{31} vibration mode because of the ring-shaped, then this vibration can be generated through the inside generator section of the transformer with a higher output value by the 33 mode. Since the vibration wave transmit through the radial direction of the ring, it can direct the energy to the center of the device with less loss in energy.

The poling process of the device should be separated into two parts. Since the poling direction is vertical, and the internal electrode is quite complex. Especially when

we try to pole the generator (output) section in the radial direction, we need to increase the poling voltage quite carefully. Because the ceramic near the ring-shaped electrode has small cracks, due to the shrinkage mismatch problem in the co-fire process, and these cracks will cause electrical break down when poling. So how to improve the co-fire result and how to improve the design of the ring-shaped electrode will need further work in the future.

Experimental Results

Table 8.1 Physical properties of the radial mode MPT

k_{31}	0.3	k_{33}	0.55
d_{31}	50 (pm/V)	d_{33}	90 (pm/V)
s^E_{31}	0.7*E*-11 (m^2/N)	Density	7500 (kg/m^3)
Q_m	70	Fundamental resonance frequency	~0.34 MHz
v^E_{33}	3300 m/s	Total thickness	~2 mm
Inner radial dimension	9~10 mm	External radial dimension	3~4mm

Some preliminary experimental results have been obtained and shown in Table 8.1. Further work will be done on this RMPT device, the optimization of its fabrication process and working mode selection will be further pursued.